AFWL-TR-89-35

(2)

AN EXPERIMENTAL STUDY OF MICROWAVE TRANSMISSION THROUGH A DECAYING PLASMA

Kyle James Hendricks

May 1989

Final Report

Approved for public release; distribution unlimited.

AIR FORCE WEAPONS LABORATORY
Air Force Systems Command
Kirtland Air Force Base, NM 87117-6008

This report contains color plates: All DTIC reproductions will be in black and white.

This final report was prepared by the Air Force Weapons Laboratory, Kirtland Air Force Base, New Mexico, Job Order 57972401. Kyle J. Hendricks (AWPB) was the Laboratory Project Officer-in-Charge.

When Government drawings, specifications, or other data are used for any purpose other than in connection with a definitely Government-related procurement, the United States Government incurs no responsibility or any obligation whatsoever. The fact that the Government may have formulated or in any way supplied the said drawings, specifications, or other data, is not to be regarded by implication, or otherwise in any manner construed, as licensing the holder, or any other person or corporation; or as conveying any rights or permission to manufacture, use, or sell any patented invention that may in any way be related thereto.

This report has been authored by an employee of the United States Government. Accordingly, the United States Government retains a nonexclusive, royalty-free license to publish or reproduce the material contained herein, or allow others to do so, for the United States Government purposes.

This report has been reviewed by the Public Affairs Office and is releasable to the National Technical Information Service (NTIS). At NTIS, it will be available to the general public, including foreign nationals.

If your address has changed, if you wish to be removed from our mailing list, or if your organization no longer employs the addressee, please notify AFWL/AWPB, Kirtland AFB, NM 87117-6008 to help us maintain a current mailing list.

This report has been reviewed and is approved for publication.

Kyle J. Hendricks

KYLE J. HENDRICKS
Captain, USAF
Project Officer

Rex L. Schlicher

REX L. SCHLICHER
Major, USAF
Ch, Beam Physics Branch

FOR THE COMMANDER

William L. Baker

WILLIAM L. BAKER
Ch, Advanced Technology Division

DO NOT RETURN COPIES OF THIS REPORT UNLESS CONTRACTUAL OBLIGATIONS OR NOTICE ON A SPECIFIC DOCUMENT REQUIRES THAT IT BE RETURNED.

UNCLASSIFIED

SECURITY CLASSIFICATION OF THIS PAGE

REPORT DOCUMENTATION PAGE

Form Approved OMB No. 0704-0188

1a. REPORT SECURITY CLASSIFICATION: Unclassified	1b. RESTRICTIVE MARKINGS
2a. SECURITY CLASSIFICATION AUTHORITY	3. DISTRIBUTION/AVAILABILITY OF REPORT: Approved for public release; distribution unlimited.
2b. DECLASSIFICATION/DOWNGRADING SCHEDULE	
4. PERFORMING ORGANIZATION REPORT NUMBER(S): AFWL-TR-89-35	5. MONITORING ORGANIZATION REPORT NUMBER(S)
6a. NAME OF PERFORMING ORGANIZATION: Air Force Weapons Laboratory; 6b. OFFICE SYMBOL (If applicable): AWPB	7a. NAME OF MONITORING ORGANIZATION
6c. ADDRESS (City, State, and ZIP Code): Kirtland Air Force Base, New Mexico 87117-6008	7b. ADDRESS (City, State, and ZIP Code)
8a. NAME OF FUNDING/SPONSORING ORGANIZATION; 8b. OFFICE SYMBOL (If applicable)	9. PROCUREMENT INSTRUMENT IDENTIFICATION NUMBER
8c. ADDRESS (City, State, and ZIP Code)	10. SOURCE OF FUNDING NUMBERS

PROGRAM ELEMENT NO.	PROJECT NO.	TASK NO	WORK UNIT ACCESSION NO
62601F	5797	24	01

11. TITLE (Include Security Classification)

AN EXPERIMENTAL STUDY OF MICROWAVE TRANSMISSION THROUGH A DECAYING PLASMA

12. PERSONAL AUTHOR(S)

Kyle James Hendricks

13a. TYPE OF REPORT	13b. TIME COVERED	14. DATE OF REPORT (Year, Month, Day)	15. PAGE COUNT
Final	FROM Jan 86 TO Feb 88	1989, May	132

16. SUPPLEMENTARY NOTATION

17. COSATI CODES			18. SUBJECT TERMS (Continue on reverse if necessary and identify by block number)			
FIELD	GROUP	SUB-GROUP	Rf	Afterglow	Ionization	Interferometry
20	09		Plasma	Microwave	Transmission	Propagation
20	06		Decay	Breakdown	Radiofrequency	

19. ABSTRACT (Continue on reverse if necessary and identify by block number)

The physics of pulsed microwave, or radio frequency (rf) transmission through a decaying plasma column is studied experimentally. A plasma column is formed in argon or nitrogen gases, to represent the neutral gas breakdown due to an rf pulse. Initially the electron density of the plasma column is such that the plasma electron frequency (ω_{pe}) is greater than the microwave frequency (ω_{rf}). An rf pulse capable of plasma reionization is applied across the plasma column at varying times in the plasma's decay phase (the plasma afterglow). We have studied the variation of the transmitted rf pulse characteristics, pulse width and amplitude, as a function of the time into the afterglow. The ionization frequency of argon by a microwave pulse is found experimentally to be within 20% of the theoretical value. The comparison of ionization frequency is useful in establishing the applicability of earlier cavity measurements to present day open geometry systems used in transmission/propagation experiments. The rf energy contained in the transmitted pulse is found to reach half its maximum value for afterglow times of order 50 milliseconds (argon)

(over)

20. DISTRIBUTION/AVAILABILITY OF ABSTRACT	21. ABSTRACT SECURITY CLASSIFICATION
☒ UNCLASSIFIED/UNLIMITED ☐ SAME AS RPT. ☐ DTIC USERS	Unclassified

22a. NAME OF RESPONSIBLE INDIVIDUAL	22b. TELEPHONE (Include Area Code)	22c. OFFICE SYMBOL
Kyle J. Hendricks	(505) 844-0121	AFWL/AWPB

DD Form 1473, JUN 86 — Previous editions are obsolete.

SECURITY CLASSIFICATION OF THIS PAGE
UNCLASSIFIED

19. ABSTRACT (continued)

and 1 millisecond (nitrogen). These time intervals are consistent with theoretical predictions indicating that by applying high power pulses at less than 1 millisecond intervals it is possible to maintain the plasma density above the cutoff density.

We have also investigated the utility of high-power microwave interferometry. This diagnostic technique differs from the classical use of interferometry in that the microwave signal used is capable of modifying the medium (plasma) under study. In fact, the microwave pulse is capable of changing the medium to such an extent that the microwave signal is completely cut off. This diagnostic technique requires that a spatial profile for the plasma density be supplied for the numerical solution of the integral for the phase shift. The resulting relation then gives the time dependence of the phase shift or of the plasma density. For argon, the results of this technique compare favorable with other in situ and potentially perturbing diagnostic techniques.

The data for the ionization frequency for the case of nitrogen do not show the agreement found for argon. We are unable to resolve this disagreement. However, we list probable sources which might contribute to the observed differences in the behavior of the gases. Future work is necessary to examine these speculations more critically.

ACKNOWLEDGMENTS

I wish to express my deepest appreciation to my dissertation committee members, namely, Professors H.S. Ahluwalia (Chairman) and Howard Bryant of the Physics Department, Professor Norman Roderick and Dr. Joseph Mather of the Chemical and Nuclear Engineering Department, and Dr. M. Collins Clark of Sandia National Laboratory. I am deeply indebted to Professor Ahluwalia for his guidance in the presentation of this work and in preparing the manuscript, and to Dr. Clark for his guidance in completing the experiment. I also am grateful to the High Power Microwave Group of the Weapons Laboratory for supporting this work. Specifically, I wish to thank Capt. Gary DeMuth, Dr. Don Voss, Dr. Mike Hayworth, Dr. Bob Platt, Jim Metz, and Carl Noggle for many valuable discussions and their assistance at difficult points in this work. I am deeply grateful to Maj. Rex Schlicher for allowing me to devote the time needed to complete the experiment and the manuscript. Last but not least, I deeply appreciate the support and encouragement of my parents, Bryce and Sara Hendricks; my wife Carla and my daughters Jenna and Morgan, throughout the completion of this work.

AN EXPERIMENTAL STUDY OF MICROWAVE TRANSMISSION THROUGH A DECAYING PLASMA

Kyle James Hendricks

B.S., Physics, University of Iowa, 1980
M.S., Physics, University of Iowa, 1982
Ph.D., Physics, University of New Mexico, 1989

The physics of pulsed microwave, or radio frequency (rf), transmission through a decaying plasma column, is studied experimentally. A plasma column is formed in Argon or Nitrogen gases, to represent the neutral gas breakdown due to an rf pulse. Initially the electron density of the plasma column is such that the plasma electron frequency (ω_{pe}) is greater than the microwave frequency (ω_{rf}). An rf pulse capable of plasma reionization is applied across the plasma column at varying times in the plasma's decay phase (the plasma afterglow). We have studied the variation of the transmitted rf pulse characteristics, pulse width and amplitude, as a function of the time into the afterglow. The ionization frequency of argon by a microwave pulse is found experimentally to be within 20% of the theoretical value. The comparison of ionization frequency is useful in establishing the applicability of earlier cavity measurements to present day open geometry systems used in transmission/propagation experiments. The rf energy contained in the transmitted pulse is found to reach half its maximum value for afterglow times of order 50 milliseconds (argon) and 1 millisecond (nitrogen). These time intervals are consistent with

theoretical predictions indicating that by applying high power pulses at less than 1 millisecond intervals it is possible to maintain the plasma density above the cutoff density.

We have also investigated the utility of high-power microwave interferometry. This diagnostic technique differs from the classical use of interferometry in that the microwave signal used is capable of modifying the medium (plasma) under study. In fact, the microwave pulse is capable of changing the medium to such an extent that the microwave signal is completely cutoff. This diagnostic technique requires that a spatial profile for the plasma density be supplied for the numerical solution of the integral for the phase shift. The resulting relation then gives the time dependence of the phase shift or of the plasma density. For argon, the results of this technique compare favorably with other *in situ* and potentially perturbing diagnostic techniques.

The data for the ionization frequency for the case of nitrogen do not show the agreement found for argon. We are unable to resolve this disagreement. However, we list probable sources which might contribute to the observed differences in the behavior of the gases. Future work is necessary to examine these speculations more critically.

TABLE OF CONTENTS

PAGE

List of figures

INTRODUCTION

High frequency, low to moderate power, radio waves (microwaves) have been used routinely in telemetry systems to communicate with and guide aircraft and spacecraft. Microwaves have also been used in special scientific projects such as echo ranging, topological studies of planetary surfaces, and modification of the characteristics of the local ionosphere at several locations around the globe. For some applications in atmospheric studies large amplitude microwave pulses are used. Transmission of large amplitude pulses may result in ionization of the atmospheric gases. The large oscillating electric fields inherent in these microwave pulses accelerate free electrons thereby losing energy to them. The energetic electrons collide with neutrals (atoms and molecules) creating a plasma. If the amplitude of the pulse is large enough and the pulse width is long enough, the number density of the electrons can increase very rapidly until it attains a critical value (n_c). At this stage the plasma acts like a reflector for the remainder of the pulse. If the time between the pulses is sufficiently large, the plasma will decay and the gases will return to a neutral state. Therefore, it is clear that only pulses of certain width and repetition rate can be transmitted through the atmosphere. The physical processes involved in the propagation and breakdown in air of the short burst, high power microwaves are poorly understood at present. This is not surprising because nonlinear phenomena are involved. An

experimental investigation is useful in identifying and understanding the main physical processes that contribute to the observed phenomena.

In this dissertation we have made an attempt to understand the physics of transmission of a pulsed microwave signal through a decaying plasma, by experimental means. Argon and nitrogen gases are used separately as transmitting media. A plasma column is formed in each gas and a microwave pulse is transmitted across it. The electron density in the plasma column is such that the plasma frequency (ω_{pe}) is greater than the microwave frequency (ω_{rf}). During the plasma's decay (the plasma afterglow) a short microwave pulse capable of reionizing the plasma is transmitted. We have studied the changes in the characteristics of the transmitted microwave pulse, such as the pulse width and the amplitude, as a function of the time into the afterglow. The pulse width is used to draw inferences about the ionization rate (the ionization frequency). The determination of the ionization frequency is useful in establishing if the earlier results, obtained by others from cavity measurements, are applicable to open systems used in contemporary transmission experiments. In our experiment we measure the microwave energy contained in the incident, the reflected, and the transmitted pulses. The change in the energy contained in the transmitted pulse is indicative of the change of the electron number density in the plasma column. The transmitted microwave pulse energy data are also useful in determining

the minimum inter-pulse time separation for large amplitude microwave pulses.

To understand how this experiment fits into contemporary plasma physics research, we review the various types of microwave-plasma interactions. The range of interactions extends from use of low amplitude microwaves as a diagnostic technique (standard interferometry) to using a single microwave pulse with sufficient energy to ionize the neutral gas.

The first type of interaction reported in the literature is the classic use of a low power microwave source for microwave interferometry[1,2]. Low power in this case implies that the microwave source is unable to alter the plasma properties. The plasma density must be below the critical value corresponding to the microwave frequency used. The experimental arrangement used in [1] is very similar to the arrangement used by us.

The second type of interaction involves the transmission of a microwave pulse which is resonantly absorbed in the plasma region thereby increasing the electron number density until it reaches the critical value, thereafter the plasma region becomes a perfect reflector[3]. The experimental arrangement used in [3] is similar to that used in the present work but the microwave energy is not transmitted across the plasma region.

The third type of interaction involves a study of the microwaves scattering from the plasma column[4]. The experimental setup used is again quite similar to that used in the present investigation. The difference lies in the way the plasma column is used. For scattering experiments the plasma column simply acts as a diffracting medium to low power microwaves. The microwave signal does not perturb the plasma in [4].

The fourth type of microwave-plasma interaction relevant for our review involves a study of the ionization produced by a single pulse[5-20]. Two techniques have typically been used in these investigations. In one case, an evacuated waveguide is used to carry large amplitude pulses. Sections of the waveguide are filled with a gas to study the ionization as a function of the amplitude of the electric field and neutral gas pressure[5,6]. The second method uses a large volume at atmospheric pressure. A reflector is used to act as a second source. If the incident and the reflected waves are in phase, the resultant amplitude of the electric field of the microwave signal causes ionization inside the region under study[7-13]. Both of these techniques are dependent on the availability of seed electrons to initiate the breakdown of the neutral gas. The point is that the size of the interaction is so small that naturally occurring free electrons may not be present. To overcome this difficulty, β-emitters are used in some experiments[10]. The study of such interactions has dominated the research for the past

decade to understand and appreciate the role played by the system parameters. The parameters used have a range covering power levels of watts to gigawatts, frequencies of a few hundred megahertz (MHz) to tens of gigahertz (GHz), pulse widths of a few nanoseconds to a few microseconds, and pulse repetition rates of up to a few kilohertz (kHz).

Standard theory indicates that once the gas is ionized and the plasma electron number density reaches the critical value complete reflection of the microwave signal will occur[12,13,14]. Various research groups[5,6,7,8,10,11] have studied breakdown in laboratory systems, with a view to understanding whether scaling laws exist. If scaling laws exist, it may be possible to specify the pulse width, amplitude, frequency, and neutral gas pressure over the range of interest, for a given experimental setup.

Solutions to the Boltzmann equation have been obtained under various approximations, using numerical simulations[15-20]. In the absence of scaling laws, the physical significance of the available solutions cannot be appreciated. From a practical point of view one has to understand how to propagate high power microwave pulses through a decaying plasma. The amplitude and period of the microwave pulse are such that the gas reionizes and forms a plasma of density n_c. In the present investigation, a plasma column is preformed. It acts as a medium for the transmission of the microwaves which have an amplitude of the electric field comparable to that required for the breakdown

of the gas. The plasma is then allowed to decay, and the transmission characteristics of the microwave pulse are studied. The lower limit to the inter-pulse separation is clearly zero. In this case the electron density remains at the critical value so that subsequent microwave power is reflected. The upper limit is closer to a few plasma decay time constants (about 0.1 sec). For this case, the plasma is so rarefied that the gas is effectively neutral.

To complete the review, we wish to point out that researchers at the Los Alamos National Laboratory are studying the inverse problem using air[18,21]. They are investigating how often one must apply microwave power to keep the plasma at the critical density. They find that a greater than 1 kHz repetition rate (< 1 msec inter-pulse separation) is required to accomplish this. This value is within the extreme limits discussed by us in the preceding paragraph.

The experimental setup used in the present investigation provides us with a complete freedom for selecting any time separation between plasma formation and microwave pulse transmission. This is indeed useful, since high power microwave devices do not currently have the capability of providing arbitrary inter-pulse separation. The investigation reported here probably represents the first attempt to transmit a microwave pulse through a plasma, where the pulse also modifies the refractive index of the medium.

We have also investigated the merit of using high-power microwave interferometry as a diagnostic technique. This technique is easy to implement. The necessary data are obtained by taking a fraction of the incident and transmitted pulses to a detector which provides a measure of the phase difference between the two signals. The phase difference provides a direct measure of the variation of the index of refraction of the medium modified by the microwave pulse. It should be emphasized that this technique does not perturb the boundary conditions of the system under study. A plasma is extremely sensitive to the insertion of probes, which cause changes in the boundary conditions. In the case of argon the technique of using high powered microwave interferometry has been found to give results which agree well with those obtained from other *in situ* and potentially perturbing diagnostic techniques.

The dissertation is organized as follows. In Chapter 1 we discuss the basic aspects of the standard theory of the breakdown in gases and reionization. In Chapter 2, we describe the various pieces of hardware used to perform the work. The description is kept brief, more detailed explanations (or derivations) are given in the appendices. For example, the two principal plasma diagnostic techniques, namely the double Langmuir probe and the two coil conductivity probe, are described in Appendices 1 and 2. In Appendix 3, the optimum window thickness for microwave transmission is calculated. The window is used to introduce

the microwave pulses into the vacuum chamber. In Appendix 4, we discuss the methods used to calibrate the various microwave devices used in our experiment. The derivation of the equation used to compute the phase shift, due to the microwave pulse crossing the plasma column, is presented in Appendix 5. In Chapter 3, the experimental data obtained by us are presented. Finally, we discuss the conclusions reached from analyses of the data, and suggest questions unanswered by this work which require further investigation. We also discuss some suggestions for modifications to the present experiment.

1. THEORETICAL DISCUSSION

This chapter summarizes our present understanding of the interaction between the microwave pulses and the plasma. The breakdown of a gas is discussed and the relaxation processes, observed for the atmospheric gases are described. The reionization process of a decaying plasma column is also discussed.

1.1 PLASMA IONIZATION

The ionization of a neutral gas by both cw and pulsed microwave sources has been studied for over 30 years. Typically experiments are done in cavities to increase the range of electric field amplitudes. Some free electrons must be present to be accelerated by the electric field of a microwave pulse. These accelerated electrons cause the breakdown of the gas. In microwave propagation experiments, as one goes to higher altitude the probability of finding an electron increases due to the increasing intensity of cosmic rays and ionizing radiations from the sun. Additionally the mean free path for electrons increases due to the lower particle density. This may allow the electron to reach a very high energy in the presence of large amplitude microwave signals. It is known that each gas has an optimum energy for collisions[22]. After exceeding that energy the collision cross-section decreases drastically. One would therefore prefer that a free electron be available with a mean free path approximately equal to the wavelength of the

incident microwaves. This process is described by the continuity equation which deals with a balance between the creation and loss processes of the plasma. If more electrons are created than are lost we have an exponential growth in the electron number density. If losses dominate, the rate of decay will vary depending upon the dominant loss mechanism. Typical loss mechanisms include electron attachment characterized by an exponential decay, and recombination characterized by a t^{-1} decay. On a much longer time scale the plasma will diffuse out of the region of interest. For example, in Section 3.1 we present data from the conductivity probe which indicates that N_2 plasma decayed by electron attachment. This phenomena has been observed before for air[17].

1.2 PLASMA REIONIZATION

The plasma reionization process is best described by using the continuity equation which may be written as follows:

$$\frac{\partial n}{\partial t} = \nu_i \, n - \nu_L \, n \, , \qquad (1.2.1)$$

where ν_i is the rate of ionization of neutrals by electrons, ν_L represents the rate of loss of plasma electrons, and n is the electron number density. It should be noted that ν_i and ν_L are not necessarily simple coefficients but may be complex functions. The loss of electrons by diffusion is neglected due to the longer time scale involved.

Immediately after the pulse enters the plasma the loss mechanism is still dominant and the plasma continues to decay. After a short time, the production and loss processes balance and the density tends to remain constant. Afterwards, the rate of production of electrons by microwaves exceeds their loss rate. The initial density determines the fraction of the pulse that passes through the plasma unchanged. The variation of the density with time is given by:

$$n(t) = n_0 \, e^{\nu_i t} . \qquad (1.2.2)$$

The above equation is derived from [Eq. 1.2.1] by neglecting the plasma loss term and assuming that the ionization frequency is independent of time. The time (t_0) required for the density to reach the critical value (n_c) may be obtained from [Eq. 1.2.2] and is given below:

$$t_0 = \frac{1}{\nu_i} \ln \left(\frac{n_c}{n_0} \right) . \qquad (1.2.3)$$

The value for n_0 depends on the afterglow time when the microwave pulse is applied. The calculated value for t_0 has been compared with argon data, and the value of ν_i is found to be 1.4×10^8 Hz (see Chapter 3 for details).

We can also compute a value for the collision frequency (ν_i) by using the data from Brown[22] on the breakdown studies in cavities. Brown has grouped together data for the values of electric field amplitude, gas pressure, and microwave frequency for different gases. He groups these data by defining a quantity $\Lambda^2 = D/\nu_i$ where Λ is an effective

diffusion length and D is the diffusion coefficient. The quantity Λ^2 is given by Brown for several gases, including argon. By computing the value of D we can determine the value of ν_i as follows. We note that the diffusion coefficient is given by:

$$D = \left\{ \frac{v_{av}^2}{3\,\nu_m} \right\}, \qquad (1.2.4)$$

where v_{av} is the average electron velocity in the plasma and ν_m is the electron (momentum transfer) collision frequency. We can compute the average electron velocity by using a distribution function $f = N\, e^{-(H/T)}$ where H is the total energy of the system, T is the thermal energy of the system, and N is the normalization factor such that

$$\int f \; d^3v \; d^3x = 1.$$

The total energy of the system during the transit of the microwave pulse is given by:

$$H = \tfrac{1}{2}\, m\, v^2 + q\, E\, \ell_m \qquad (1.2.5)$$

where m and q are the electron mass and charge respectively, E is the electric field amplitude due to the microwave pulse, and ℓ_m is the mean free path for electron-neutral collisions. Using the fact that $\ell_m = v/\nu_m$ and then completing the square for the total energy. We find:

$$H = \tfrac{1}{2}\, m\, (v + qE/m\nu_m)^2 - \tfrac{1}{2}\, (qE/\nu_m)^2/m \; . \qquad (1.2.6)$$

To find v_{av} we must evaluate:

$$v_{av} = \left[\int v^2 \, f \, d^3v\right]^{\frac{1}{2}}$$

$$= \left[\frac{3\,T}{m} + \left[\frac{q\,E}{m\,\nu_m}\right]^2\right]^{\frac{1}{2}}$$

$$\sim qE/m\nu_m \, , \qquad (1.2.7)$$

the thermal energy T of the electrons in the afterglow is orders of magnitude smaller than the energy of electrons accelerated by the microwave pulse and therefore dropped from the equation. Combining all the factors together we obtain an expression for ν_i in terms of E, f, ν_m, and Λ, given below:

$$\nu_i = \frac{1}{3\,\nu_m^3} \left(\frac{eE}{m\Lambda}\right)^2 . \qquad (1.2.8)$$

We know from classical electrodynamics[23] that

$$\Delta P/_{\Delta a} = \tfrac{1}{2}\,\epsilon_0\,E^2\,v_g . \qquad (1.2.9)$$

Where ΔP is the amplitude of the rf pulse, Δa is the interaction area crossed by the pulse, ϵ_0 is the dielectric constant of free space, E is the magnitude of the the electric field, and v_g is the microwave group velocity. In our experiment $v_g \approx c$, where c is the speed of light. Assuming that Δa is of the order of the cross-section of the vacuum chamber interaction region, we obtain $\Delta a \sim \pi r^2$ where r is the radius of the plasma chamber (7.62 cm). Expressing E in terms of the power of the pulse and the cross-sectional area of the plasma slab we find that the ionization rate is given by:

$$\nu_i = \frac{1}{3}\left(\frac{e}{m\Lambda}\right)^2 \frac{1}{\nu_m^3} \frac{2\,\Delta P}{\Delta a} \frac{1}{\epsilon_0\,c} . \qquad (1.2.10)$$

In our experiment, $\Delta P \sim 270$ kW, $\Delta a \sim .018$ m^2, and $e/m = 1.76 \times 10^{11}$ coul/kg. For argon, $\nu_m \sim 10^{10}$ Hz and $\Lambda = .00103$ m, means that $\nu_i = 1.1 \times 10^8$ Hz. The calculated value of ν_i agrees quite well with the experimentally determined value mentioned earlier.

However it should be noted that several assumptions have been made in the above derivation. They are listed below.

1. Microwave power illuminates the plasma column uniformly.
2. That the value of $\nu_m \sim \nu_{en}$ for argon (see App. 1).
3. Use of the value of Λ given by Brown is valid.

To make the above calculations applicable to different experiments we want to parameterize the time to reionization (t_0) by the fraction of the incident pulse ($\alpha = t_0/\tau$) that traverses the plasma prior to the time when the critical density is reached. Substituting the calculated value for ν_i in Eq. 1.2.2 leaves only one unknown, i.e., the density of the plasma remaining after waiting for a time t into the afterglow. Choosing $\alpha = \frac{1}{2}$ and using representative values for our experiment while using argon we find that $n_0 \sim 10^7$ cm^{-3}. Given that the argon plasma decays by recombination, and that the initial electron density is of the order of 5×10^{13} cm^{-3} (see Section 3.1) requires that the plasma must decay for a time t ~ 10 to 30 milliseconds. This means that if microwave pulses are applied at a rate greater than 100 Hz the plasma would not decay enough between pulses to allow propagation of one-half of the energy contained in a square pulse.

We can also calculate the ionization rate for N_2. To do this, we can use the same values for N_2 as we did earlier for argon with the exception of the electron collision frequency which we take as $\nu_m = 4 \times 10^9$ Hz[22]. We find that $\nu_i \sim 1.7 \times 10^9$ Hz. The accepted value is $\nu_i \sim 1.5 \times 10^9$ Hz [18] which is not significantly different from our calculated value.

2. THE EXPERIMENTAL SYSTEM

The details of the apparatus used to complete this experiment are provided in this section. The various pieces of equipment needed to produce the plasma column and to generate the microwave pulse are described. Also, we discuss the various diagnostic techniques employed, details are provided in the appendices. Since this experiment involves a study of the changes in the pulse shape of the microwave signal passing through a plasma region created by a previous pulse, our discussion begins with the creation and the geometry of the plasma column. We then discuss the diagnostic techniques used for measuring parameters which determine the properties of the plasma column. A discussion of the microwave source and the radiated pulse is presented next. Finally, we discuss how a streak camera is employed to determine the location of the region where reionization of the plasma occurs.

2.1 THE EXPERIMENTAL ARRANGEMENT

The schematics of the experimental set-up is shown in Fig. 1. The vacuum chamber is made of pyrex glass and has a T-shaped configuration. The diameter of the tube of the chamber is 15.2 cm. The vacuum chamber is enclosed in a box made of anechoic sheets, made by Advanced Absorber Products (Type ML-P). The sheets are flat and about 5 cm thick. They have 17 dB of absorption (for normal incidence) relative to a

perfect reflector. The anechoic sheets suppress extraneous microwave signals from entering the plasma column. Thereby we ensure that transmission of microwaves through the plasma column can be treated as a one dimensional problem.

Typically the vacuum chamber is pressurized to about 2 Torr when using argon and about .5 Torr when using nitrogen. The lowest pressure obtained in the chamber using the mechanical pump is about 70 millitorr. So, the impurity level is always less than 14% for nitrogen and less than 3.5% for argon. A Leybold-Hereus mechanical gauge (model Diavac-M) is used for the measurement of pressures. The scale on the gauge is calibrated to read pressures over the range 1 Torr to 1000 Torr. A McLeod gauge is used to check the scale of the Diavac gauge over the range 1 Torr to 150 Torr. Also, the Diavac gauge calibration is extended, by using the McLeod gauge, to read pressures between 0.25 Torr and 1 Torr.

The plasma is created between two high voltage electrodes, about 24 cm apart. We find that the cylindrical plasma column is homogeneous over radial distances greater than 3 cm. This does not strictly meet the requirement for a plasma slab approximation of $\lambda/r \ll 1$, where λ is the free space wavelength and r is a measure of the radius of homogeneity for the plasma column. However, $\lambda/r \lesssim 1$ which crudely satisfies our assumption. Measurements of the plasma parameters are presented in Section 3.1.

The coordinate system used, as shown in Fig. 1, is as follows. The origin (O) lies at the intersection of the

plasma column axis with the center line of the waveguide. The $\hat{x}$ axis points toward the grounded electrode and the $\hat{y}$ axis points out of the figure. Later in our discussion we assume that the plasma forms an infinite slab in the x-y plane, and the direction of propagation ($\vec{k}$) of the microwave pulse is along the $\hat{z}$ axis.

The pulser used to create the plasma column is shown schematically in Fig. 2. The following sequence of steps are involved in its operation.

1) An AC voltage level is selected by using a variac.
2) The AC voltage drives a power supply to give a proportionate DC voltage (~ 50 V_{dc}/V_{ac}).
3) This voltage is applied to a 3 μf capacitor.
4) A trigger pulse of 300 V amplitude and FWHM of 100 ns is used to close the KN-6B switch which shorts the positive side of the capacitor to ground.
5) A large negative pulse then appears at the output for 10 μsec.
6) The switch is typically triggered once per minute, but operation at a frequency of 4 times per minute has also been used.

The reader should note the ammeter circuit on the positive side of the power supply is used as a voltage monitor.

The voltage (V(t)) appearing across the electrodes of the plasma chamber is monitored through a 1/1000 resistive divider, displayed on an oscilloscope, and recorded for later use. The current (I(t)) flowing through the plasma is monitored through two self-integrating current monitors. Typical pulses are shown in Fig. 3. It should be pointed out that the gas does not always ionize immediately after application of the voltage pulse but may hold off the voltage for a finite amount of time and then it suddenly ionizes.

This phenomenon is illustrated in Fig. 3 by three examples encountered in the operation of the apparatus. Each pair of traces begins when the voltage pulse is applied to the chamber. In Fig. 3(a) the discharge occurs about 50 μs after the voltage pulse is applied to the chamber. In Fig. 3(b) the gas breakdown occurs almost immediately, while in Fig. 3(c) the gas breakdown does not occur until after 200 μs. The point is that the time between the application of the voltage pulse and the breakdown of the gas is not reproducible. Therefore the beginning of the current pulse serves as a better reference point from which to measure the afterglow time. The current monitor provides accurate information on the variation of the current flowing through the plasma. This information is used to obtain an estimate of the plasma impedance and thereby provides an estimate of the conductivity of the plasma, as discussed below.

Initially, open-shutter photos are taken of hydrogen, argon, nitrogen, and room-air plasmas. They are displayed in Fig. 4. The hydrogen and argon plasma columns are well formed and by varying the aperture of the lens it is found that the column does fill the chamber. However, for nitrogen and room air, the radius of the column is much smaller. In Fig. 4 a plasma column is shown for air at a pressure of 3 Torr. This is due to the difference in the ionization characteristics of nitrogen and argon. For example, given the voltage pulse available ($\lesssim$ 5 kV) and the electrode spacing in the chamber, the neutral gas pressure must be less

than 50 Torr for Argon and less than 5 Torr for Nitrogen to allow for breakdown[22,24,25].

The open shutter pictures are used to estimate the plasma conductivity (σ), in the following manner. The homogeneous plasma column may be approximated by cylinder of length l, cross-section πr^2 and uniform conductivity (σ). The following formula is used to calculate σ:

$$R = \frac{V}{I} = \frac{l}{\sigma \pi r^2} . \qquad (2.1.1)$$

Where V and I are measured with the voltage and current monitors, and r is measured from the open shutter photo of the plasma column. The value of $\sigma \sim 50$ to 60 mho/m, obtained in this case agrees with the value of the conductivity obtained by other methods (discussed in the next section), within a factor of three.

2.2 PLASMA DIAGNOSTIC TECHNIQUES

The principal diagnostics employed to measure the various properties of the plasma column are a double Langmuir probe[26] and a two-coil rf conductivity probe[27,28]. The Langmuir probe is used to investigate the degree of homogeneity of the plasma column. However, this is not a trivial task because the presence of probes within the plasma column generates a local perturbation, as discussed below. The conductivity probe measures the time variation of the plasma conductivity during the afterglow.

The double probe system is shown schematically in Fig. 5. The probe tips have a DC bias and the current drawn by the probe is measured by a self-integrating current probe[29]. Sample data obtained with the probe are shown in Fig. 6. The large current signal shown at the beginning of the pulse is induced by the pulser and is the same in every photo. This part of the pulse does not provide any useful information and is ignored because the plasma is not yet in a steady state. So the measurements are made at points marked by a circle in Fig. 5, after the spike subsides (~ 10 μsec from the start of the trace). The current is measured for each value of the bias (V) applied to the probe. So we need several traces to determine the probe characteristics. Fortunately, this is possible because the plasma column is highly reproducible.

The data obtained from the double probe are reduced in the following manner; details are given in Appendix 1. The curve shown in Fig. A1.1 is adjusted to fit the data points obtained from the traces, as described above. The parameters determined are the ion saturation current (I^{*}_{pi}) and the plasma electron temperature (T_e). This information is used to compute the plasma electron density (n) at several radial distances to establish the homogeneity of the plasma column. When the probe is on the axis or at radial distances r ≤ 2 cm the shape of the plasma column is not deformed due to the presence of the probe. As the radius is increased (2 cm ≤ r ≤ 6 cm) the column tends to bend to keep the probe inside the

body of the plasma. So reliable measurements of of n could not be made at these larger radial distances. At very large radial distances ($r \geq 6$ cm), the column returns to the straight line path between the electrodes. The data obtained with the probe can be represented analytically as follows:

$$n(r)=n_0*(1 - (r/r_{wall})^4) \qquad (2.2.1)$$

where r_{wall} is the radius of the pyrex chamber and has a value of 7.62 cm. This representation has been found to be valid for a similar setup by Jones and Wooding[4]. Equation 2.2.1 indicates that n is reduced by 10% at a radial distance of about 4.3 cm. One can therefore consider the plasma column to be quite homogeneous for radial distances of less than 3 cm.

Given that one is able to generate a homogeneous plasma column for the microwave pulse to transverse, one wants to be able to monitor the decay of n during the afterglow. In principle the double Langmuir probe is able to monitor the density decay, however the circuit available has limited time to complete the required measurement. The solution to this problem is to rebuild the circuit used to measure the current drawn by the probe, or else one could use a diagnostic technique that does not have the limitations or cause the perturbation of the plasma column as the double Langmuir probe does. A choice was made to use a 2-coil conductivity probe. The response of the probe is based on the conductivity of the medium (which is proportional to n) encircled by the

probe. Moreover, the problems associated with perturbing the plasma column as discussed above for the double Langmuir probe are circumvented. One also overcomes the limitation on how long the probe can be used to monitor the plasma column.

The conductivity probe is shown in Fig. 7. It is composed of three diamagnetic loops. The center loop is driven by a constant current oscillator. The loop generates a magnetic field which threads the outer two loops and induces a voltage in them. The two loops are of opposite helicity, therefore, they have the opposite sign voltage developed across the coaxial cables used to form the loops. These opposite voltages are then subtracted, and the difference voltage is displayed on an oscilloscope. The two signals are subtracted to remove any capacitive coupling between the center loop and either of the outer loops.

The induced voltage is a function of the conductivity, which may vary with time and space, of the medium inserted within the probe assembly, the frequency (f) of the oscillator used to drive the center coil, and the inner radius of the loops. If the conductivity or the density of the medium is homogeneous over the radius of the probe then the calculation is greatly simplified (see discussion in Appendix 2). We find that the induced voltage is a function of the product $f\sigma$. For the present application, σ is only a function of time and all other parameters are constants. This allows one to monitor the decay of the plasma for times approaching a few milliseconds.

The three coils of the probe are built on a dielectric frame of inner radius 2.54 cm. The frame has three grooves cut on the outside to hold the loops, which have radii (b) of 2.61 cm. The above assembly is inserted into an outer sleeve of the same dielectric material that is used to make the inner frame. These dielectric pieces help insulate the loops from the large current pulses that lead to the creation of the plasma column.

The plasma conductivity is determined by measuring the ratio of the voltage (V) induced in the receiver coils with a homogeneous medium present ($\sigma > 0$) of radius less than b and the voltage (V_0) induced in the coils when no medium is present ($\sigma = 0$). Instead of solving Eq. A2.9 for the product $f\sigma$, which involves inversion of various Bessel functions (see Appendix 2), one can simply calculate the values of V/V_0 for a range of values of the products $f\sigma$, and obtain a graph shown in Fig. A2.1. For a measured value of the ratio V/V_0 one determines the value of the product $f\sigma$ from the graph. Knowing the frequency of the driver coil, one then determines σ or vice versa. To obtain reasonable accuracy for the value of V/V_0, the product σf must lie in the range 10^8 Hz-mho/m to 10^{13} Hz-mho/m.

The accuracy of the measurements made by the conductivity probe is verified by inserting cylinders of POCO[30] graphite into the probe assembly. These cylinders have uniform conductivity which may be calculated from total resistance determined with a milli-ohmmeter. The two sets of

measurements are found to agree within a margin of ± 10%.

When the probe is used in the plasma chamber, the voltage output of the oscillator (not shown) and the voltage picked up by the receiver coils are recorded on a dual beam oscilloscope, as shown in Fig. 8. The data is a double exposure overlay of the signal without the plasma column (V_0) and the signal with the plasma column (V). The driver coil signal is monitored to make sure that the plasma does not change the output of the oscillator during the pulse. The receiver signal shows the outer envelope (V_0) and the inner envelope (V) as functions of the plasma afterglow time. Since one can measure the ratio of V/V_0 as a function of the afterglow time we can then determine the conductivity directly. This allows us to know the value of n at which the microwave pulse is transmitted across the plasma column, this value of n is the parameter n_0 used in Eq. 1.2.2.

The digitized image shown in Fig. 8 is representative of the decay of σ for any relaxing plasma. The figure shows the envelopes of the oscillator output which is greatly perturbed during the current pulse which forms the plasma column. After the current pulse subsides, we begin to monitor the afterglow of the plasma column. The relaxation of the inner envelope (V) to the outer envelope (V_0) is indicative of the mechanism by which the plasma column returns to the neutral state. The time required for the relaxation will vary with the neutral pressure of the gas in use. This simply means that as the ratio of plasma electrons to neutral atoms or

molecules decreases the plasma will decay faster.

2.3 A 9.0 GHz MAGNETRON SOURCE

The source used to generate the microwave pulse during the plasma afterglow is described in detail in [31]. The operation, power and frequency variability, reproducibility, and diagnostics are discussed below. The source produces a ¼ MW, 180 ns pulse (45 mJ per pulse). The frequency range is 8.5 GHz to 9.6 GHz. The electric field transmitted across the plasma column is approximately equal to that needed to to ionize the neutral gases used in the experiment ($\lesssim$ 1 kV/cm).

The microwave source is a magnetron tube (Varian Model 5780) that has two DC power supplies. The original supply used with the unit has a 6 kV, 100 mA DC output which charges a resonant LC circuit, the circuit doubles the voltage applied to the magnetron tube for all pulses but the first. The resonant circuit is designed for 1 kHz operation. This supply is useful for characterization of the rf source. However, the first pulse is less than half of the required amplitude and is not adequate for single shot operation during the afterglow.

The solution to the problem of the pulse amplitude is simply to double the DC voltage output applied to the magnetron tube. A new power supply has been built with a maximum 20 kV, 5 mA DC output. The power supply is typically only used up to 12 kV, 5 mA DC output which is equivalent to operation at 6 kV with the 1 kHz supply. As a result full power is directly obtained for each pulse, but at a much

lower repetition rate ($\lesssim$ 2 Hz).

The calibration of the magnetron output power (measured incident power) is shown in Fig. 9. This calibration uses the single pulse power supply. If one wanted the equivalent power with the 1 kHz power supply one would use half the voltage. The graph shows that for a low value of the voltage very little power is generated. As the voltage increases the beam has enough energy to balance the Lorentz force. The beam then begins to circle the cathode and resonates with the slow wave structure. At higher voltages the force due to the electric field exceeds the Lorentz force and the beam begins to go directly to the anode. At these high voltages the beam bunching does not improve and one does not gain much in the radiated microwave power. The reproducibility of the magnetron pulses is quite impressive. This makes the comparison of data in the afterglow much cleaner. Fig. 10 shows an overlay of several pulses.

The tunability of the frequency is shown in Fig. 11. The frequency is continuously varied by tuning vanes in the slow wave structure. The data shown are obtained by two different methods. The first method involved heterodyning, in which one measures the absolute value of the frequency difference from a known oscillator frequency. The second method uses a polar frequency discriminator. The discriminator technique provides two differential signals. One is proportional to the sine and the other is proportional to the cosine of the product $\omega_{rf}\,\Delta t$, where Δt is a time

difference of two cables used on the input of the discriminator. The ratio of the two voltages gives the value of the tangent of $\omega_{rf}\,\Delta t$. This means that the time variation of the ratio will give us the time variation of ω_{rf} when a known Δt is used.

The antenna system used to radiate the microwave pulse has been shown in Fig. 1. The incident power is measured by using a calibrated pickoff from a waveguide narrowwall directional coupler followed by a calibrated attenuator stack and a calibrated crystal diode detector. The reflected power is also measured with a calibrated broadwall directional coupler, calibrated attenuator stack, and calibrated crystal diode detector. The calibration gives the frequency and power response for the components used. The calibration process is discussed in appendix 4 [32,33]. The rf pulse is radiated by a modest gain (17.5 dB) pyramidal horn[34]. The horn provides for good transmission from the waveguide to free space. Sample data are shown for argon in Fig. 12 and for nitrogen in Fig. 13, for the incident and reflected power pulses.

The vacuum window used meets the condition that the reflection is minimum (actually $|R|^2 = 0$). The requirement for the window thickness (d) is given by:

$$k\,d = \pi\,\ell, \qquad (2.3.1)$$

where $k = 2\,\pi\,\tilde{n}/\lambda$, $\tilde{n}$ is the refractive index at the frequency of the magnetron, λ is the free space wavelength, and ℓ is an integer. This equation shows that the plate must

have a thickness equal to an integral number of half-wavelengths in the dielectric for good transmission (see Appendix 3)[35]. The condition on $|R|^2$ is well met because measured numbers on the incident and reflected power, in the absence of plasma, are typically $\geq$ 200 kW and $\leq$ 3 kW respectively ($\leq$ 2% reflection).

Changes in the afterglow plasma due to the microwave pulse are observed by monitoring the transmitted pulse measured on the far side of the plasma column. The transmitted pulse is measured by using a standard gain horn (to improve the directivity) which is followed by a calibrated broadwall directional coupler, calibrated attenuator stack, and a calibrated crystal diode detector. In typical use, the transmitted signal is about 10 dB down in amplitude from the incident signal when propagated in neutral gas. Sample data are also shown in Fig. 12 for argon and Fig. 13 for nitrogen. The reader should note that the transmitted pulses track the incident pulses very well for both gases, in the absence of a plasma column.

A new diagnostic tool was added after discussions with colleagues[21] at LANL. A microwave Mach - Zehnder interferometer is created by taking parts of the incident and transmitted pulses. The reference signal comes from the incident pulse, as shown in Fig. 14. The signal is fed into the local oscillator (LO) port of a double balanced mixer[36]. The sample signal is taken from the transmitted pulse. This signal is fed into the RF port of the double

balanced mixer. The intermediate frequency (IF) port of the double balanced mixer is then recorded on an oscilloscope. The IF port shows the difference in the phases of the LO and RF signals. The phase difference in the absence of the plasma column is given by:

$$\begin{aligned} \Delta\phi &= \phi_{rf} - \phi_{LO} \\ &= \{(2\pi/\lambda)\ \tilde{n}x_{rf} + \phi_0\} - \{(2\pi/\lambda)\ x_{lo} + \phi_0\} \\ &= (2\pi/\lambda)\ \ (\tilde{n}x_{rf} - x_{lo}) \end{aligned} \qquad (2.3.2)$$

where λ is the magnetron wavelength, x_{rf} and x_{lo} are the one-way path lengths for the respective section of the interferometer, $\tilde{n}$ the index of refraction of the medium in which the microwave signal propagates ($\tilde{n}$ = 1 without a plasma), and ϕ_0 is the initial phase of the wave from the magnetron. To simplify the reduction of the data to be acquired with this technique, a coaxial phase shifter[37] is added to the reference arm of the interferometer to obtain a null result when the plasma column is absent. Using this phase shifter to offset any physical path difference (x_{rf} - x_{lo}) without the plasma column, insures that any change in the measurement is due only to the presence of the plasma column.

The interferometer is considered to be balanced when the phase difference is equal to an integral number of wavelengths. A sample of a balanced interferometer signal is shown in Fig. 15. The initial and trailing spikes are due to variation in f (or λ) from the magnetron during the pulse turn on and turn off. The central part of the pulse, when the

frequency is stable, represents the portion that is balanced. The measured phase shift is also compared with a calibration curve. The curve is generated by transmitting the magnetron pulse across the vacuum chamber without plasma being present and using the phase shifter to vary the indicated phase change. The phase shifter adjustment is in deg/GHz. The x-axis gives the setting in deg/GHz multiplied by 9 GHz, the frequency of the magnetron. The voltage output by the double balanced mixer is plotted along the y-axis, and is measured during the middle part of the magnetron pulse.

The change in $\tilde{n}$ of the medium (i.e. the plasma column) may be determined in two ways by using the interferometer. One may measure the voltage output by the IF port of the double balanced mixer, and then using the calibration curve of Fig. 16 determine the phase shift from the balanced condition. One may also balance the interferometer output in the presence of the afterglow plasma, then the difference in settings of the phase shifter for balance with and without the plasma column gives the phase shift directly. Once the change in $\tilde{n}$ is found it is possible to obtain information on the average density across the diameter (L) of the plasma column[1,2]. The calculation is carried out as follows:

$$\Delta\phi = \int_0^L dz \, (k_0 - k), \qquad (2.3.3)$$

where $k_0 = 2\pi/\lambda$, $k = k_0 \tilde{n}$, and $\tilde{n} = (1 - n(z)/n_c)^{\frac{1}{2}}$, $n(z)$ is the density variation along the diameter of the plasma column, and n_c is the cutoff density for microwave radiation of frequency f. The interferometer is used to determine the

time variation of the averaged plasma density. The data from the interferometer is later compared with that obtained from the conductivity coils.

The power measurements and the interferometer measurements are all carried out during the plasma afterglow. In order to obtain the data at any point in the afterglow, a stable reference time (t_0) is needed. This is taken to be the time when one observes the onset of the current across the electrodes, indicating that a steady plasma column has formed. This is indicated by a voltage signal from a current monitor on the negative high voltage electrode, see discussion in Section 2.1. The timing circuit is shown in Fig. 17. The amplifier used for the current monitor has a high impedance (1 MΩ) and does not load down the signal. The voltage signal in addition triggers a Lecroy digital delay generator with a specified time delay, ranging from 100 ns to 1.5 sec. The delayed pulse has an amplitude of 5 volts and is used to to trigger an HP 214A pulse generator. There are two distinct pulses available; as shown in Fig. 17. One is used to trigger the magnetron, and the other is fed to a 4-way splitter that provides pulses for diagnostic purposes, and shown in Fig. 17. The time sequence of operations carried out during each measurement is shown schematically in Fig. 18. The time gap between application of the high voltage to the electrodes and t_0 represents the uncertainty in the breakdown of the neutral gas, discussed in Section 2.1.

2.4 THE STREAK CAMERA

The Streak Camera[38] is used to obtain spatial information of a qualitative nature on the location of the plasma reionization region during the transmission of the microwave pulse. It is composed of a Hamamatsu Temporal Disperser (model C1330), Hamamatsu Temporal Analyzer (model C1440-03) with a Hamamatsu SIT camera (model C1000-18). The camera is timed to image a section of a line between the lucite window and the plasma column during transmission of the microwave pulse. The camera setup and 'periscope' apparatus are shown in Fig. 19. The latter consists of several mirrors shown in the diagram connected by dashed lines, which also indicate the light path.

The periscope system is aligned by splitting a 1 mW, He-Ne laser beam as in a Michelson interferometer. One path is aligned with the center of the camera input slit, and the other is directed by a six element periscope of mirrors to the vacuum chamber. The image of the laser can be moved along the $\hat{z}$-axis (Fig. 1) from the lucite window to the plasma column. In fact this adjustment is needed because the image recorded by the entrance slit to the camera allows only about 10 cm along the $\hat{z}$-axis to be imaged at a time. The streak camera (Temporal Analyzer) is used in the 'Gate B' mode. This mode is used whenever the user needs complete control of all the camera functions. The user achieves this control of the camera by making the proper selections on the control panel, and by providing timing and control pulses

from a pulse generator that open and then hold the gate on for the necessary time interval. The gate determines when the camera is ready to record an image. The user also specifies when the camera is to be triggered during the gate, to acquire the streak image.

For our experiments the duration of the streak image must be longer than the microwave pulse. The reason for the requirement on the time duration is to allow observation of the decaying plasma before, during, and after the transmission of the microwave pulse. The available streak time which satisfies this criteria is 500 ns. The timing sequence for Gate B triggering requires that one open the gate at least 200 ns before the streak camera trigger and that one hold the gate open for the selected time interval for the streak image to be acquired. For our use a gate pulse of 730 ns is used, and the streak trigger is applied 230 ns into the gate pulse. The reader should recall the timing sequence of Fig. 18. The streak image adds another event window, about three times as wide as the microwave pulse, to the sequence. This window begins about 50 to 100 ns before the microwave pulse and lasts for 220 to 270 ns after the end of the microwave pulse. The proper timing is obtained by using three of the Lecroy digital delay generators. The first generator provides the selected afterglow time τ_D. The second and third are triggered simultaneously by the first delay generator, and both have the necessary small time delays such that the streak image

is begun immediately before the generation of the microwave pulse (~ 50 to 100 ns), and continues after the microwave pulse (~ 220 to 270 ns).

The region imaged by the last mirror of the periscope is shown in the top half of Fig. 20(a). A piece of paper with a convenient pattern is placed on top of the vacuum vessel parallel to the z-axis to provide an image plane for the alignment laser. The 'x' on the left side of the pattern indicates the position of the image of the alignment laser spot, which also provides a convenient reference for the steak image data photos. The center of the entrance slit of the streak camera is always aligned with the other half of the laser beam from the splitting prism (Fig. 19). Since the region to be viewed by the streak camera, parallel to the long line of the pattern, is about 20 cm in extent we must break the region into two parts of 10 cm each (the maximum viewing range of the entrance slit). This is achieved by adjusting the final two mirrors of the periscope to move the laser beam image along the line of the streak image of Fig. 19. The piece of paper, on which the pattern is drawn is removed prior to recording the streak image of the reionization region. The recorded data (Fig. 20(b)) are always presented in an orientation consistent with the image shown in the mirror of Fig. 20(a). That is the vertical dimension of the streak image photo is always aligned such that the plasma column is toward the lower edge of the photo, and the lucite window is toward the upper edge of the photo.

One may expect that the light intensity of a streak image should be brightest toward the plasma column axis. However, Fig. 20(a) shows a piece of wood that is used to hold the anechoic chamber together which crosses the final mirror of the periscope. This piece of the anechoic chamber shadows the lower edge of the data photos, and the shadowing or lack of light intensity is evident in all the data discussed later in Section 3.4. The streak image is made of tiny dots of light that begin at the right edge and continue to the left of the photo, i.e. the horizontal axis (time) of the streak image begins at the right and runs to the left of the photo. The reader should note that some of the dots are brighter than others. Each dot in the photo represents an aggregate of atoms or molecules which emit light as a result of being excited by the capture of accelerated free electrons.

The image processor of the streak camera system is used to enhance the contrast between the light dots and the dark background of the displayed data. The data of six shots are superimposed to improve the resolution of the low intensity light. Recording the data in this way adds a large background signal which must be subtracted from the data, so that the available information on the reionization region may be retrieved. The background is removed such that the amplitude indicator, the line located at the top of the streak image, has a constant intensity at the beginning of each streak image photo. The amplitude is set to a constant because the light emitted by the plasma column at the

beginning of the streak image is from the decaying plasma which provides a constant background on these relatively short time scales. Another artifact of the 6 shot overlay is that the gain (contrast) changes dynamically. After setting the offset one adjusts the gain to enhance the details of the image. The details to be seen are the vertical array of dots which indicate light being emitted at points along the line of the streak image (Fig. 19). It must be emphasized that we are looking for relative changes in the light intensity between images of the reionization region that are recorded at various times in the plasma column afterglow. Since we are looking for relative changes in the light intensity the offset and gain adjustments discussed above are always identical for data recorded both with and without the microwave pulse traversing the afterglow region. It may be possible to obtain quantitative information from the intensity amplitude indicator, however the indicator was not calibrated. It only serves a very limited purpose of indicating the time variation of the spatially integrated light intensity.

3. EXPERIMENTAL MEASUREMENTS

This section discusses the results of the measurements made on the plasma column and the interaction between the afterglow plasma and the microwave pulse. The measurements of the radial variation of the plasma density in the column carried out with a double Langmuir probe are presented. The plasma decay is monitored by the conductivity coil probe. There seems to be agreement between the conductivity probe (at t=0) and the double Langmuir probe results.

Measurements carried out to understand several aspects of the microwave-plasma interaction are discussed. First we present and discuss the data on the energy contained in the incident, reflected, and transmitted pulses (for both argon and nitrogen) and their variation with afterglow time. The phase measurements carried out with the Mach-Zehnder interferometer, as a function of the afterglow time are also discussed. The measured phase-shifts derived from the interferometer measurements are compared with the phase-shifts computed using Eq. 2.3.3 which uses measurements of the electron density (n) made with the conductivity coil probe. We explore the relationship between the reionization time, the time for the density to reach the critical density (n_c), of the plasma column by the microwave pulse and the afterglow time. This is determined by the pulse width (FWHM) of the transmitted signal, for both gases. Finally the data obtained with the streak camera are presented. The streak images respond to the light emitted, during the transmission

of the microwave pulse.

3.1 PLASMA COLUMN

It is of interest to know whether the plasma column is homogeneous or has an annular structure. We carried out this investigation for argon gas at 2 Torr neutral pressure. The gas is ionized by applying a pulse V ~ 3800 volts (measured current I ~ 1.13 kA). The typical parameters, on the plasma column axis are found to be n ~ 1.6 to 2.5 $\times 10^{13}$ cm^{-3}, T_e ~ 3 to 10 eV, σ ~ 35 to 45 mho/m. The relation between σ (mho/m) and n (cm^{-3}), for argon, is found to be $n(cm^{-3}) = 4.4 \times 10^{11}$ σ(mho/m) (App. 1). The radial variation of the density and conductivity are shown in Figures 21 and 22, respectively. The open circles in both figures represent data obtained with the double Langmuir probe. The data in both cases seem to fit an analytical function of the form: $\delta [1 - (r/r_{wall})^4]$. The value of δ is adjusted until a good fit of the data is obtained. The coefficients are found to be $n(r=0) = 1.8 \times 10^{13}$ cm^{-3} and $\sigma(r=0) = 37$ mho/m. The data indicate that the plasma column is homogeneous up to radial distances of 3 to 4 cm.

The data on the variation of the argon plasma conductivity with afterglow time for several different neutral gas pressures are depicted in Fig. 23. Early in the afterglow ($\lesssim$ 10 μsec), the value of the conductivity appears to be independent of time and pressure. This may not be physically significant since sufficient time has not yet elapsed for the plasma to be in equilibrium. The data

(indicated by the different symbols) show that the plasma column decays with time as $(1 + \beta t)^{-1}$ (the solid line), which is indicative of argon decaying by recombination[22,39]. One should also note that the conductivity measured early in the afterglow (20 to 100 μsec) is between 100 and 150 mho/m. This is about a factor of 3 to 4 larger than the value of 37 mho/m, found using the double Langmuir probe. Considering that the plasma is perturbed by the presence of the double probe, and that the plasma column is constrained to a smaller diameter by the conductivity probe than when the double Langmuir probe is used, the disparity between the two sets of estimates is not unexpected.

Figure 24 shows the variation of the argon plasma conductivity with neutral pressure, which is measured early in the afterglow (~ 20 μsec). The data (indicated by the symbols) seem to indicate that σ decreases linearly (on the log-log plot) with pressure (shown by the two solid curves). The observed power-law dependence of σ on p_0 supports the assumption that the electron-neutral collision frequency is dominant in the momentum transfer process; see the discussion in App. 1. Since the typical operating voltage used to create the plasma column lies between 3500 and 3800 V, the above inference is valid for all the argon data.

The conductivity probe is also used to monitor the decay process in nitrogen (N_2). The data are shown in Fig. 25. The data seem to fit an exponential decay which is typical of decay by electron attachment[22]. The observed e-folding

time is 61 μsec. There is some ambiguity in the early time and late time characteristics of the data. Early in the afterglow there is difficulty in aligning the t=0 point. Later, the conductivity probe has difficulty in resolving changes in the density because the value of V/V_0 tends to unity, as discussed in Section 2.2. One may compute n for each value of σ given in Fig. 25 by using Eq. A1.7. The data indicate that the initial density due to the pulser discharge is 4.3×10^{12} cm^{-3}. The value of n may be compared with the value 5×10^{13} cm^{-3} obtained for the case of argon. We note that the density for N_2 has a lower value, but it is still greater than the cutoff value n_c corresponding to 9 Ghz microwaves.

3.2 MICROWAVE PULSE AFTERGLOW MEASUREMENTS

The results presented in this section are representative of the changes in the transmission of microwave energy during the plasma afterglow. These measurements are carried out in both argon ($p_0 \sim 2$ Torr) and nitrogen ($p_0 \sim .5$ to .6 Torr) neutral gases. The pressures for each gas are chosen to setup a plasma column that fills the vacuum chamber completely, but the reader is reminded that the plasma column is homogeneous for up to a radial distance $r \lesssim \frac{1}{2} r_{wall}$. The experimental measurements for each gas are discussed separately. The microwave power amplitudes and pulse widths (FWHM) for the incident, the reflected, and the transmitted signals are displayed on the oscilloscope screen and

photographed. We take the product of the amplitude and pulse width (FWHM) to represent the total energy contained in each of the pulses. In our opinion, this product provides a better measure of the changes occurring in each of the pulses than indicated by the microwave power amplitudes alone. The phase change of the microwave pulse due to travel across the plasma column is monitored to obtain data on the plasma column decay. These data channels are recorded for various afterglow times.

The results obtained with argon are considered first. The variation of the energy measured for the incident, the reflected, and the transmitted signals are shown in Fig. 26. The data for the incident signal can be used to provide an estimate of the amplitude of the electric field traversing the plasma region. The incident power (~ 250 kW) indicates that the electric field is of order 1 kV/cm. This electric field is almost capable of directly ionizing argon and N_2[13,22]. The transmitted pulse energy is seen to reach a value equal to half the maximum value transmitted across the plasma column in 50 milliseconds. The implication is that if one tries to transmit large amplitude microwave pulses across a decaying argon plasma region, less than half of the maximum energy would be transmitted if the time between successive microwave pulses is less than 50 milliseconds.

The reader is reminded that the transmitted signal does track the incident pulse in the absence of a plasma. Late in the afterglow (> 1 msec) the transmitted pulse still tracks

the incident pulse until some free electrons are accelerated and the reionization process begins. In the case of argon the reduction of the transmitted signal is observed to be coincident with the rise of the reflected signal. The pulse width (FWHM) for all three signals show that the pulse width of the transmitted plus the reflected signals equals the pulse width of the incident signal. This indicates that very little, if any, absorption of microwave energy occurs in argon.

The phase change for argon, measured by the interferometer seems to match the type of time-variation of the electron density measured by the conductivity coils as seen in Fig. 27. The calculated time variation of the phase change has been compared to the decay of the density. The calculation used the time variation and radial profile discussed earlier for argon. The initial axial plasma electron density used is 5×10^{13} cm^{-3}, as measured by the conductivity coil. The observed decay of the density as measured by the conductivity coils for two different shots indicated by the symbols: □ and △ are shown in Fig. 28. The plotted data provide an estimate of the reproducibility of the decay of the plasma density. The time profile of the observed argon decay is typical of decay by recombination. The solid line indicates the expected time variation in the electron density if the decay is by recombination. The expected time variation is given by[25]:

$$n(t) = \frac{n_0}{1 + \beta t} \qquad (3.2.1)$$

where n_0 is the initial plasma density and β is the decay rate. The values for n_0 and β are determined by measuring the values of the plasma electron density at two times t_1 and t_2 ($t_1 < t_2$), one then solves for β by noting that,

$$\frac{n(t_1)}{n(t_2)} = \frac{1 + \beta\ t_2}{1 + \beta\ t_1}. \qquad (3.2.2)$$

Having found β one then finds $n_0 = n(t_1)\ (1+\beta t_1)$. One can now use Eq. 3.2.1 in Eq. A5.2 to compute a phase shift in a microwave pulse due to traveling across the plasma column. The calculated phase is compared with measured data in Fig. 29. The data are only obtained after two milliseconds into the afterglow. Earlier in the afterglow the plasma density exceeds the critical density (n_c) over most of the plasma volume. Since no pulse is transmitted to the sample arm of the interferometer, no output is produced. Also when $\Delta\phi$ is under 0.01 radians (= .57°) the phase change is effectively zero.

The results of the energy transmitted through N_2 are not qualitatively different from the data for argon. Sample data and reduced data are shown in Fig. 13 and 30, respectively. The incident signal is identical to the incident energy levels used for argon. The reader should note that the reflected energy is not as high as for argon. The transmitted signal again shows that to transmit half of the maximum transmitted pulse energy one must allow for the

plasma to decay for an afterglow time of ~ 500 μsec to 1 msec. Also the observation for the incident, the reflected, and the transmitted pulse widths made for the case of argon does not hold for N_2. We have observed that the incident pulse width (FWHM) is greater than the sum of the reflected pulse width (FWHM) and the transmitted pulse width (FWHM). This was illustrated by the data recorded at 100 μsec into the N_2 afterglow which are shown in Fig. 13. This data shows that initially the reflected pulse and the transmitted pulse amplitudes are very small. Later in the microwave pulse the reflected pulse amplitude then increases, even though the transmitted pulse amplitude remains small. This data clearly illustrates that the incident microwave pulse energy is lost from the problem by some mechanism other than reflection from the plasma column or transmission through the plasma column. Possible mechanisms that are candidates for this additional loss of microwave energy are molecular absorption by N_2, electron runaway of accelerated electrons out of the plasma column region, or scattering of the microwave pulse in a direction orthogonal to the line between the two waveguide horns.

The interferometer data are also considerably different for N_2 than for argon. The plotted data, the circles, of Fig. 31 show the density decay measured by the conductivity coils. The solid line indicates the expected time variation in the electron density if the decay is by attachment. The expected time variation is given by[25]:

$$n(t) = n_0 e^{-\gamma t} \tag{3.2.3}$$

where n_0 is the initial plasma density and γ is the decay rate. The values for n_0 and γ are determined by measuring the values of the plasma electron density at two times t_1 and t_2 ($t_1 < t_2$), one then solves for γ by noting that,

$$\frac{n(t_1)}{n(t_2)} = e^{-\gamma(t_1 - t_2)} \tag{3.2.4}$$

Once γ is determined then $n_0 = n(t_1)\, e^{\gamma t_1}$. Again, one can use Eq. 3.2.3 in Eq. A5.2 to compute a phase shift in a microwave pulse due to travel across the plasma column. The phase shift computed as described above is compared in Fig. 32 with the measured phase shift data. One can see that the experimental data (indicated by the symbols) deviate considerably from what one would expect from the computed phase shift (indicated by the solid line). This discrepancy between data and theory is not understood. The same mechanism that may account for energy loss may also account for the observed differences between the computed and measured phase shifts.

3.3 TAIL EROSION

Tail erosion of the microwave pulse[19,20] is observed when the leading part of the microwave pulse accelerates free electrons which ionize the neutral gas creating a plasma. This causes the index of refraction to change sufficiently to reflect or attenuate the trailing part of the pulse. This phenomenon is seen at work in our data. In Section 3.2 we referred to the decay of the transmitted pulse amplitude as

the reflected pulse amplitude increased. This late time attenuation of the pulse is indicative of the plasma being reionized to the critical density, which will then reflect the remainder of the pulse. Tail erosion is discussed separately for both argon and nitrogen.

As pointed out earlier, the conductivity coil data indicate that the argon plasma decays by recombination. The ionization by microwaves however causes an exponential increase in the density. When this information is used the continuity equation (Eq. 1.2.1) becomes:

$$\frac{\partial n}{\partial t} = \nu_i \, n - \alpha \, n^2, \qquad (3.3.1)$$

where n is the plasma density, ν_i is the ionization rate due to the incident microwave signal, and α is the coefficient for recombination. After the point where $\partial n/\partial t = 0$ the growth overwhelms the decay, and we find that $n(t) = n_0 \, e^{\nu_i t}$. From the transmitted signal pulse width we obtain a measure of how much of a square pulse is transmitted through the afterglow plasma. If we plot the data for the transmitted pulse width (FWHM) as a function of afterglow time, and then compare that data with a curve for t_0 (see Eq. 1.2.3) we can determine ν_i by fitting the curve for t_0 to the data. This has been done in Fig. 33 for the case of argon. We obtain $\nu_i = 1.4 \times 10^8$ Hz. From theoretical arguments given in Section 1.2 we computed $\nu_i = 1.1 \times 10^8$ Hz. At a time early in the afterglow ($\tau_D \sim 1$ msec) the curve in Fig. 33 does not pass through the data point. This may be due to the fact that the

given curve represents a solution to Eq. 3.3.1 after neglecting the recombination term.

Nitrogen seems to behave quite differently. The data for N_2 that are depicted in Fig. 34 indicate that the transmitted pulse width is independent of afterglow time. The solid line in Fig. 34 is the calculated pulse width as a function of the afterglow time. The reader should note that the change in the pulse width is very slight, but that the predicted pulse width is about 2 orders of magnitude smaller than the measured values. We are unable to explain how this discrepancy comes about.

3.4 DATA OBTAINED WITH A STREAK CAMERA

As stated in Section 2.4 the streak camera is used to determine if the breakdown region occurs near the plasma column or the lucite window used to introduce the microwave pulse into the vacuum chamber. We will show that the reionization occurs near to the plasma column axis for both gases. The data for the two gases are considered separately.

Data obtained near the argon plasma axis are shown in Figures 35 and 36, the photos are oriented in the same way as the photo of Fig. 20(b). The orientation is such that the plasma column axis is toward the bottom of each photo. The reader should ignore the dark vertical band which appears in all the streak photos. This is an artifact of the recording of the video display and is not physically meaningful. Note that early in the afterglow (Fig. 35) there is approximately

uniform light over the region of view with or without the magnetron being pulsed, except that the intensity is brighter with the microwaves present. At a later time ($\geq$ 1 msec) no light is emitted from the observed area without the microwave pulse to reionize the plasma. Also note that in the data for 1 msec into the afterglow that the intensity across the photo is initially constant and then decreases as the streak goes from right to left. This is consistent with the streak time beginning immediately after the turn on of the magnetron pulse and lasting longer than the magnetron pulse. A final point for the photo taken during the microwave pulse at 1 sec into the afterglow. The light intensity has decreased considerably relative to the intensity earlier in the afterglow. This is indicative of a small concentration of free electrons, as one would expect for plasmas that are many decay times into their afterglow.

The data recorded near the lucite vacuum window (Figures 37 and 38) have many similar characteristics to the data taken near the plasma column axis. The main distinction is that the emitted light is more intense for the on axis view (Fig. 35) than the emitted light for the window view (Fig. 37). This indicates that the plasma reionization is occurring near the plasma column axis and not on the vacuum side of the dielectric window. The data in Fig. 38 are taken later in the plasma afterglow. Again light is not observed if the microwave pulse is not transmitted. The fact that light is seen during the rf pulse indicates that there are

some free electrons that diffuse through the region and then recombine with ions to form excited neutrals.

The N_2 streak data are shown in Figures 39 through 43. Figures 39, 40, and 41 show on axis views for different afterglow times. The N_2 data are similar in many ways to the data for argon. One example is that more light is emitted during the rf pulse. One should also note the difference between Fig. 35 and Fig. 39. The photographs are identical in all but two aspects. One difference is the neutral gas used, and the other is the relative intensity. More light is emitted from near the plasma column axis for N_2 than for argon. The reader's attention is drawn to the bright band that appears in many of the late afterglow time photos for N_2. This bright band occurs near the end of the microwave pulse, which seems to occur at the same time in the microwave pulse as the growth of the reflected microwave signal shown in Fig. 13. These data seem to further support the observation on the microwave pulse energy being lost from the plasma column region by some mechanism other than transmission or reflection.

Figures 42 and 43 show the window view at different afterglow times. Note that in this case also the brighter light occurs for the later afterglow time. However the data, during transmission of the microwave pulse, show the light emitted near the plasma column axis are still more intense than the light emitted near the lucite window, for all afterglow times.

CONCLUSIONS

We have investigated the transmission of a microwave pulse through a decaying plasma column. A plasma column has been created using argon and nitrogen as neutral gases. A microwave pulse, with the electric field ($\vec{E}$) polarized perpendicular to the plasma axis, has been transmitted across the plasma region at various times during the plasma decay. The microwave pulse has sufficient intensity to cause the plasma to reionize the neutral gas, to a density exceeding the critical density for the microwave frequency in use.

The transmission characteristics of the two gases used are found to be very different. With argon as the neutral gas we find the following. The initial axial electron density is typically 5×10^{13} cm^{-3}, and the plasma decays by recombination of electrons and ions. The transmitted pulse energy reaches one-half of the maximum measured value for afterglow times of the order of 10 milliseconds. This number is in agreement with the prediction of the continuity equation in Section 1.2. The microwave ionization frequency indicated by the variation of the transmitted pulse width with the afterglow time agrees with the calculated value.

When nitrogen gas is used, some of the results are quite different. The data from the conductivity probe indicates a lower initial axial density of 4.3×10^{12} cm^{-3}. This is not surprising, because we know from the DC breakdown properties that N_2 needs a lower pressure than argon does to create a plasma column that fills the plasma chamber for a voltage

pulse of a given amplitude. The N_2 plasma is found to decay by attachment of electrons to neutrals. The data also indicate that there is a large difference between the measured and the calculated values of the ionization frequency. The transmitted pulse width is also found to be insensitive to variation of the afterglow time. The only similarity between argon and N_2 is the agreement between the predicted and measured afterglow time for the transmitted pulse energy to reach one half of the maximum transmitted value. The predicted value and the measured value for the afterglow time for N_2 are 1 millisecond.

The calculations mentioned above also help establish the confidence in the use of the coefficients measured in microwave cavity experiments, for use in open geometry experiments. The question has always been whether one can take measurements from closed systems which have conducting walls to systems which are open. The assumed answer has always been in the affirmative. This experiment supports that assumption.

The breakdown of the calculations in the case of nitrogen raises many questions about the models currently used. An obvious first attempt to understand the difference in their responses to microwave pulses would be to see whether the observed differences can be explained in terms of distinct physical properties of the two gases used. One notes that argon is a monatomic gas and nitrogen is a diatomic gas. This difference allows nitrogen to have

additional molecular energy levels due to rotational and vibrational excitation of the outer molecular electrons.

Absorption of microwaves by diatomic and even polyatomic gases has been been reported in the literature[40]. The energy is typically coupled in through the electric or magnetic multipole moments. These types of excitations are typically unavailable to homopolar molecules such as nitrogen and oxygen. However, for strong amplitude pulses multipole moments can be induced by polarizing the electron cloud of the molecule. An example is the absorption of 64 GHz microwaves[41] by the induced magnetic dipole moment in molecular oxygen.

Another explanation of the different response of N_2 may lie in the relatively large electron mean free path due to the low background neutral pressure used for N_2 (.5 Torr). Pitchford, et al[15] discuss the process of electron runaway. Electron runaway occurs when the electrons accelerated by the microwave pulse cannot lose energy by reionizing the plasma. According to calculations by Pitchford, runaway becomes a problem if $E/n_0 \gtrsim 1500$ Td $= 1.5 \times 10^{-14}$ V-cm^2, where E is the electric field amplitude from the microwave pulse and n_0 is the neutral gas density. For N_2 the value of $E/n_0 \sim 7000$ Td, while for argon $E/n_0 \lesssim 1500$ Td. However, we are not sure whether the observed differences can be explained by this hypothesis. Although we have suggested some plausible mechanisms, the list of possibilities is by no means exhaustive. We must emphasize that we are not able to

provide an acceptable model for understanding the observed differences. Further work is necessary to develop a more comprehensive understanding.

So far as we know, high powered microwave interferometry has been used as a diagnostic technique, for the first time, for the measurement of the plasma column parameters. Agreement between the interferometer and the two coil conductivity probe is found in the case of argon. The time dependence of the plasma column decay is the same for both diagnostic techniques. Both techniques have problems when making the measurement early and late in the afterglow. Early in the afterglow the assumption about the homogeneity of the plasma column made in the calculations for the conductivity coils may be invalid. As mentioned in Section 3.2, early in the plasma afterglow the interferometer does not have the microwave signal from the sample arm because the plasma is beyond the critical density which causes the technique to be unavailable. Late in the afterglow, both techniques suffer from a lack of sensitivity due to the low plasma density. Even with these limitations, the use of the technique remains an excellent alternative for diagnostic purposes in a high powered microwave experiment. The necessary apparatus is already in use for the transmitting and receiving antennas. One only needs to split the two signals to obtain the necessary data. This is much simpler than adding *in situ* diagnostics that perturb the system under study.

We have shown that the propagation of repetitively pulsed microwaves of large enough amplitude to ionize the neutral gas is possible. However, the interpulse separation is several lifetimes into the plasma afterglow ($\lesssim$ 50 msec). This insight may be helpful in easing the design requirements for future high powered microwave sources.

This project has raised many questions for further research to improve the applicability of the currently accepted models. These models explain the interaction between microwave pulses and atmospheric plasmas. The questions to be addressed include:

1) Why does nitrogen respond differently to 9 GHz microwave pulses than argon?

2) How does the absorption of microwave pulses, by neutral and weakly ionized atmospheric gases, vary as a function of the pulse amplitude and frequency?

3) What is the dependence of the pulse width on the afterglow time required (the duty cycle of the microwave source) for transmission of a large fraction of the microwave energy contained in a pulse?

4) What are the two and three dimensional scattering effects of high powered microwave pulses from finite plasma regions?

To answer these questions major advances are required in the electrical pulsed power and the microwave sources. However, analytical study will continue until new experiments can be performed.

From our perspective the following are areas where improvements must occur in high power microwave sources. The changes that are discussed are those that must happen to microwave sources to enable experimentalists to answer the above questions, using a single source. This requires a

major advance in the technology of electrical pulse compression devices (called prime power pulsers). It is also desirable that the efficiency of high power microwave sources be increased. Below we discuss the limitations of presently available microwave sources.

The electrical pulse power puts a primary constraint on the ability to do repetitively pulsed experiments. For example, consider an energy storage system which holds 10 kilojoules and is to be cycled at 100 Hz with a 100 ns pulse width. If one ignores, for the moment, the efficiency of the microwave source in using electrical power, one needs to have about 1 MW average AC power to operate the power supply for this experiment. For a typical efficiency of a few percent, one needs about 100 to 200 MW average power for a single experiment. It is clear that we are beginning to require a large fraction of the power generated by a small substation. A second limitation is that pulse power technology available at present can deal with the single pulse parameters described above at perhaps a 1 Hz rate. Since the pulse repetition rate for the experiment described in this dissertation is less than a few hundred kilohertz, it is clear that considerable development work is needed to meet this requirement. However, one may need only a finite number of pulses in succession. One can achieve this by developing the ability to store the total energy needed prior to beginning the sequence of pulses. One can then draw on this stored energy during a burst of a few pulses.

The microwave source should also be redesigned. Most high power microwave devices have a plasma (cold) cathode that generates an electron beam. These plasma cathodes emit electrons by having large electric fields applied between the cathode and the anode. The process of electron emission rapidly degrades the cathode material. The degradation of the two primary cathode materials, velvet[42] and graphite, is by a catastrophic process. The velvet will continue to emit until the material is used up, i.e. until the nap of the velvet is gone. The graphite fails due to its being a fragile material. This leads one to look at other methods for emitting the electron beam, none of which are suitable for bursts of several pulses.

One has also to worry about the ionizing radiation caused by the 'left over' electron beam. High power microwave sources are inherently inefficient (~ 2%) so a large part of the electron beam is left over to generate ionizing radiation. The unused part of the beam leads to a requirement for an ionizing radiation shield. In practice, a system involving about 7 kJ per pulse and 5 pulses per hour requires a wall of high density concrete about 1 m thick or an exclusion zone of about 7 m radius around the electron beam diode. The point is that a more efficient high power microwave (HPM) source is required.

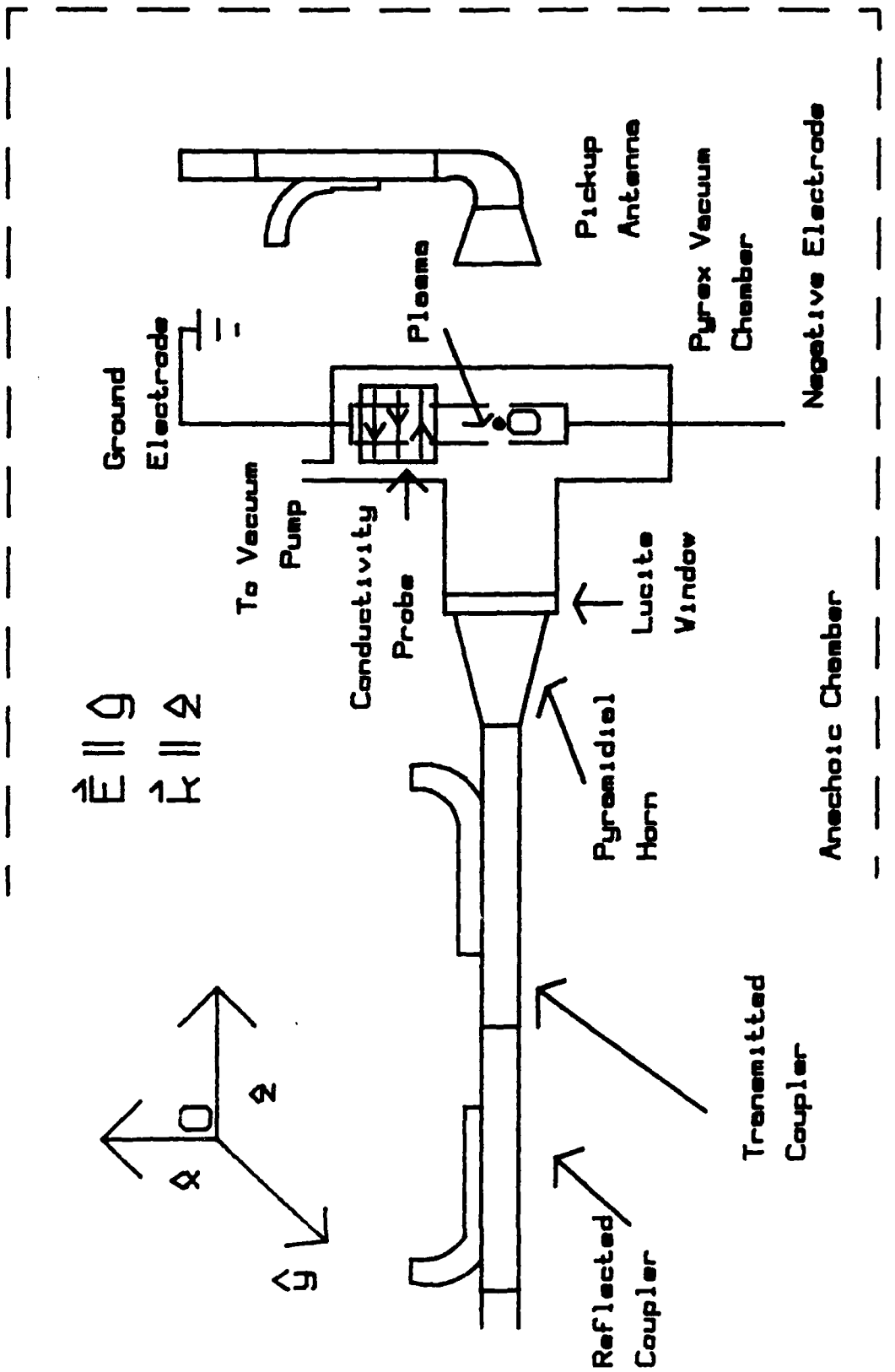

Figure 1. Schematic of the experimental set-up

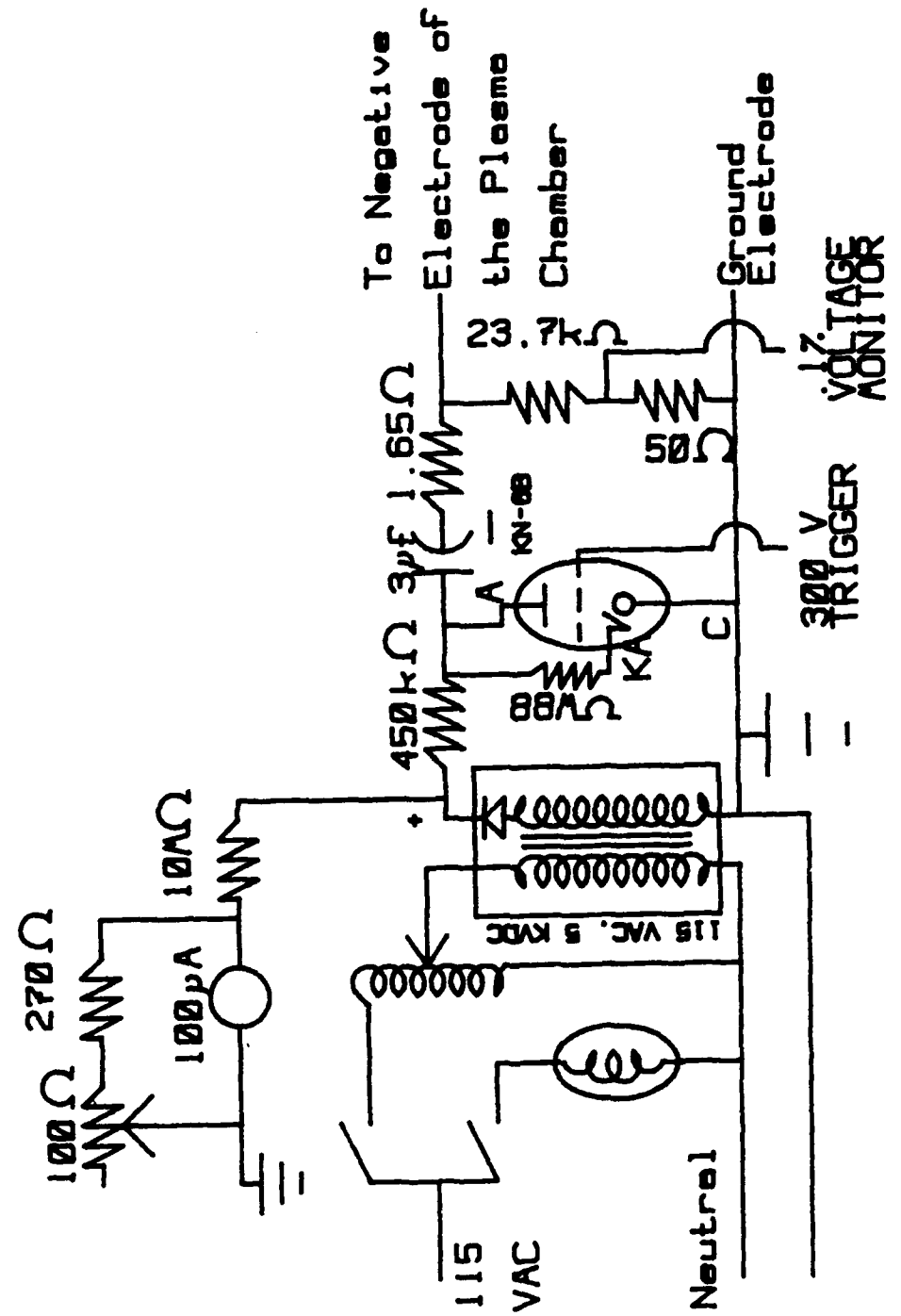

Figure 2. Schematic of the pulser used to generate the plasma column

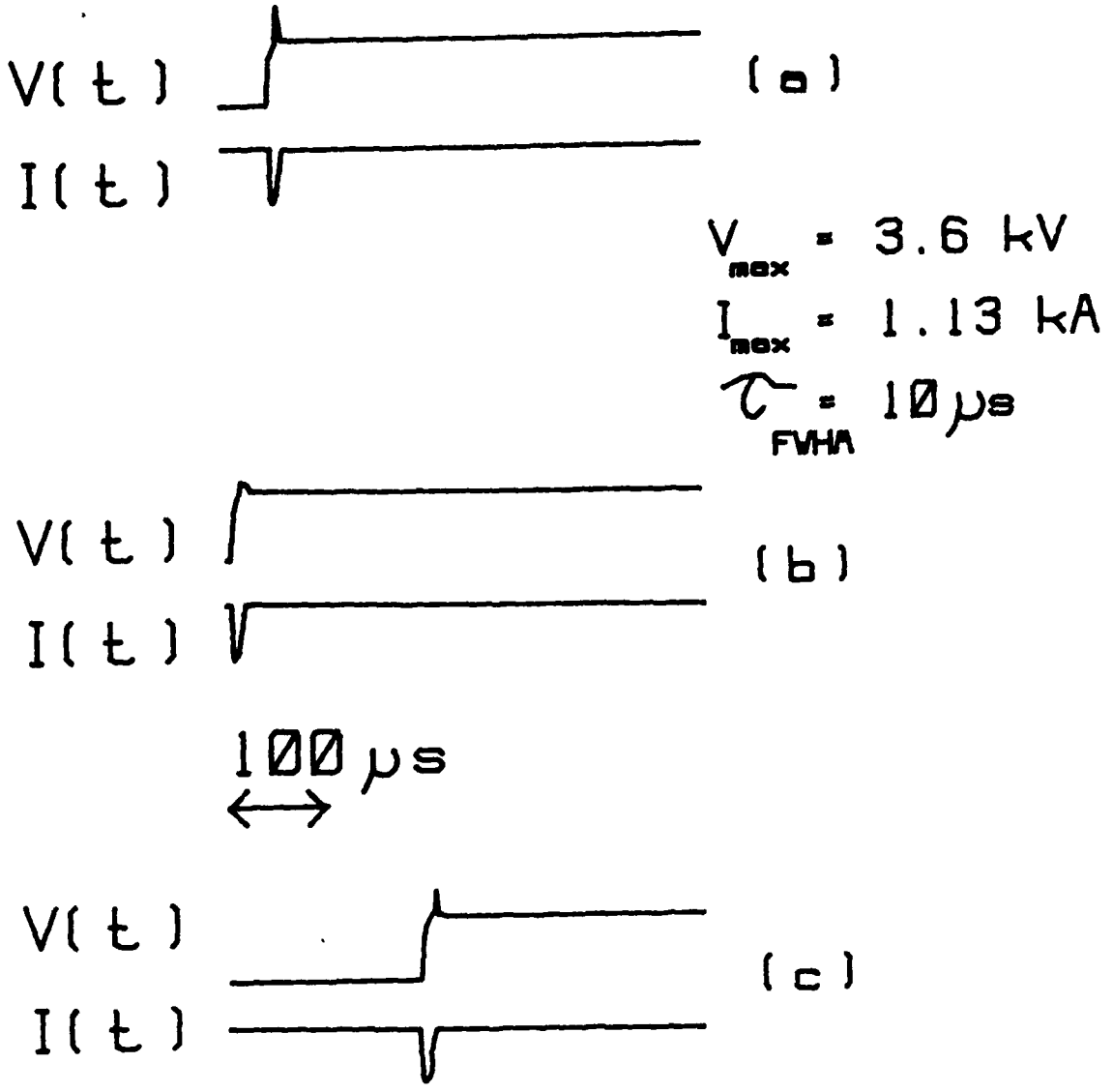

Figure 3. Output characteristics of the pulser used to create the plasma column

(a) H_2 at 3 Torr neutral pressure.

(b) Ar at 3 Torr neutral pressure.

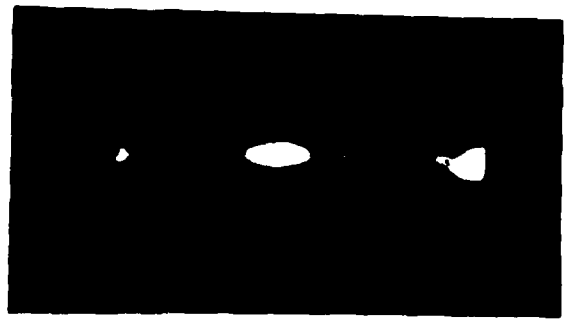

(c) Room air at 3 Torr neutral pressure.

(d) N_2 at .6 Torr neutral pressure.

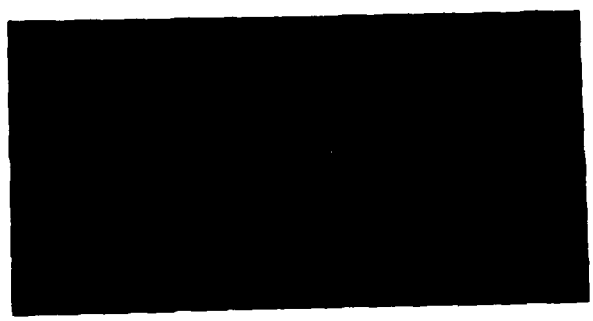

Figure 4. Sample open shutter pictures for various plasma columns produced. The arcs for H_2, Argon, and room air are 23 cm long. The arc for N_2 is 16 cm long.

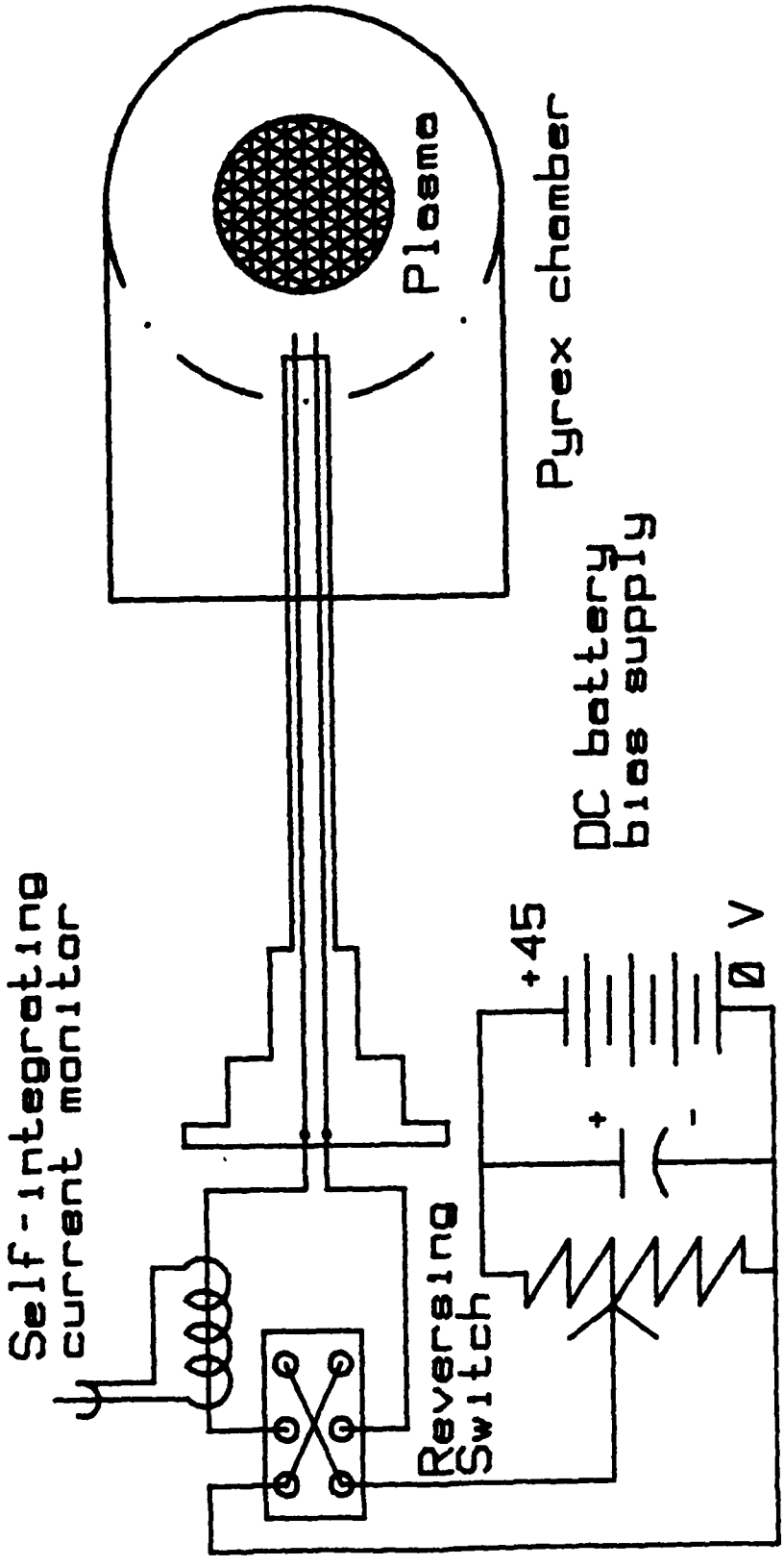

Figure 5. Schematic of the double Langmuir probe.

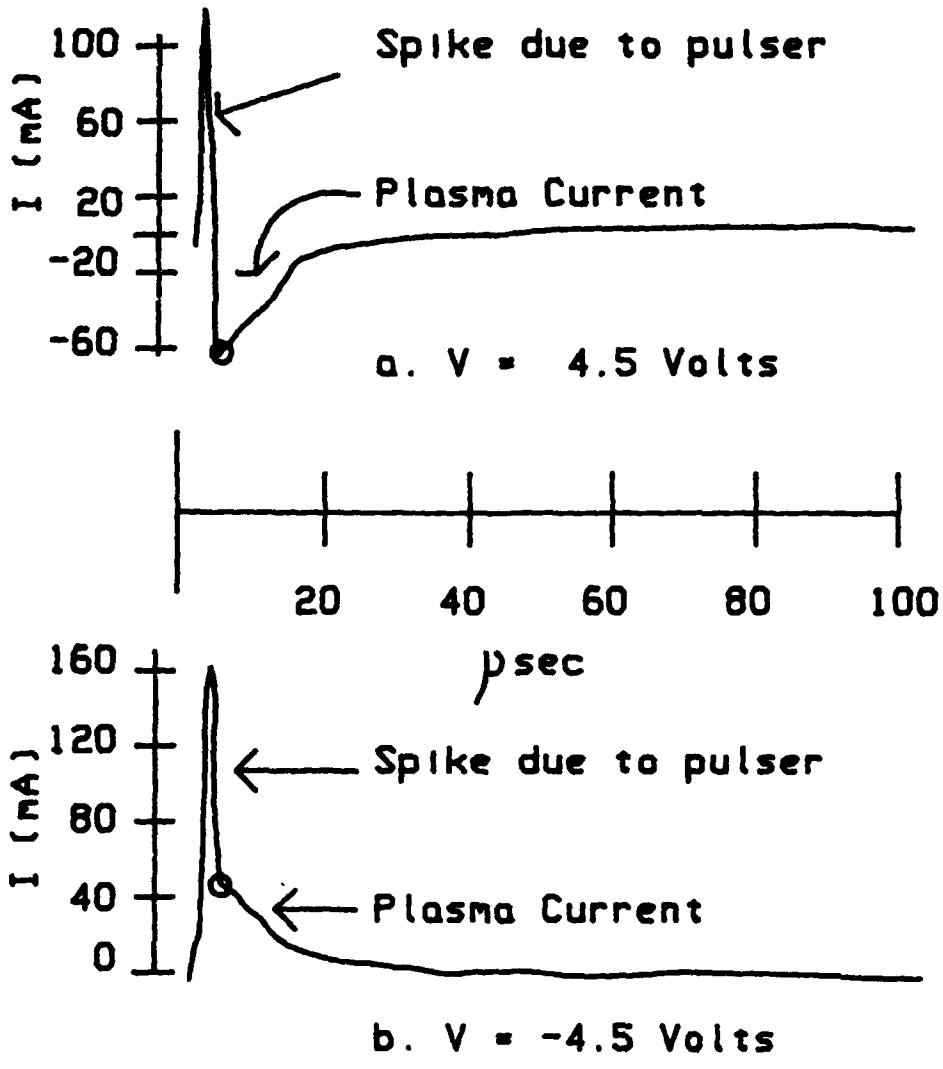

Figure 6. Typical double Langmuir probe traces for fixed bias

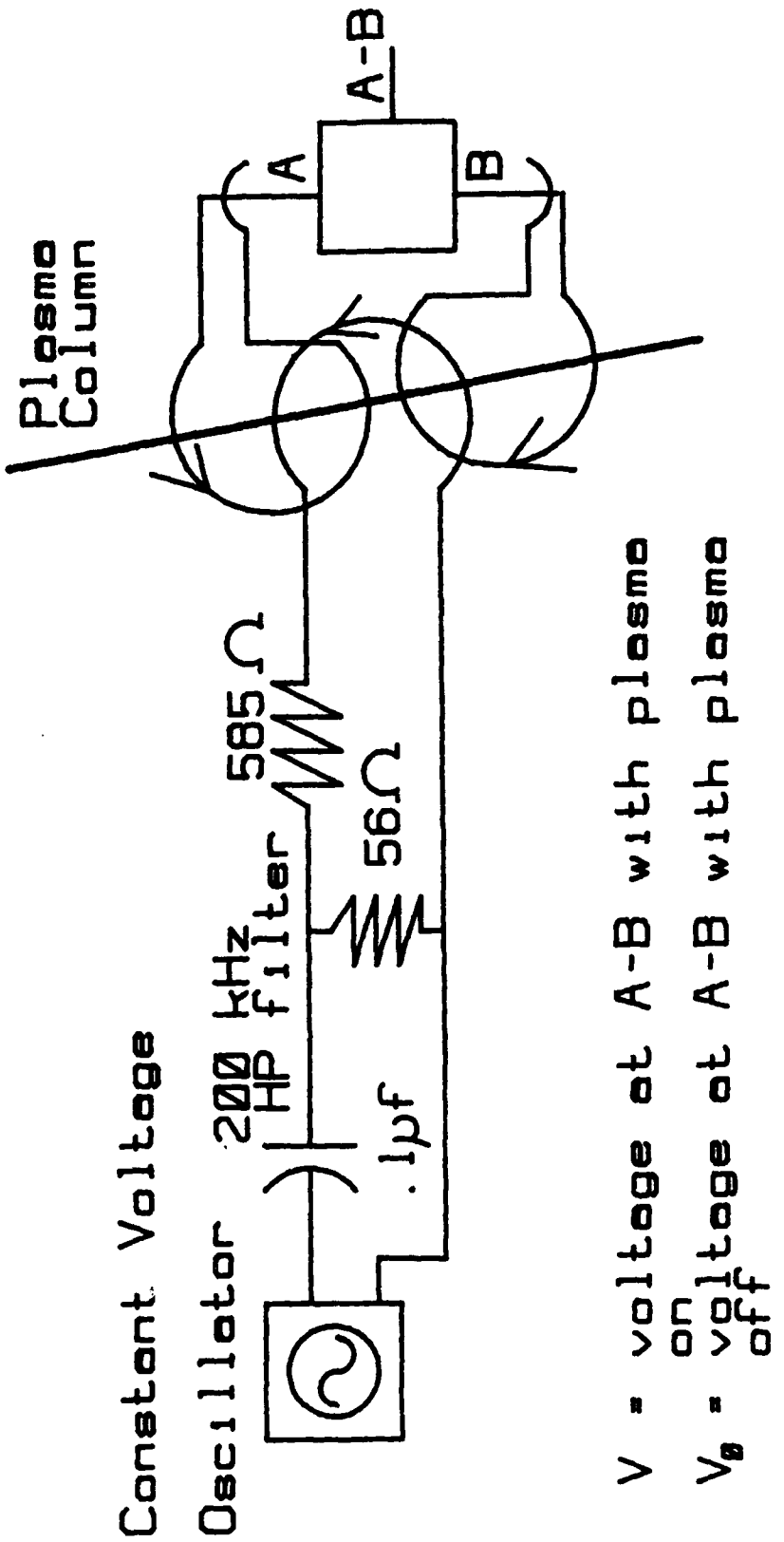

Figure 7. Schematic of the 2-coil Rf conductivity probe.

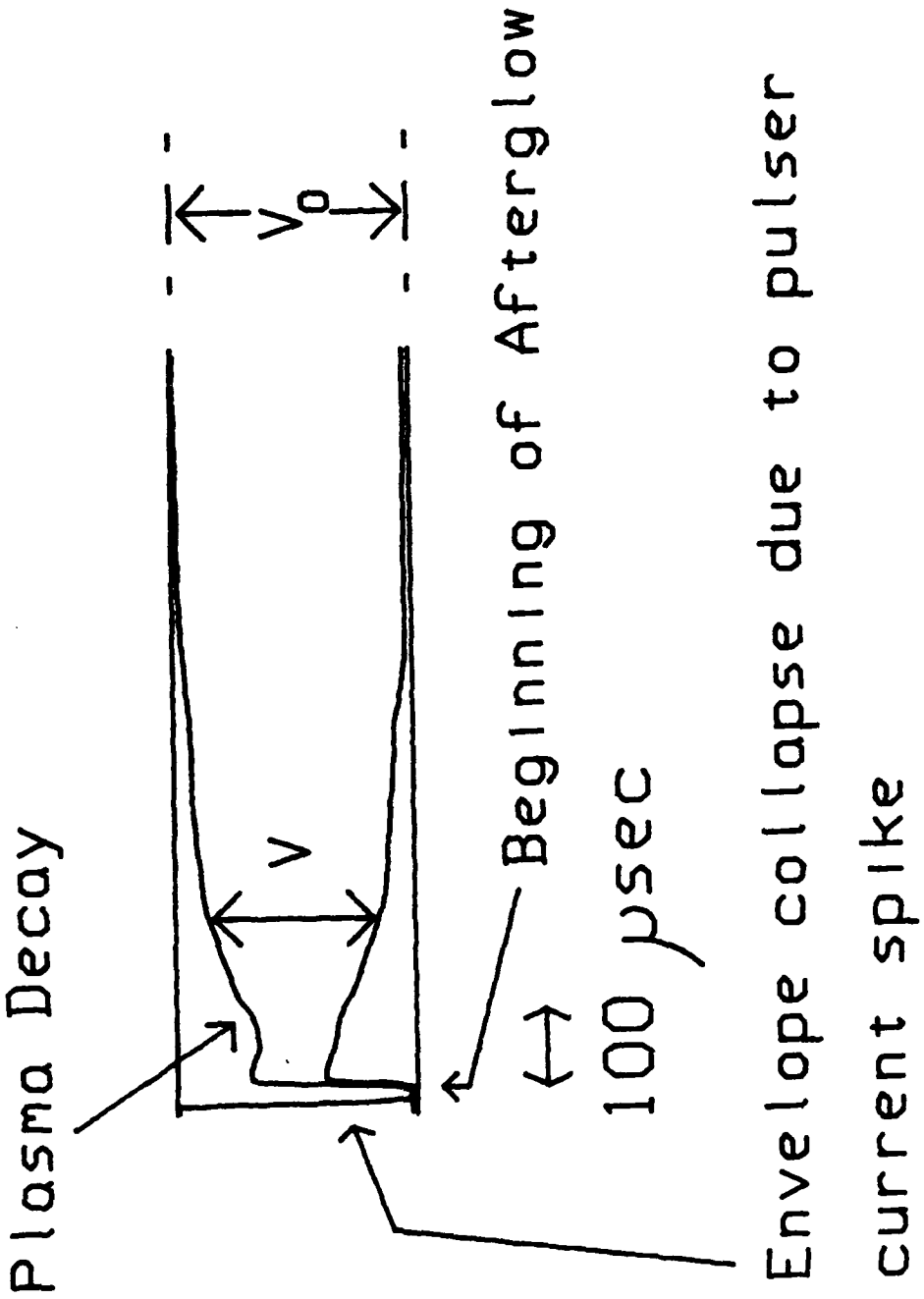

Figure 8. Typical data from the conductivity probe showing V and V_0

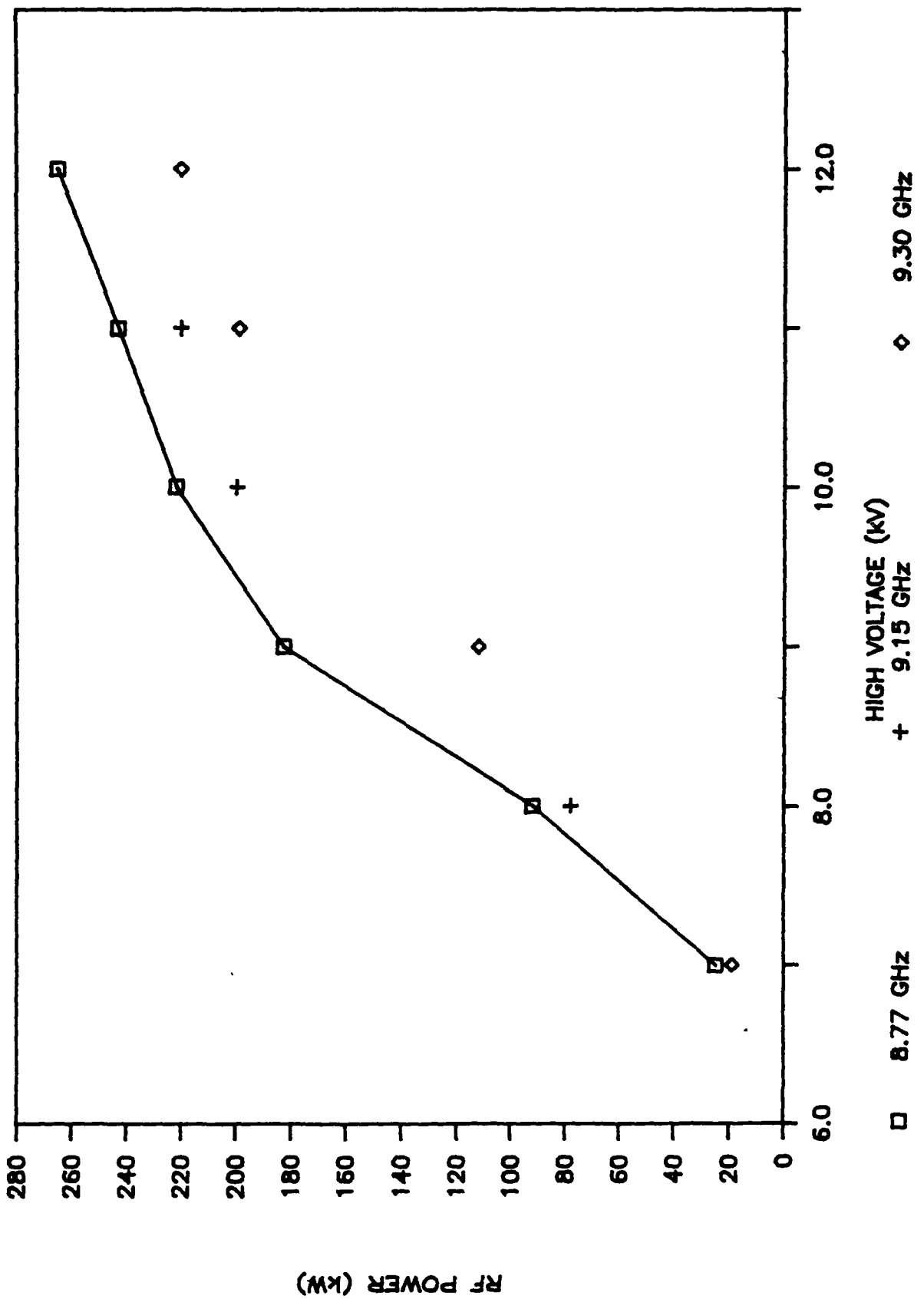

Figure 9. Rf power output calibration for the magnetron

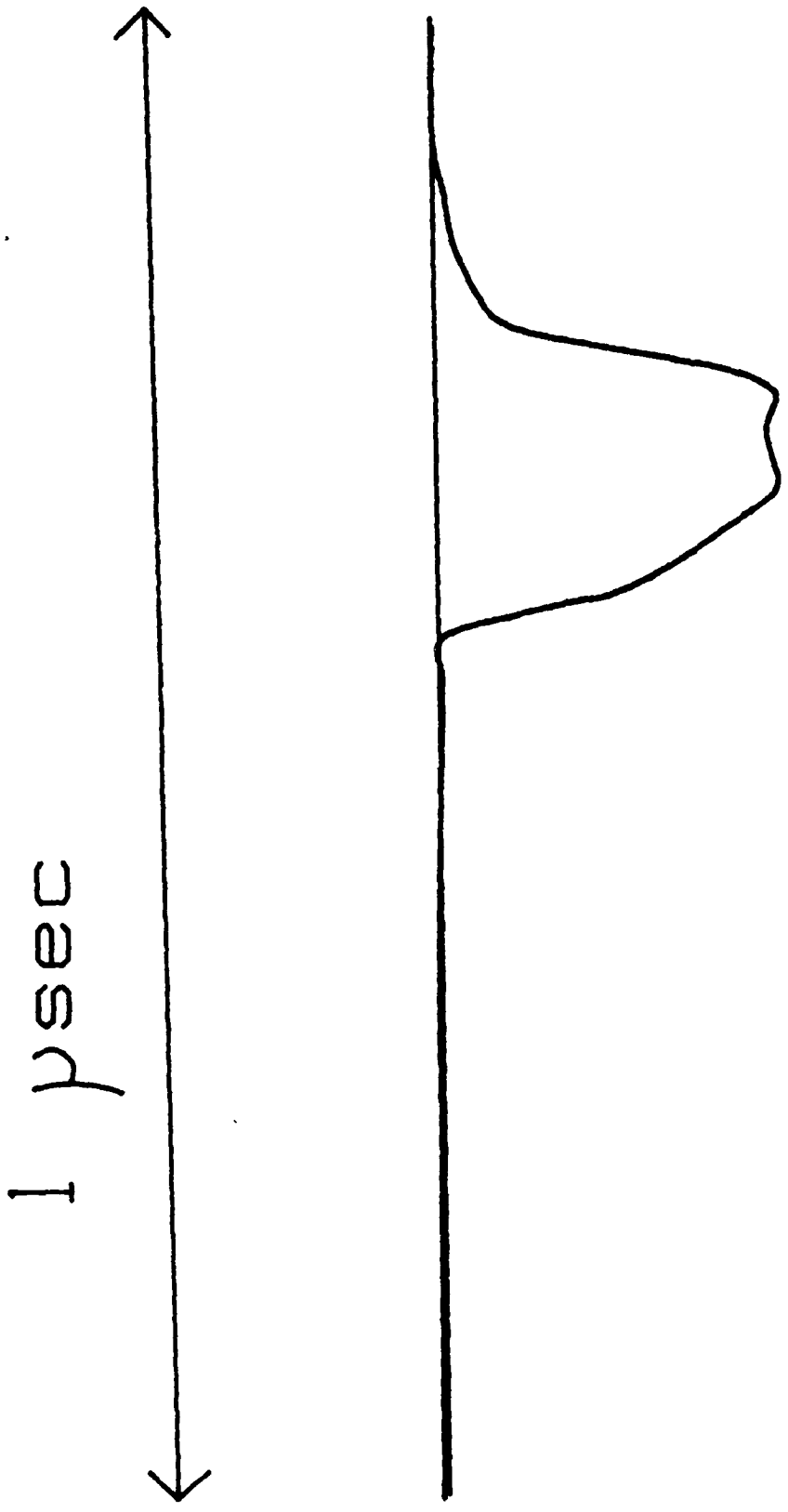

Figure 10. An overlay of 5 microwave pulses. The pulse amplitude is 260 kW.

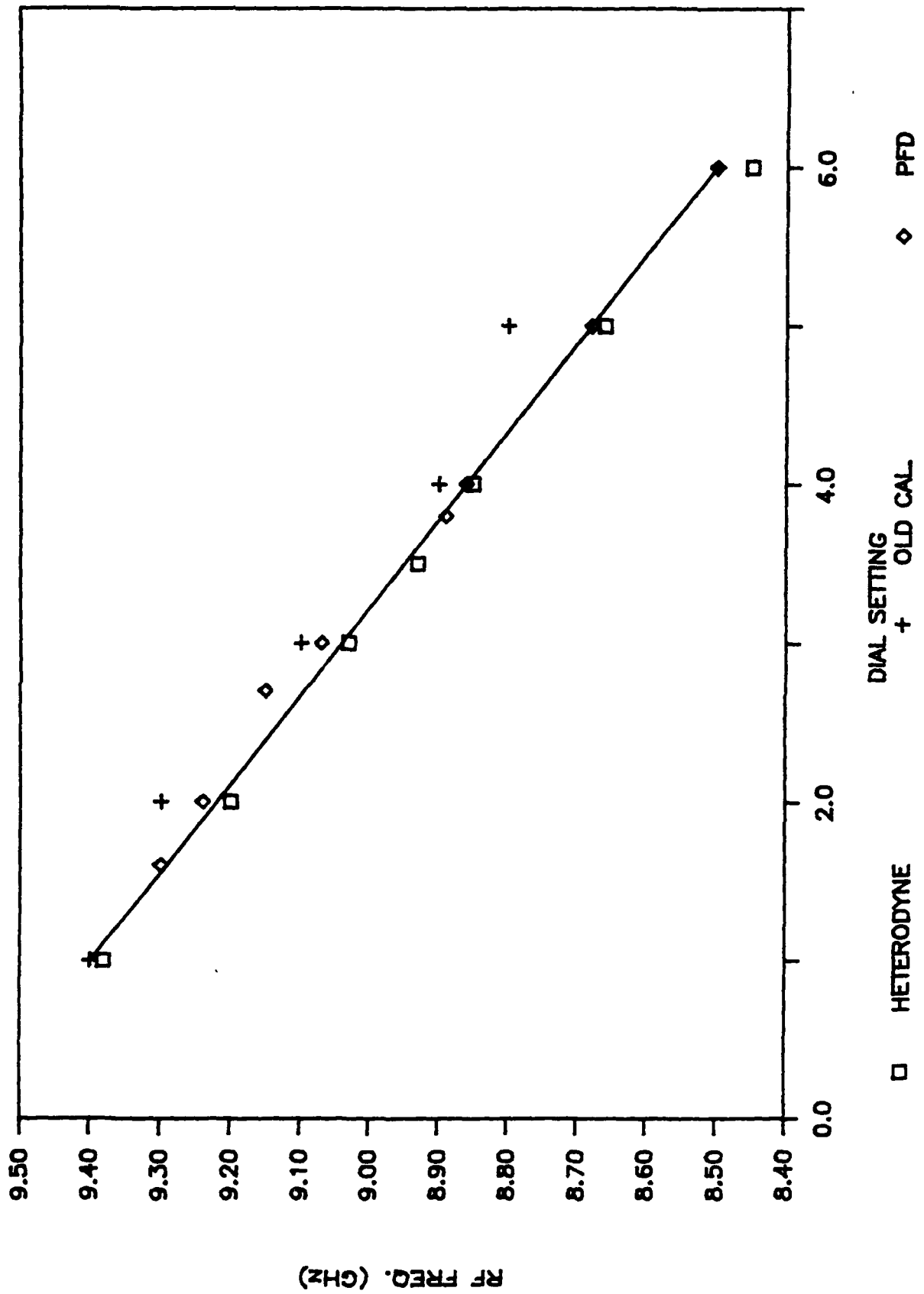

Figure 11. Magnetron frequency calibration

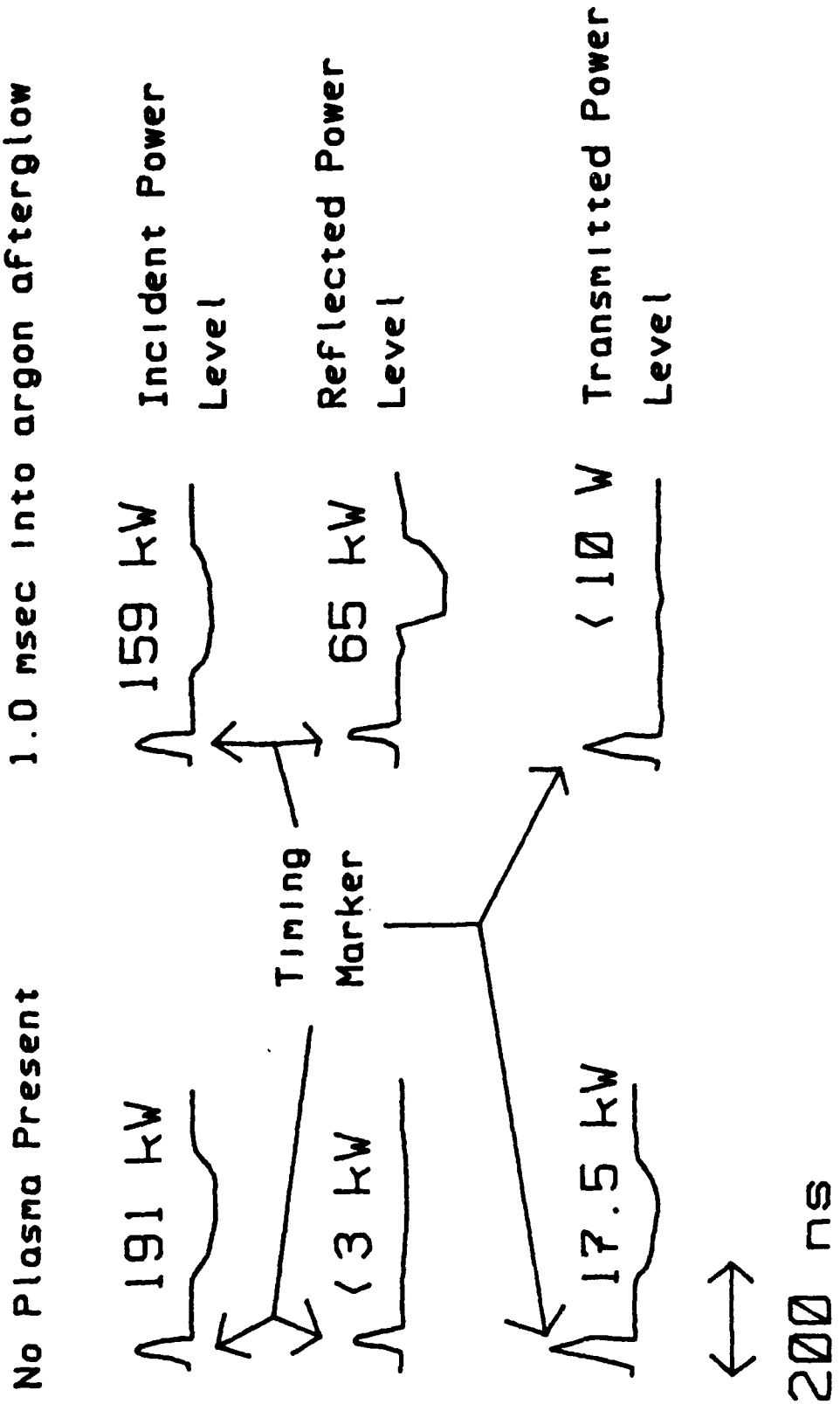

Figure 12. Sample data of microwave transmission through Ar.

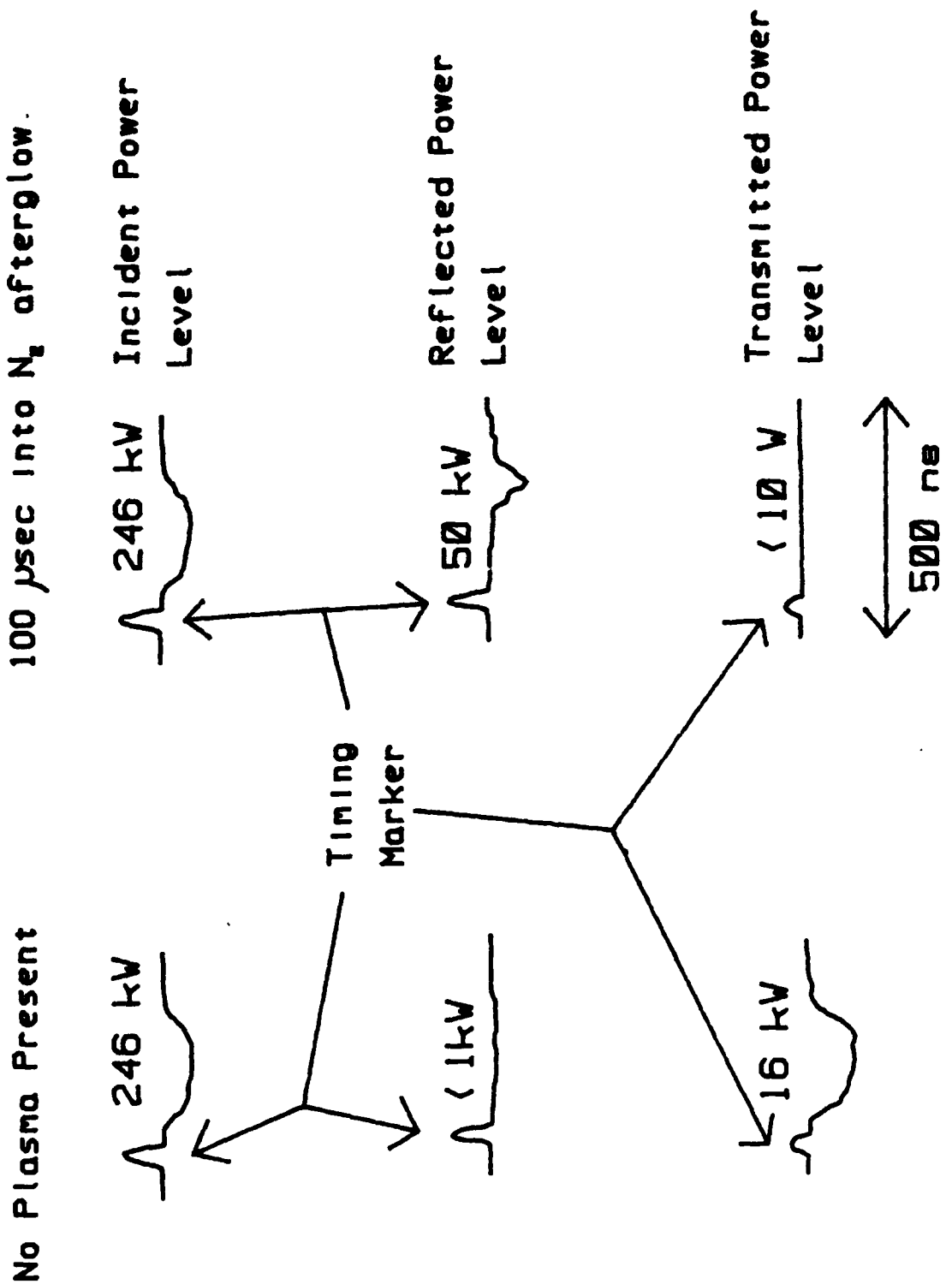

Figure 13. Sample data of microwave transmission through N_2.

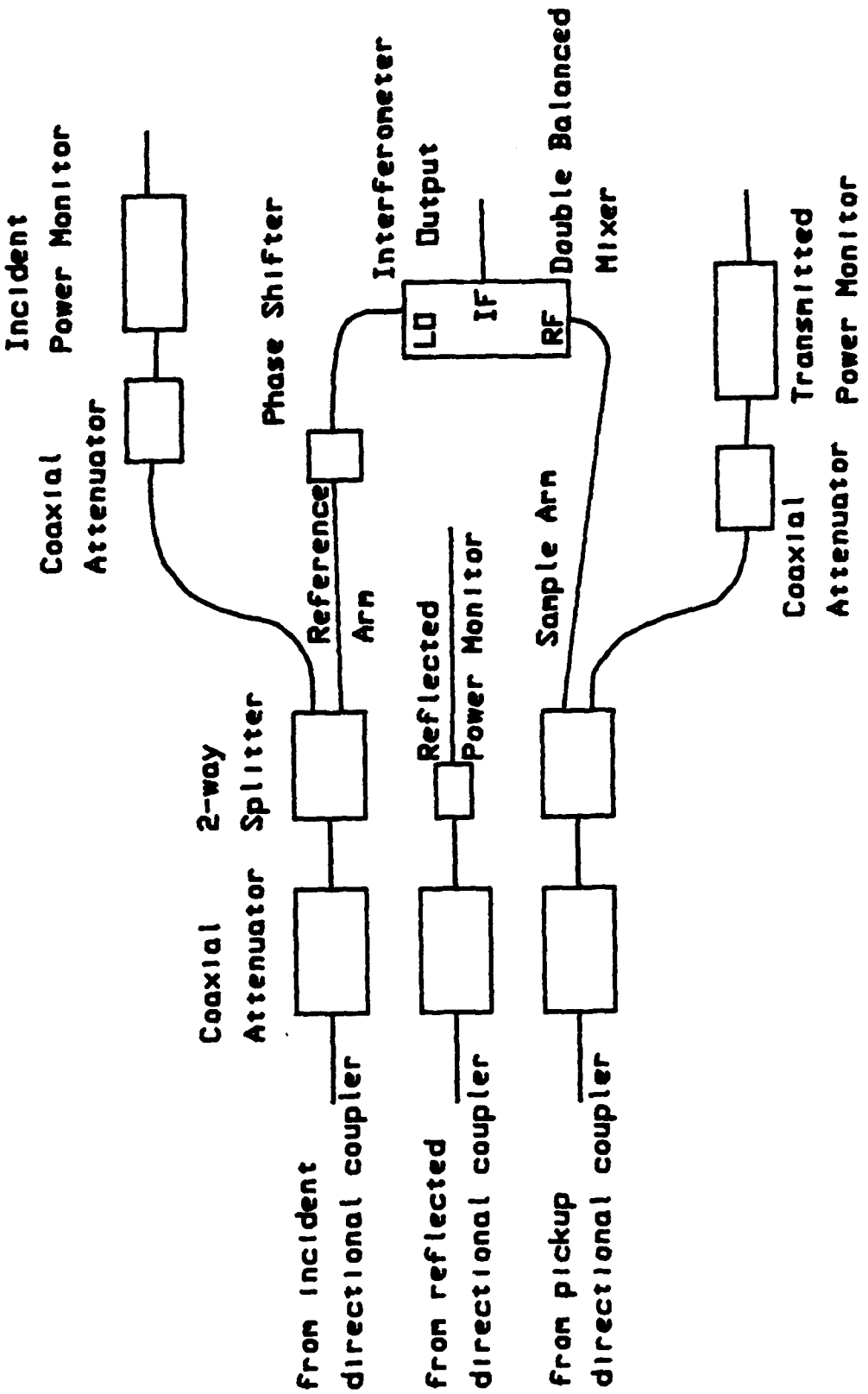

Figure 14. Schematic for the hookup of the microwave diagnostic channels

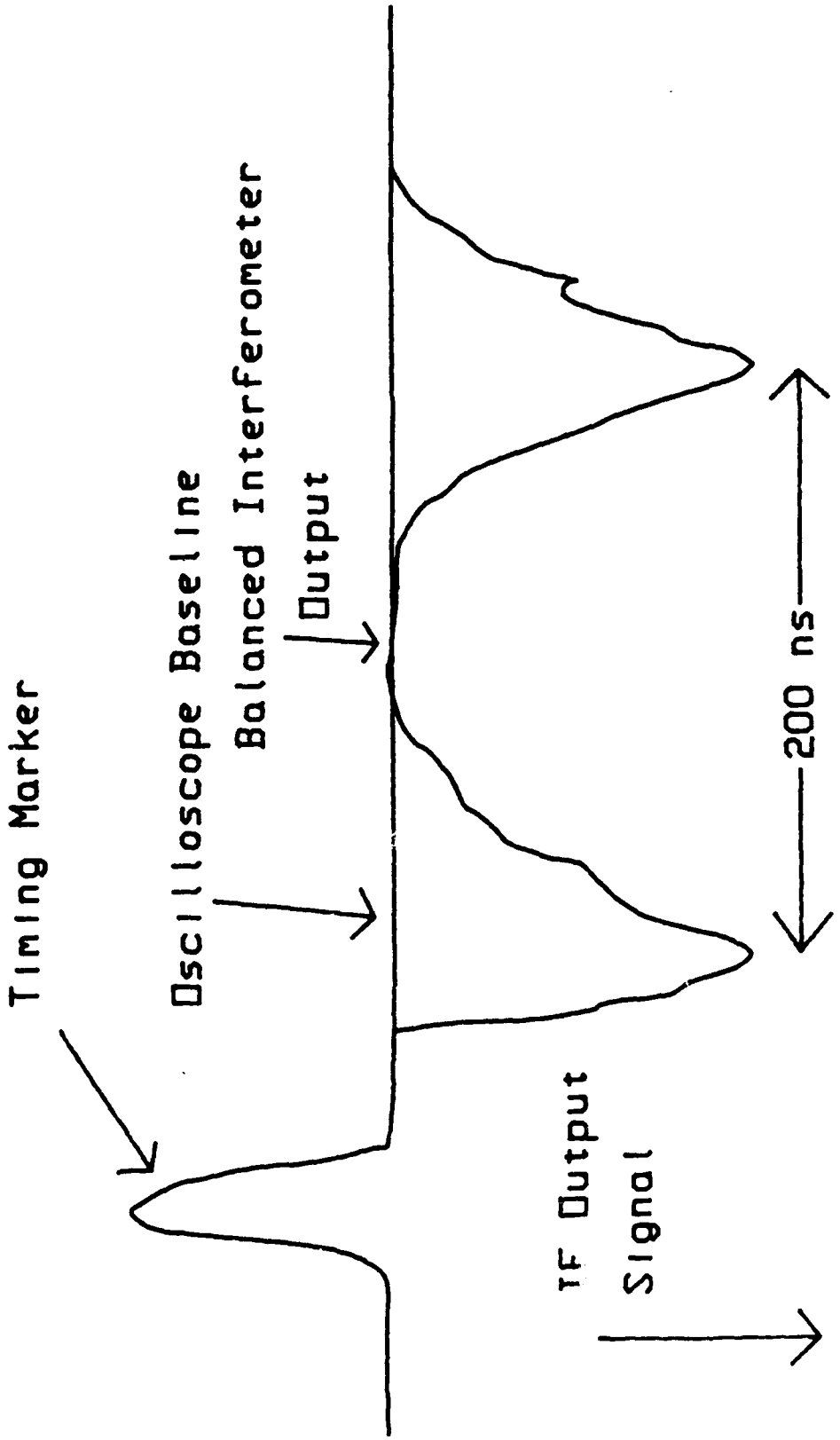

Figure 15. Datum indicating a nulled interferometer

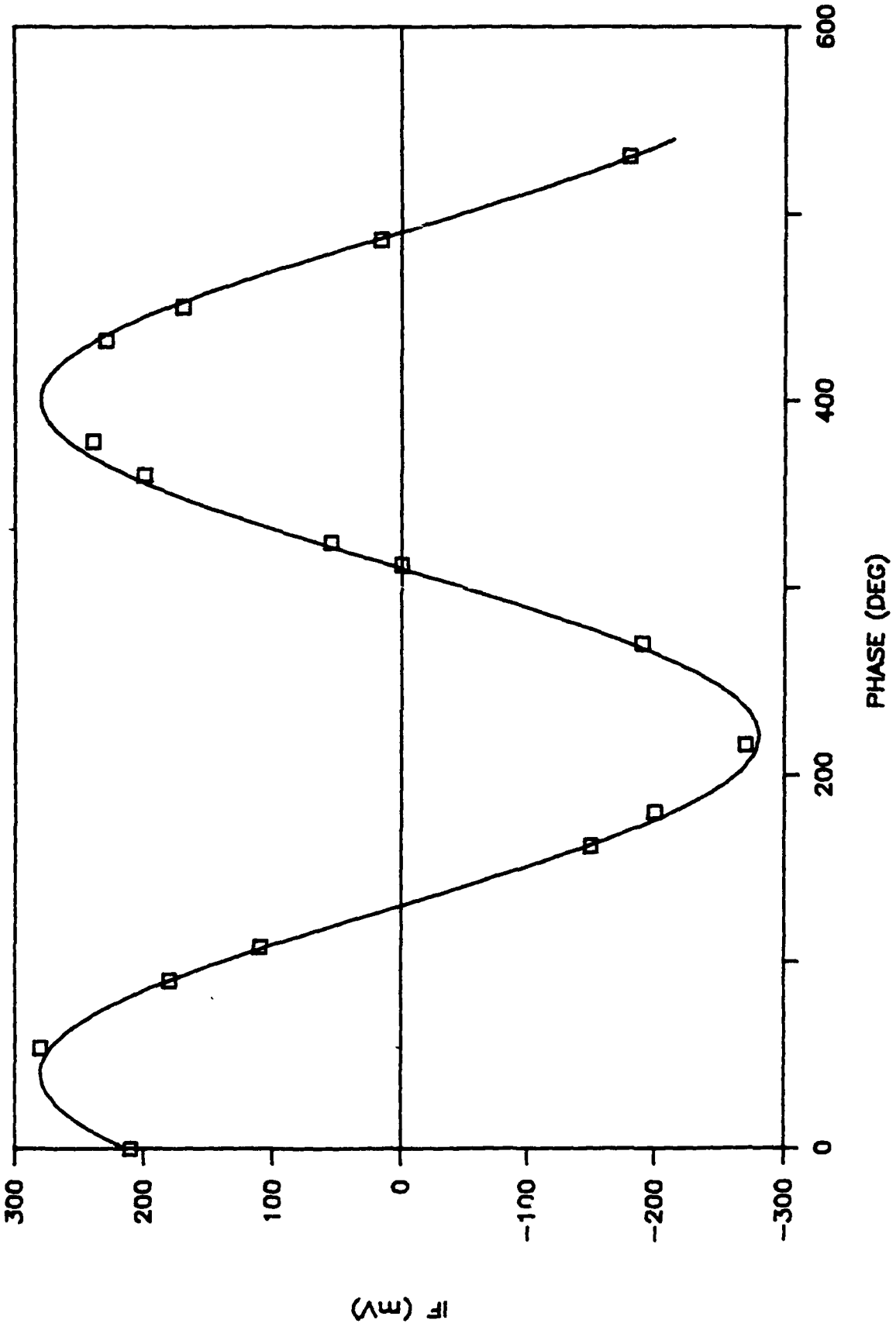

Figure 16. Interferometer calibration for 9 GHz

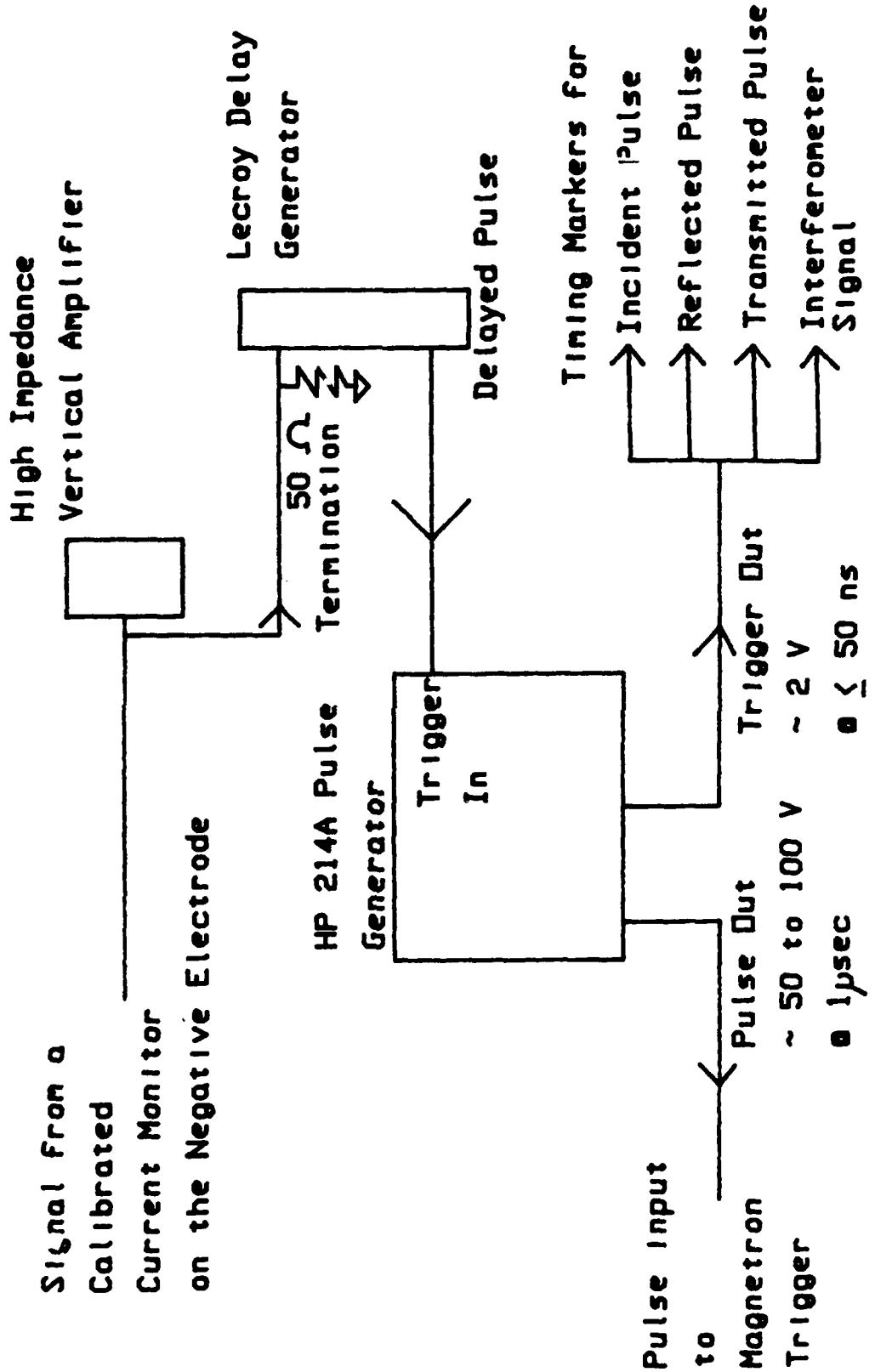

Figure 17. Afterglow timing circuit for triggering the magnetron

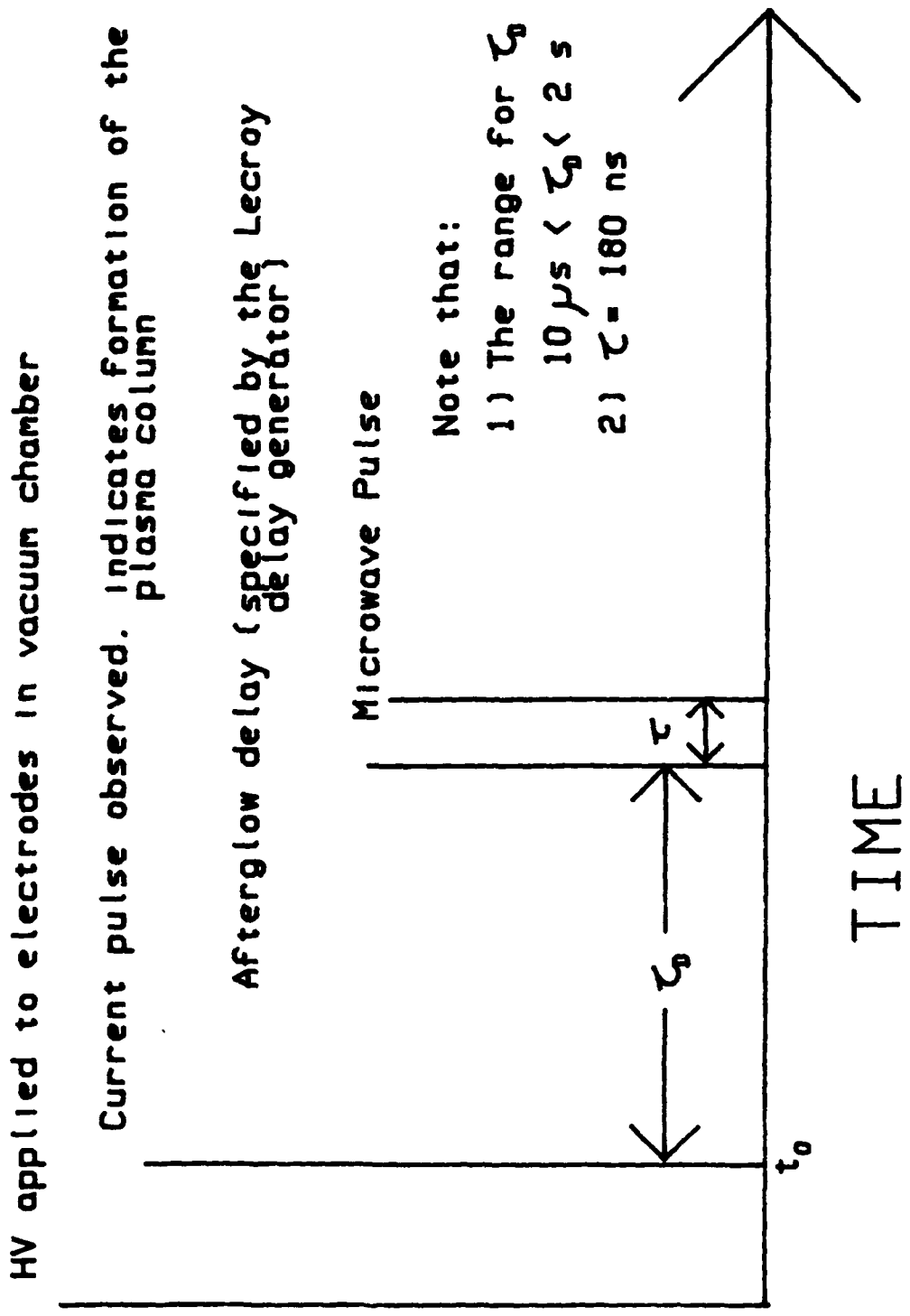

Figure 18. Relative timing diagram indicating various points in a given pulse sequence

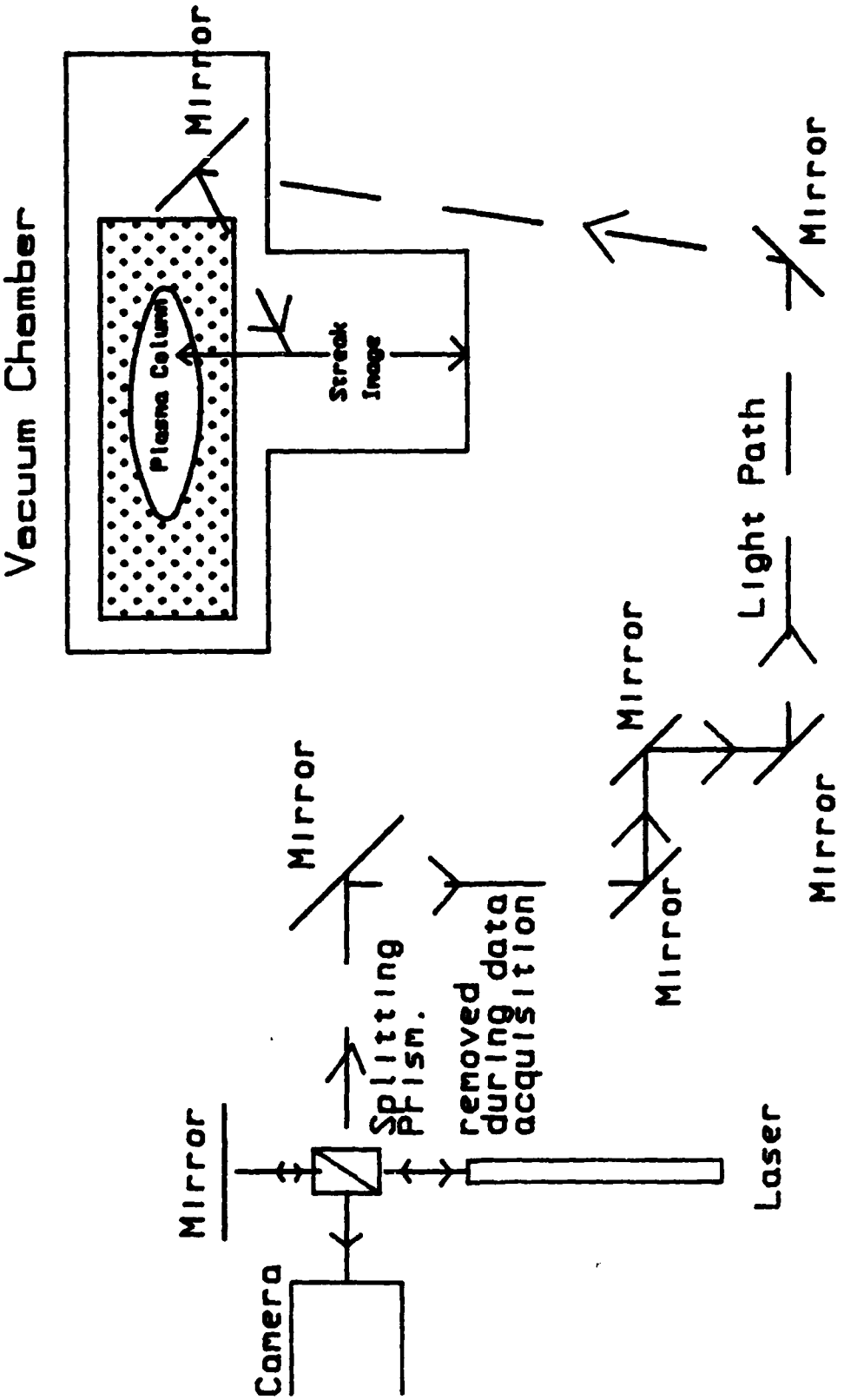

Figure 19. Streak camera setup

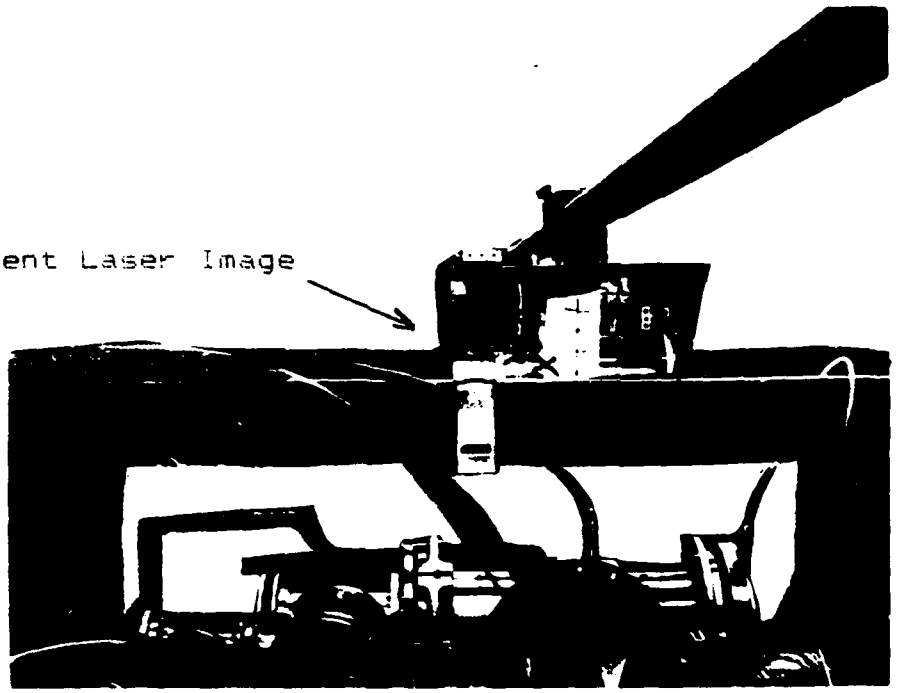

(a)

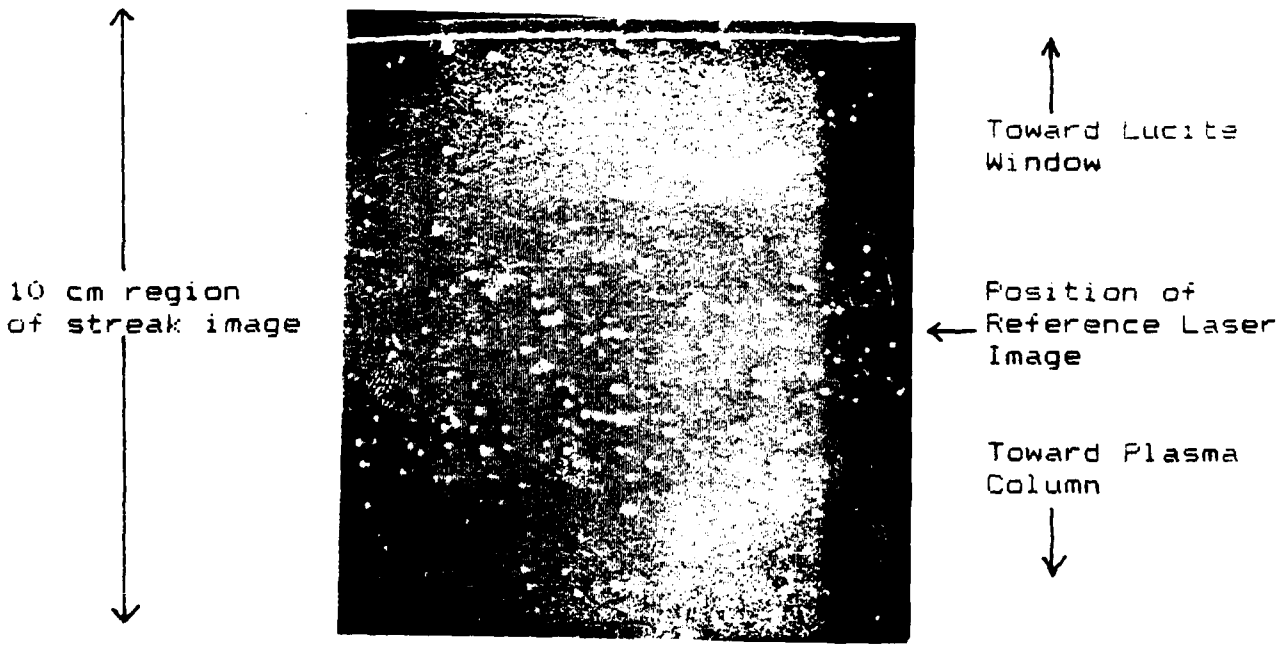

(b)

Figure 20. (a) Photo of the plasma chamber looking into the last mirror of the periscope and (b) a sample streak photo.

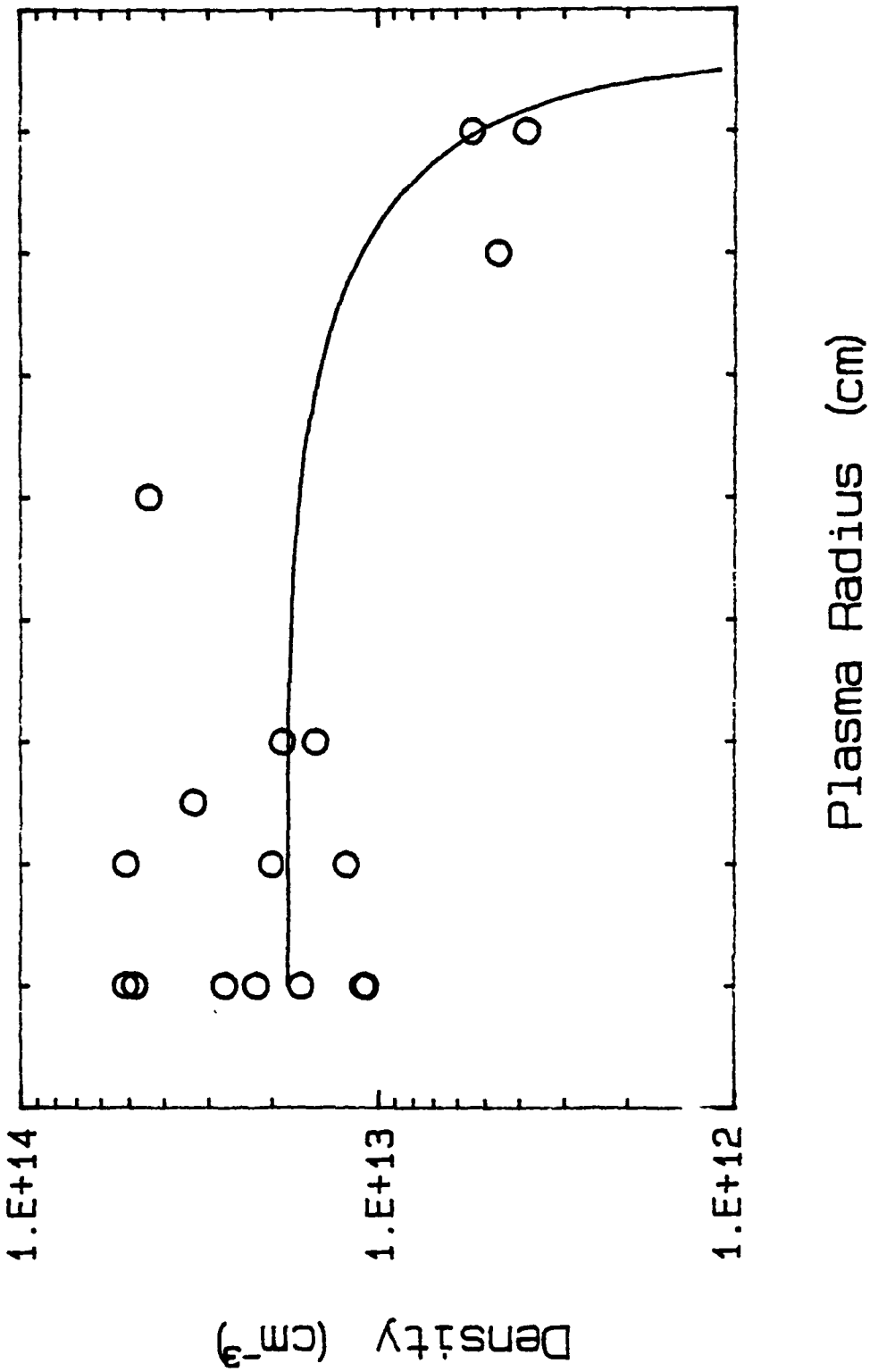

Figure 21. Plasma density measured by the double Langmuir probe

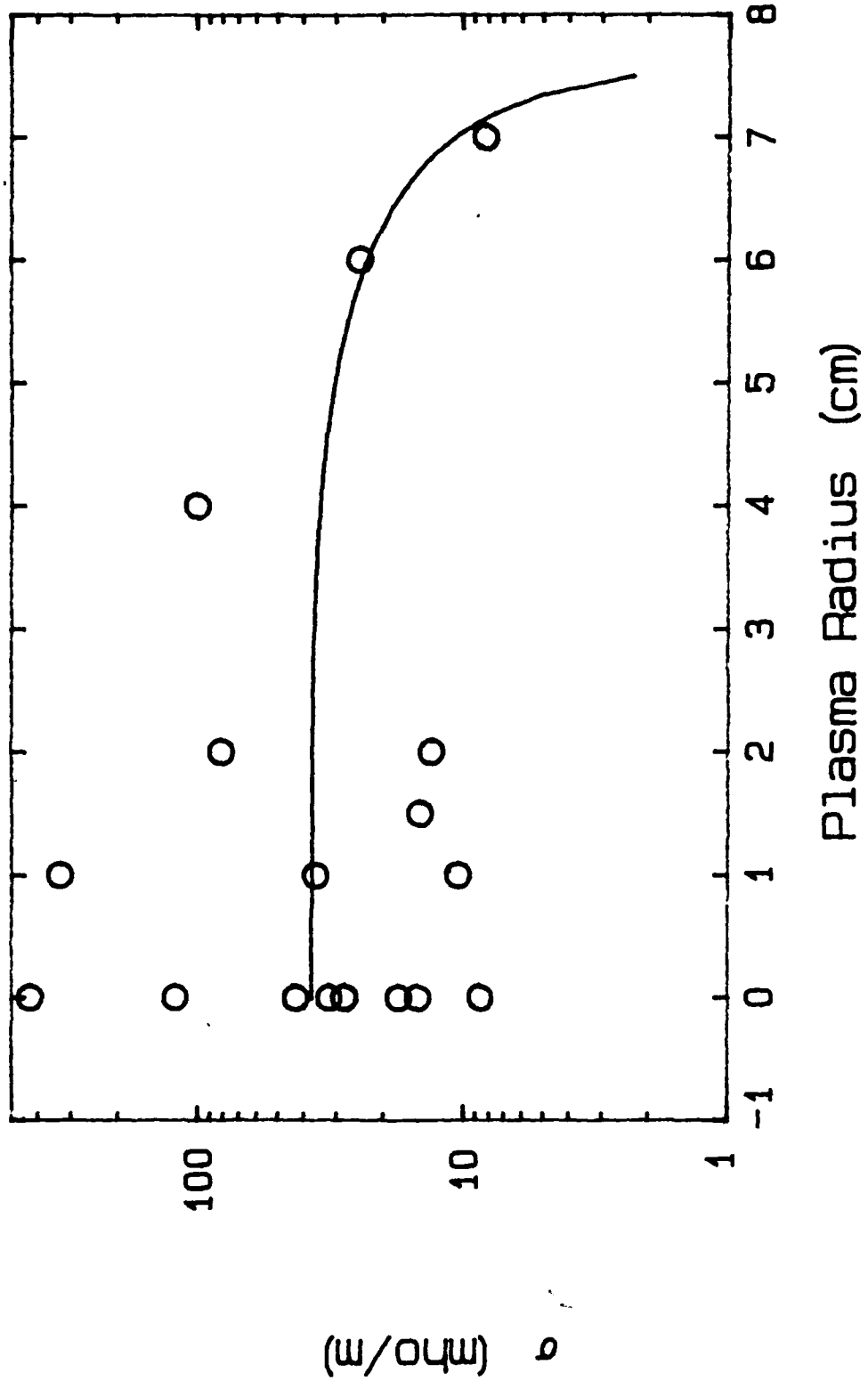

Figure 22. Plasma conductivity calculated from double probe data

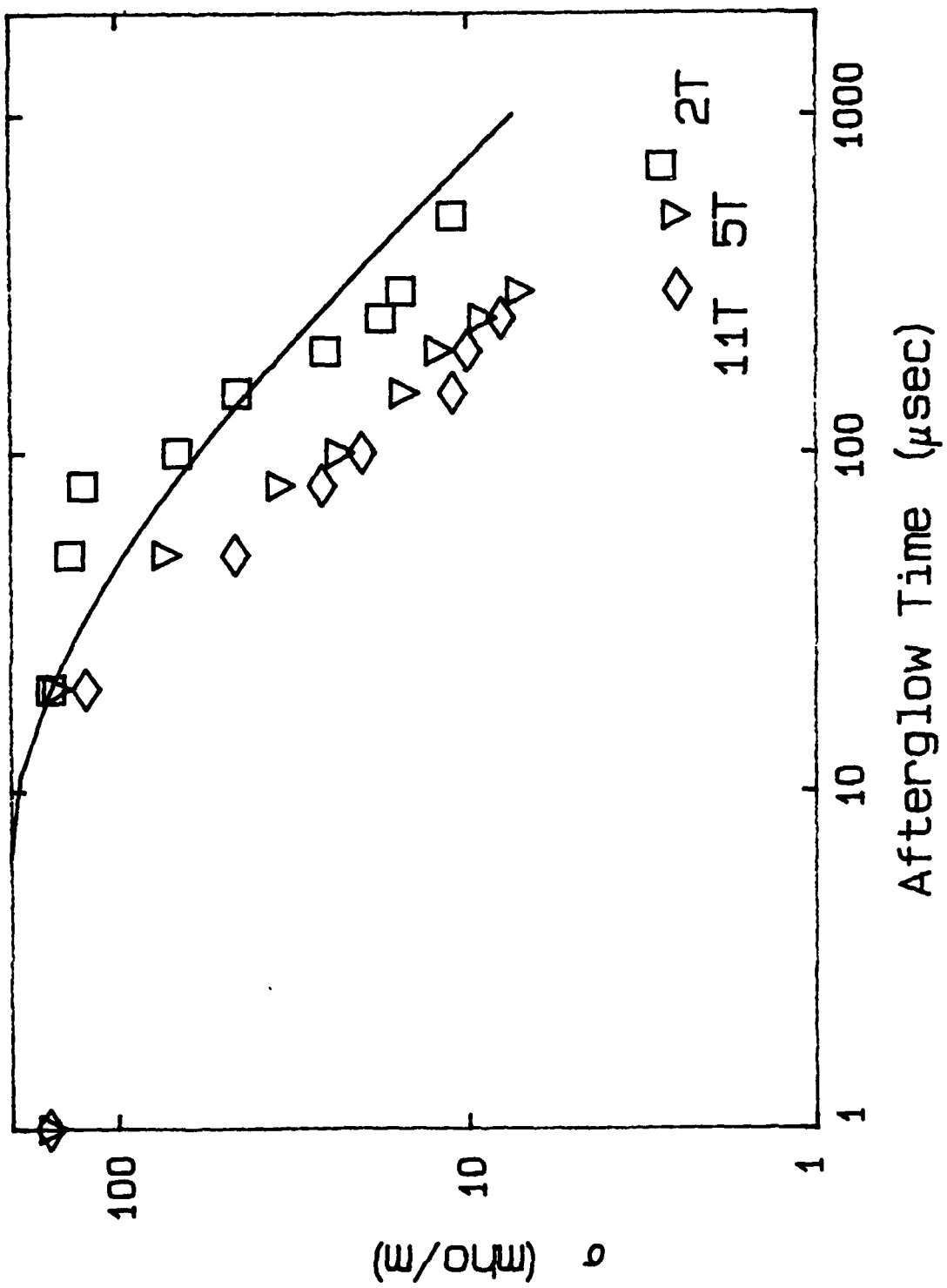

Figure 23. Ar conductivity decay measured by the rf coil probe

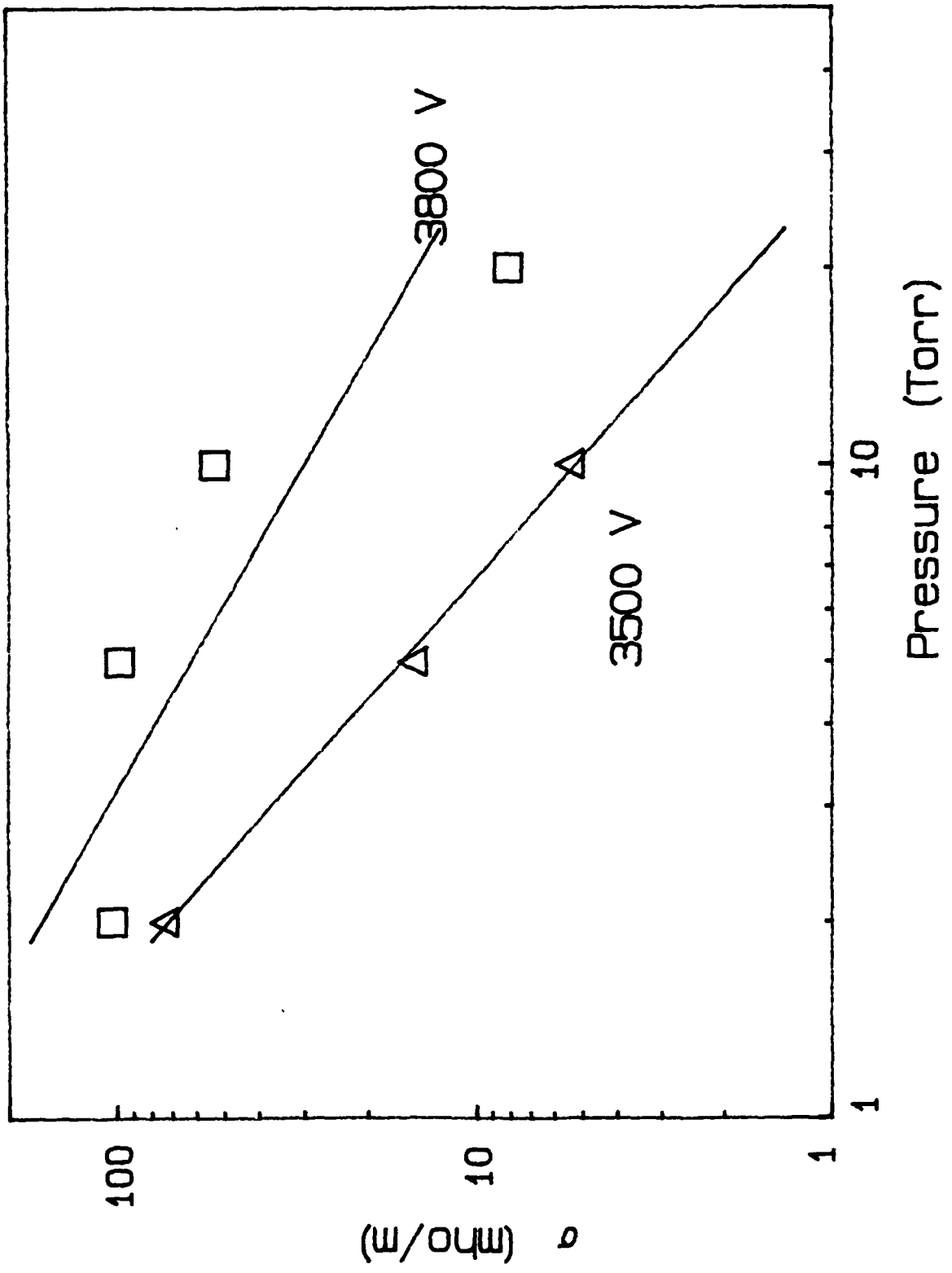

Figure 24. Ar conductivity changes due to pressure changes

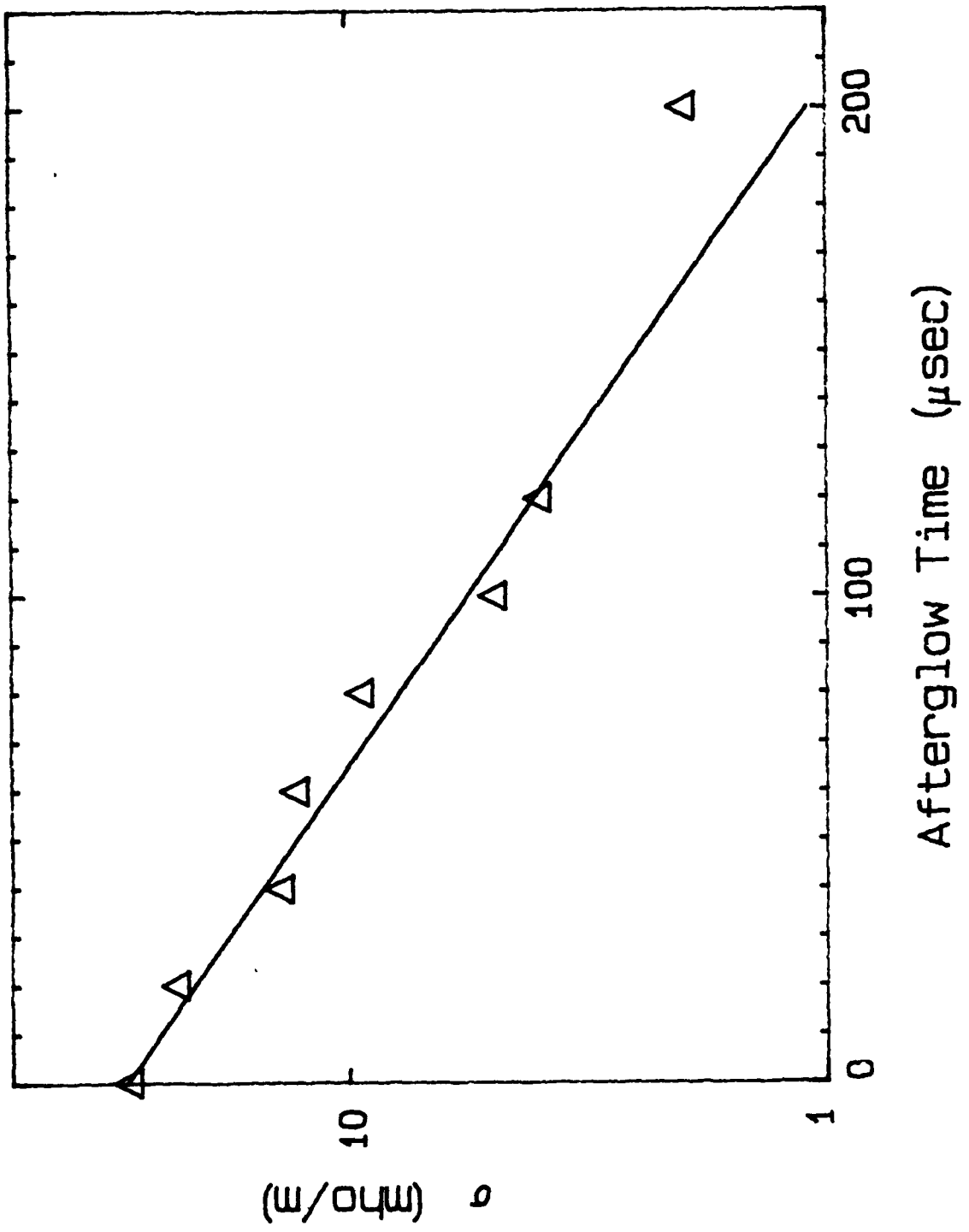

Figure 25. N_2 conductivity decay measured by the rf coil probe

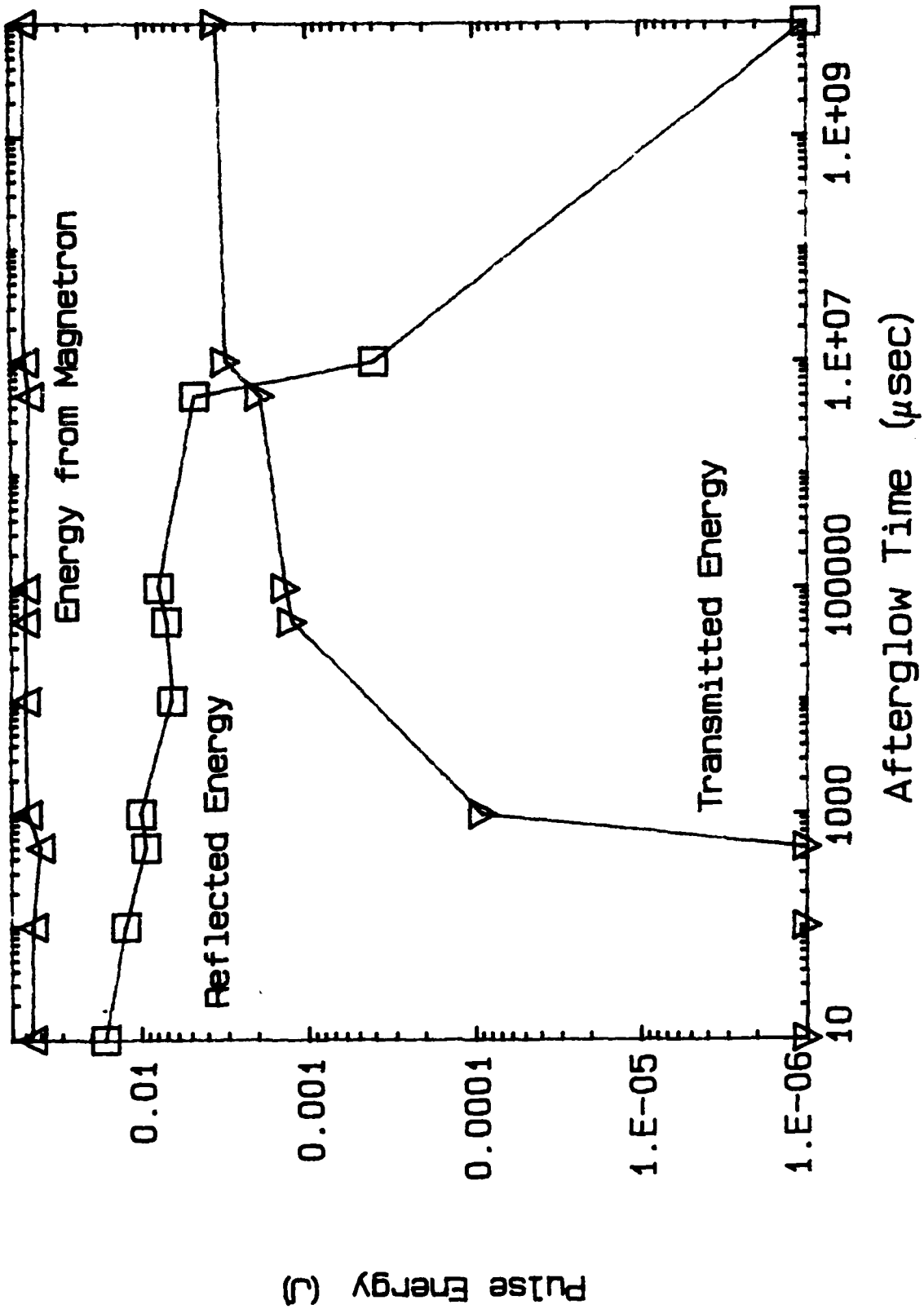

Figure 26. Variation of the various rf pulse energies with time, for the case of Ar.

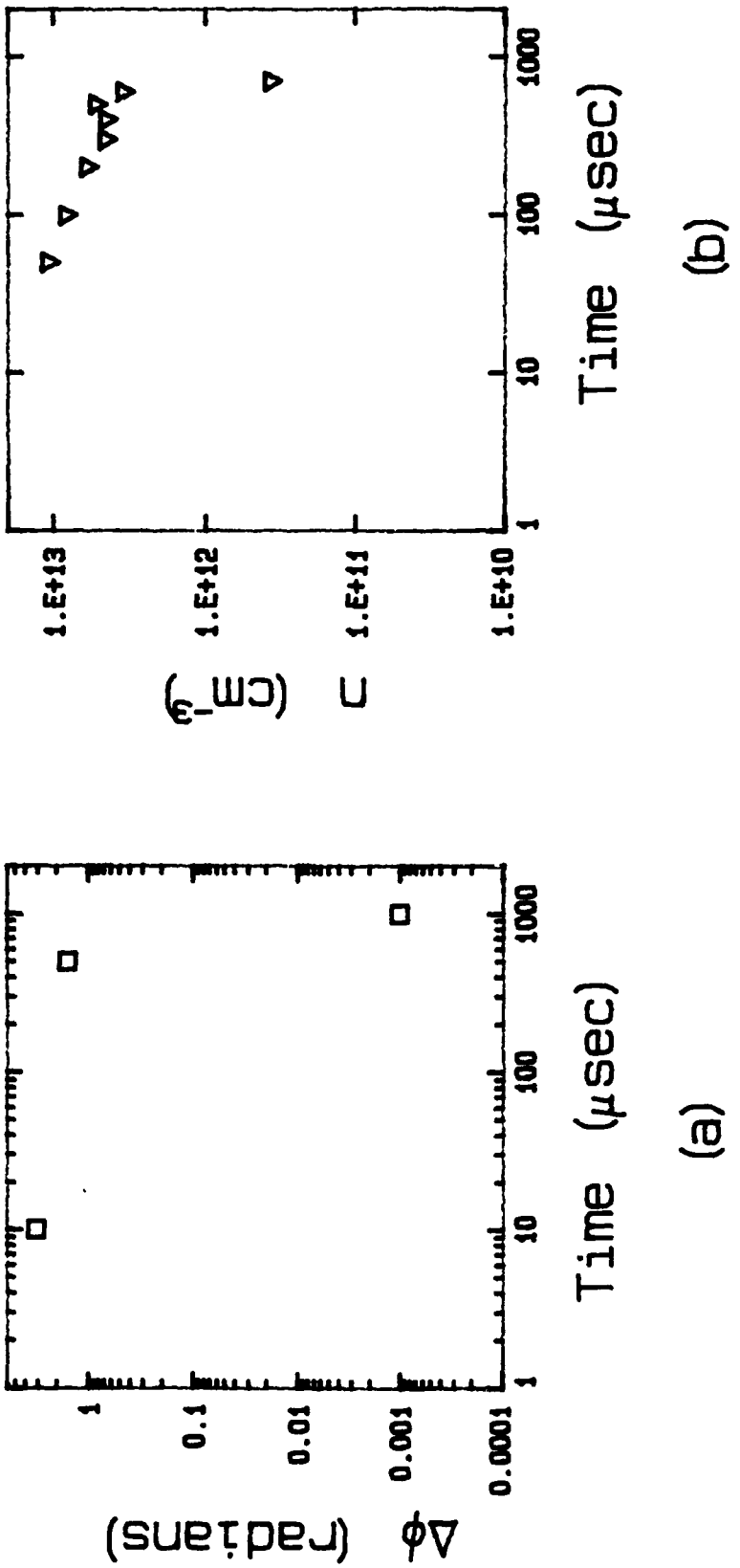

Figure 27. Comparison of time variation of the phase shift measured by the interferometer and the variation of the density determined by the conductivity probe

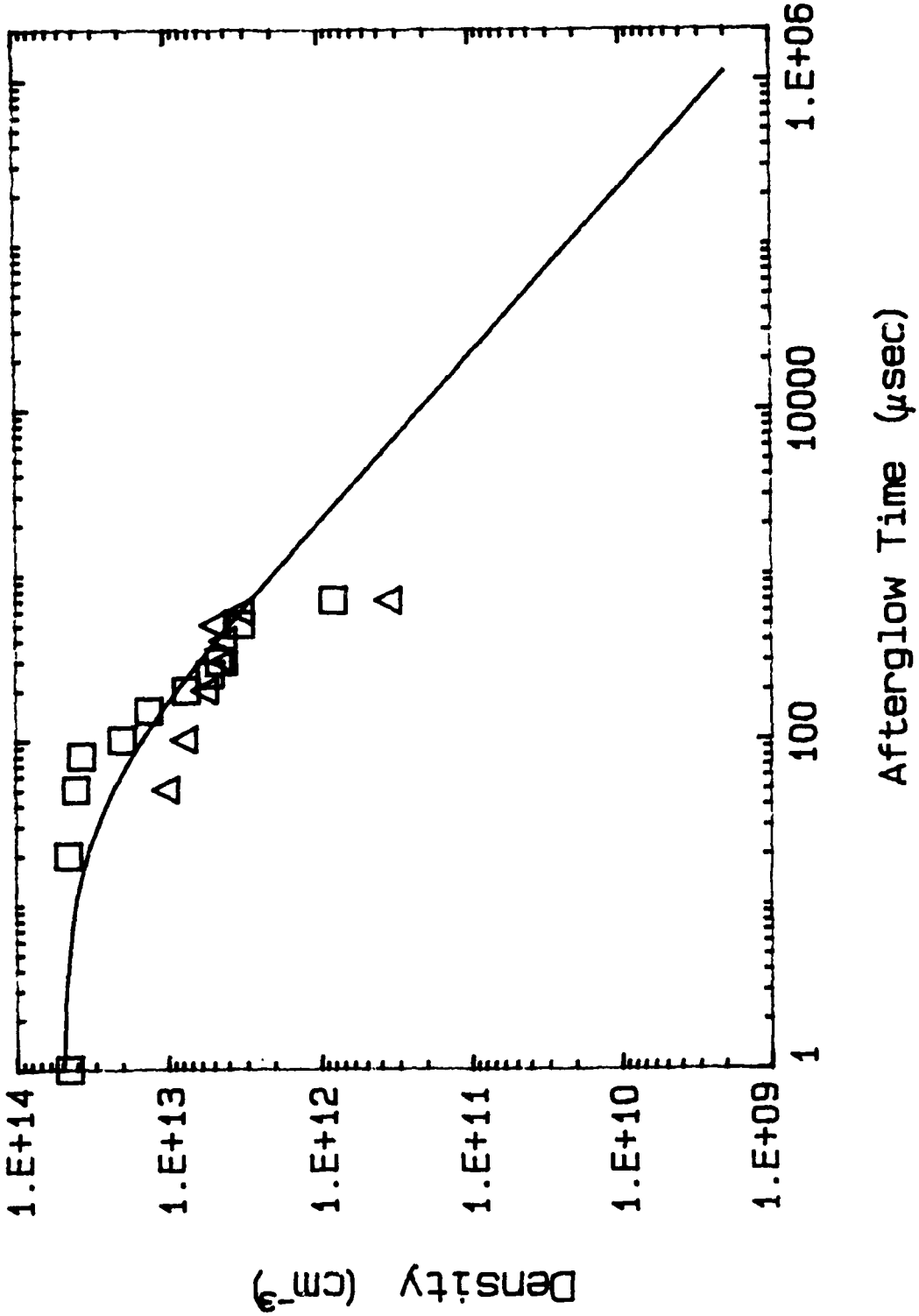

Figure 28. Comparison of the on axis density used in eq. 3 and that measured by the conductivity probe (Ar 2T)

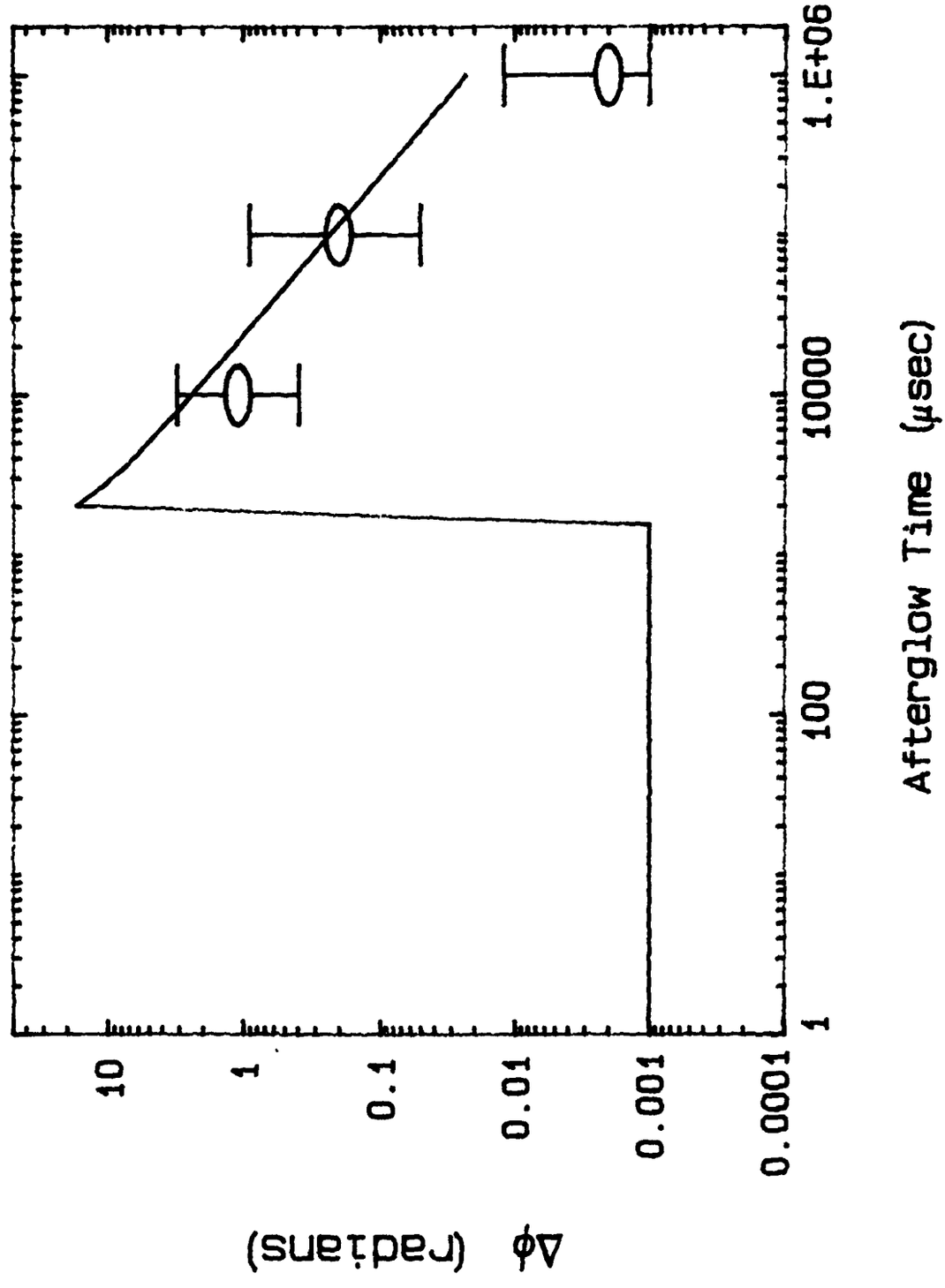

Figure 29. Comparison of the calculated and measured phase change for Ar at 2 Torr

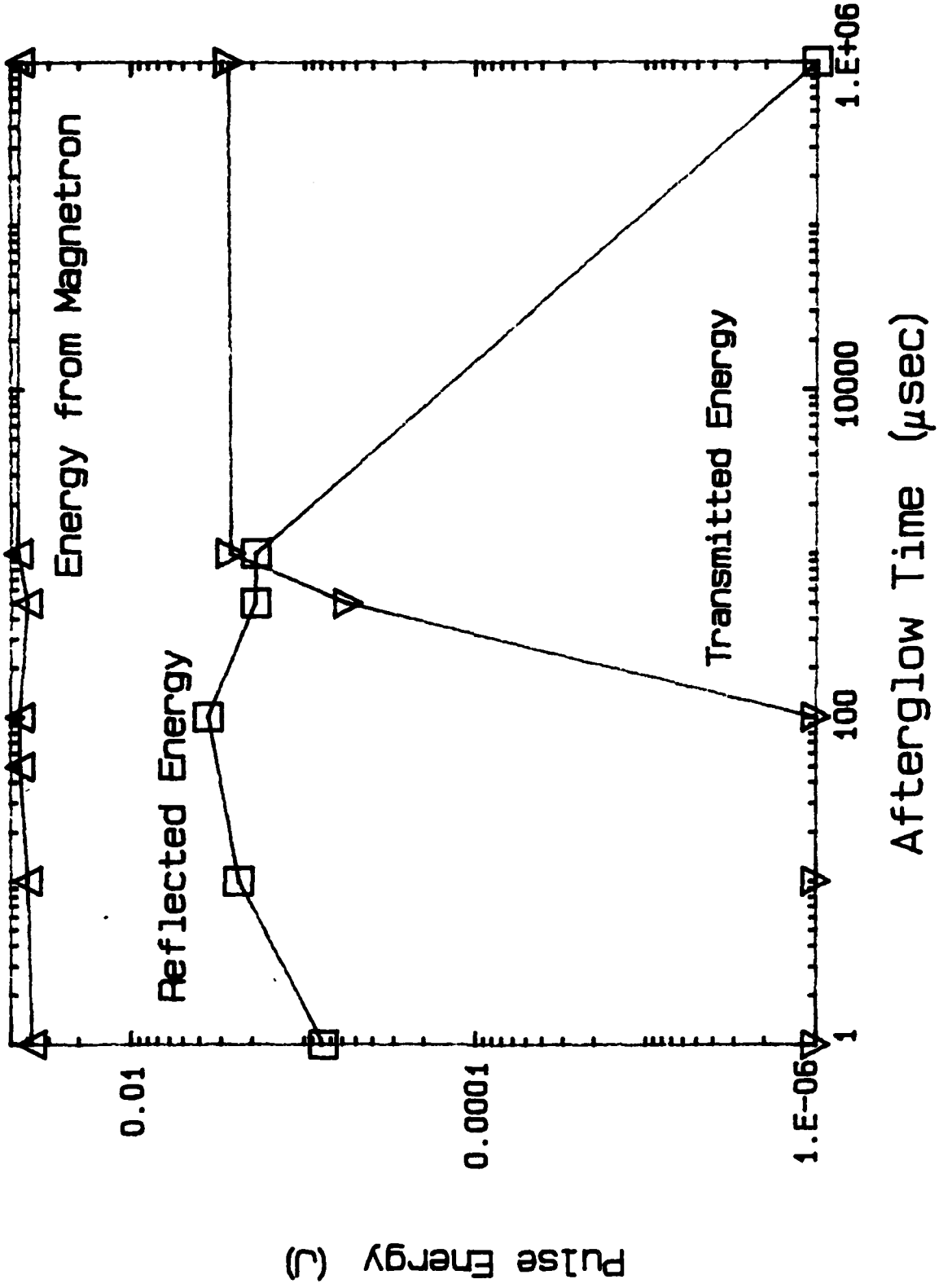

Figure 30. Variation of the various rf pulse energies with time in N_2

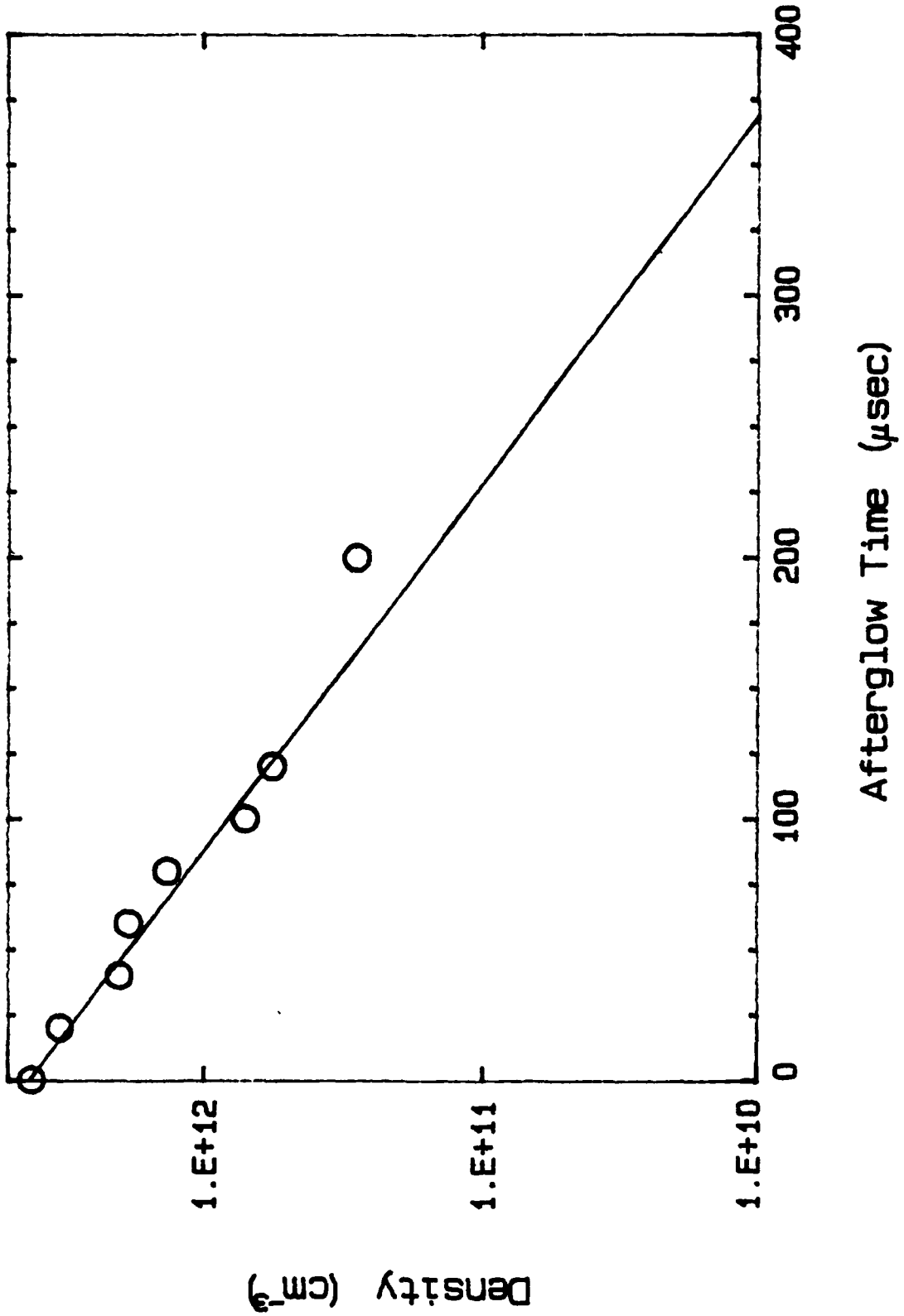

Figure 31. Comparison of the on axis density used in eq. 3 and that measured by the conductivity probe (N_2 .5 Torr)

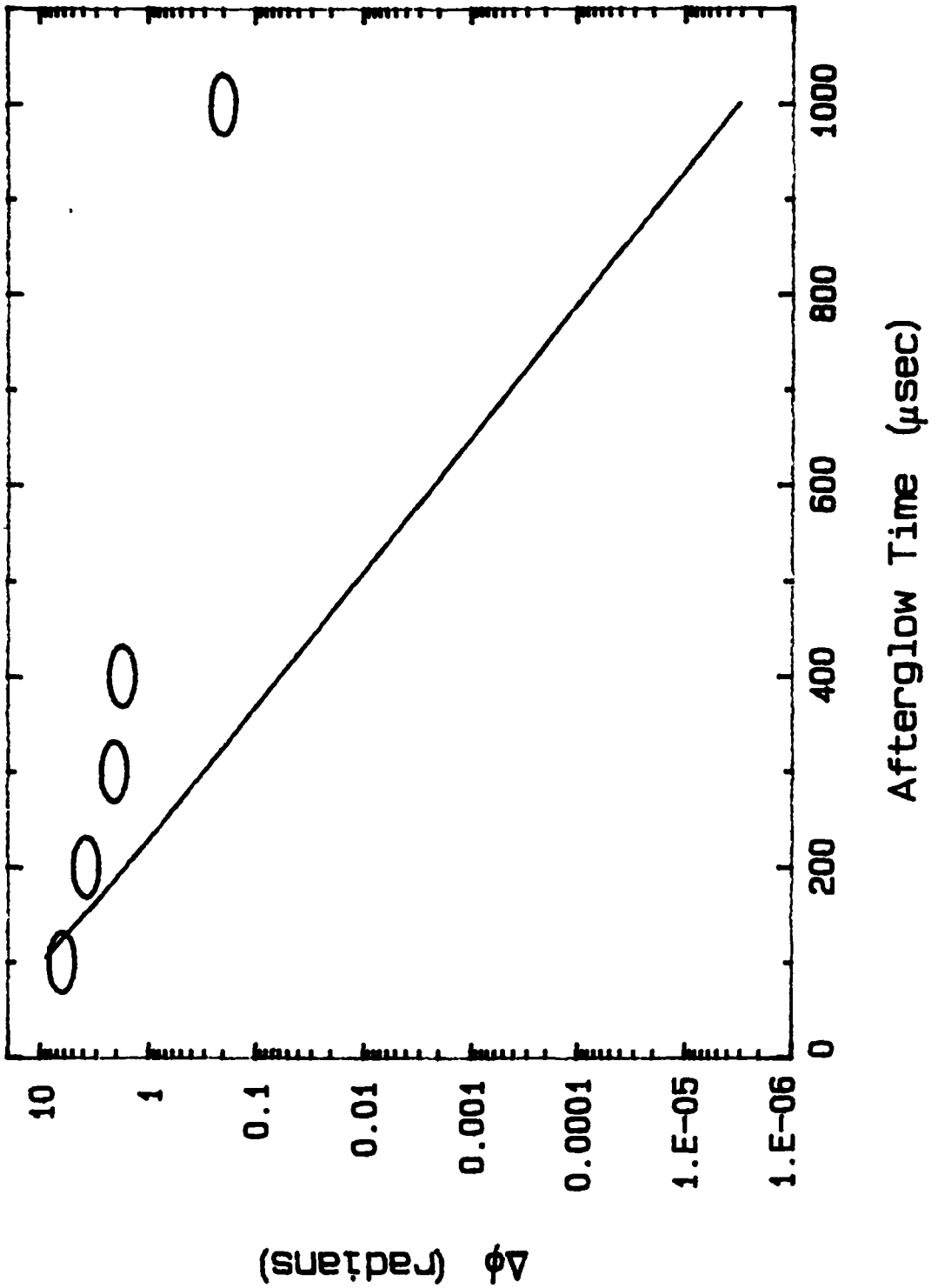

Figure 32. Comparison of calculated and measured phase change for N_2

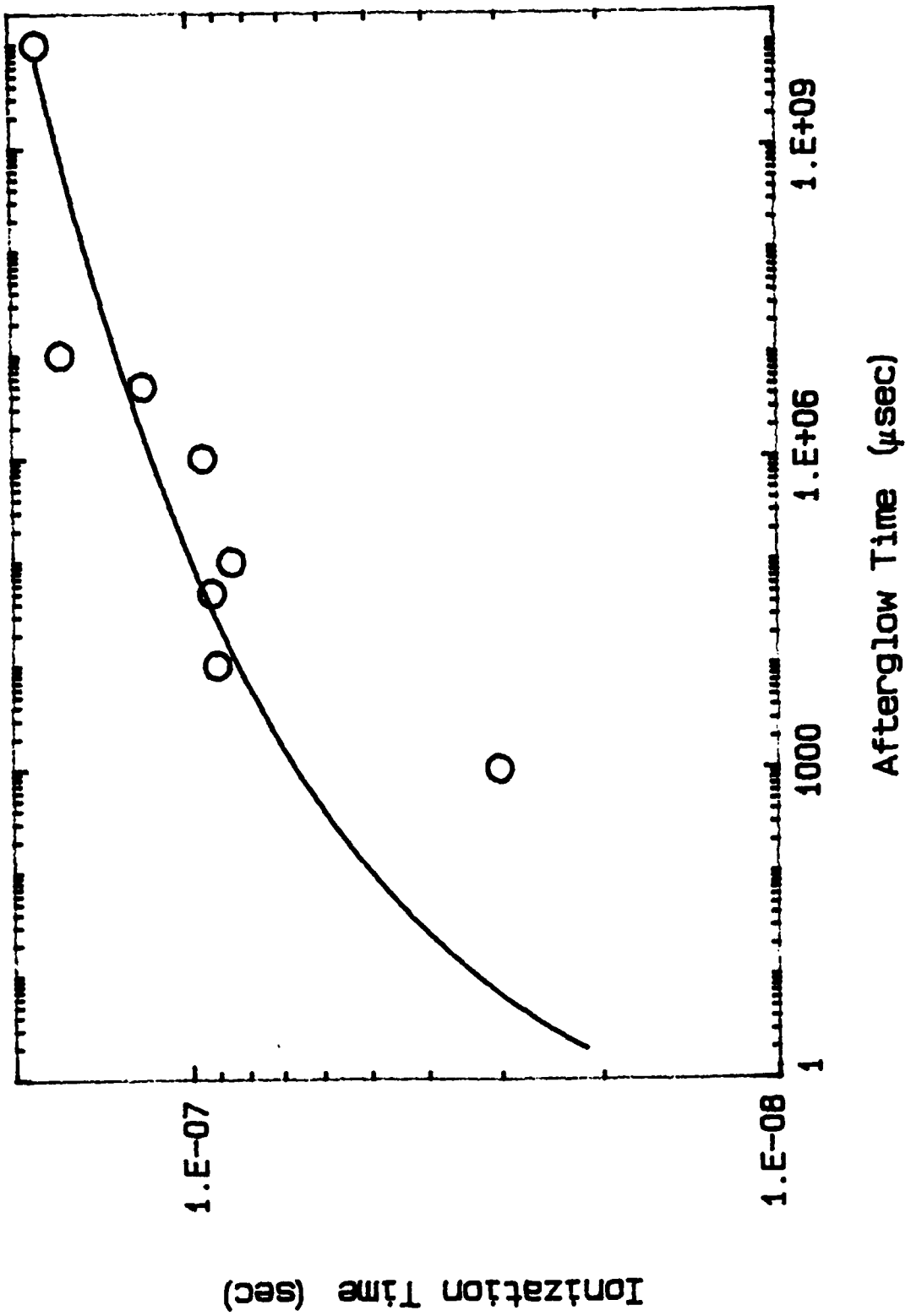

Figure 33. Comparison of Ar reionization theory and measurement

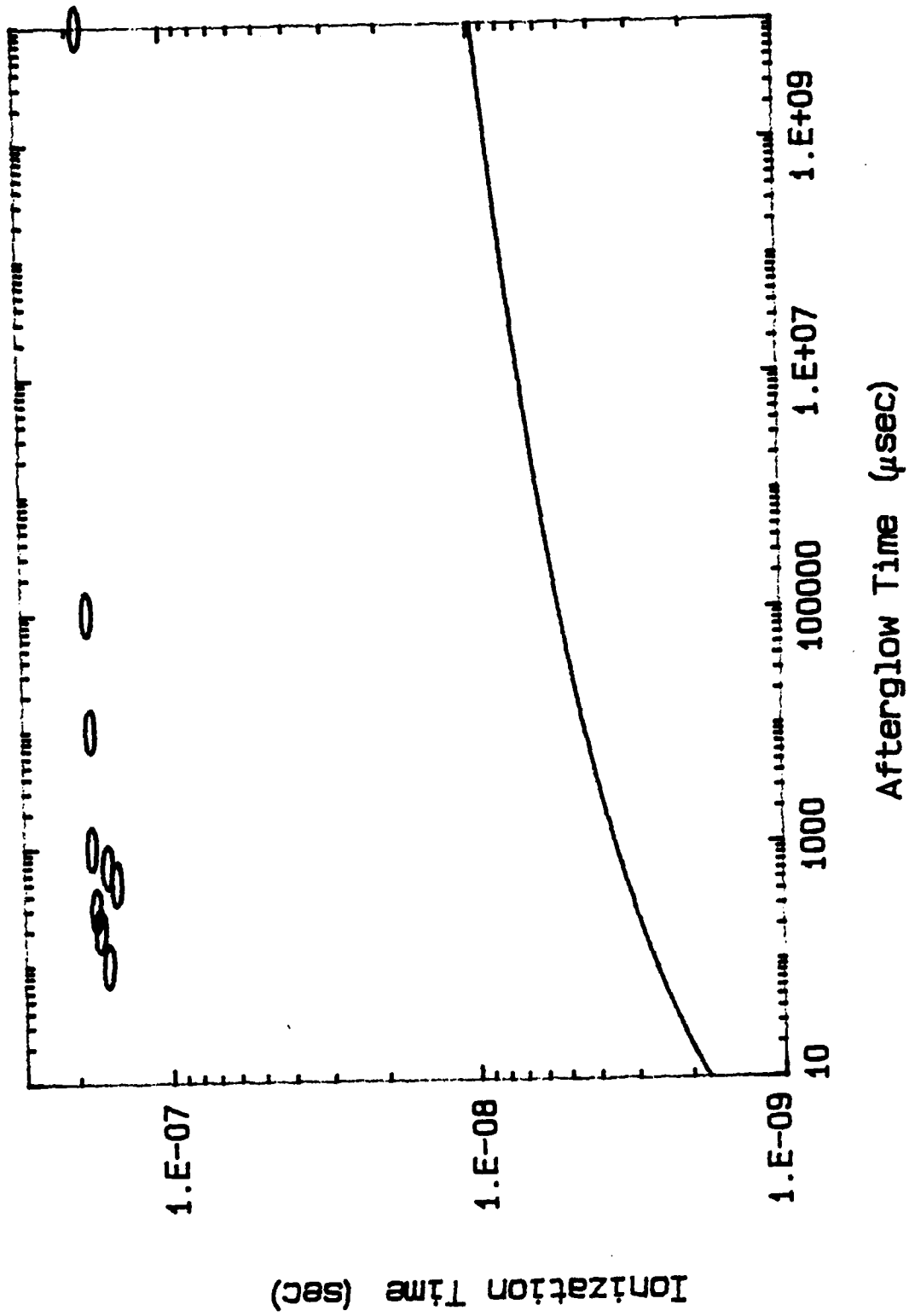

Figure 34. Comparison of N_2 reionization theory and measurement

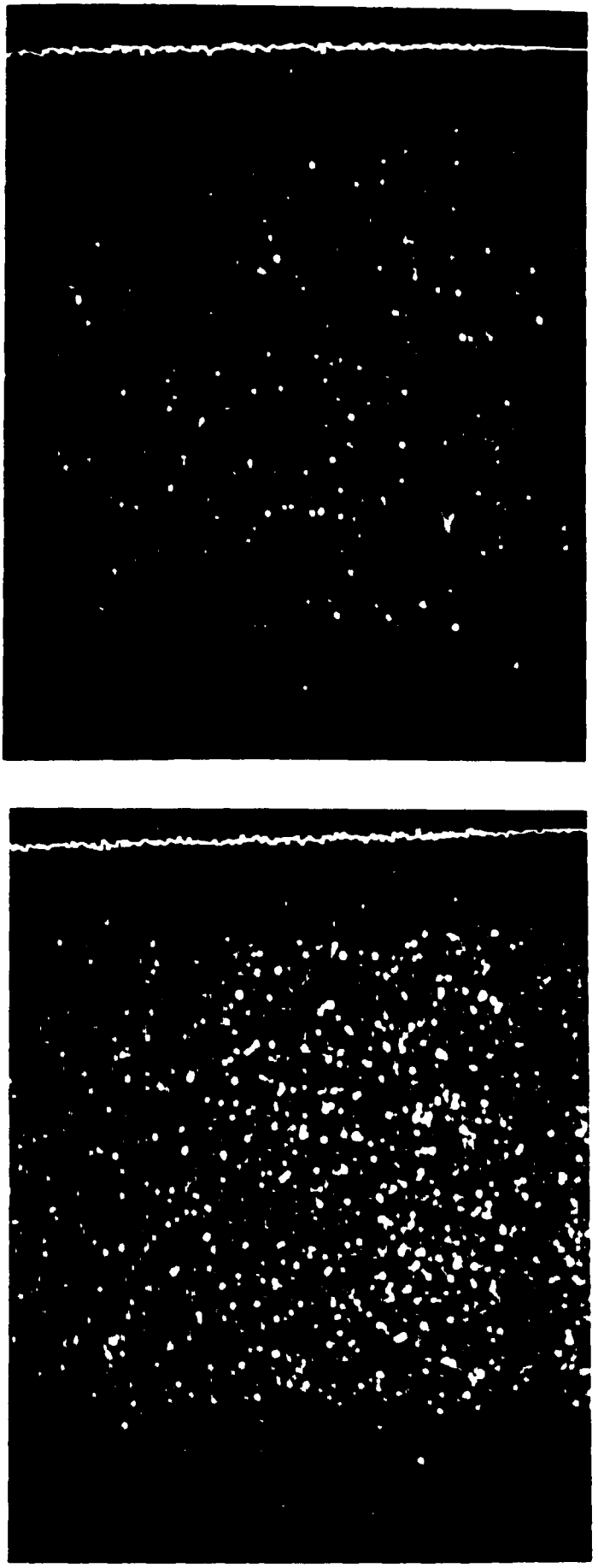

Figure 35. Streak data of Ar plasma column axis at τ_D = 10 μs. The upper photo is without the rf pulse and lower photo is during the rf pulse.

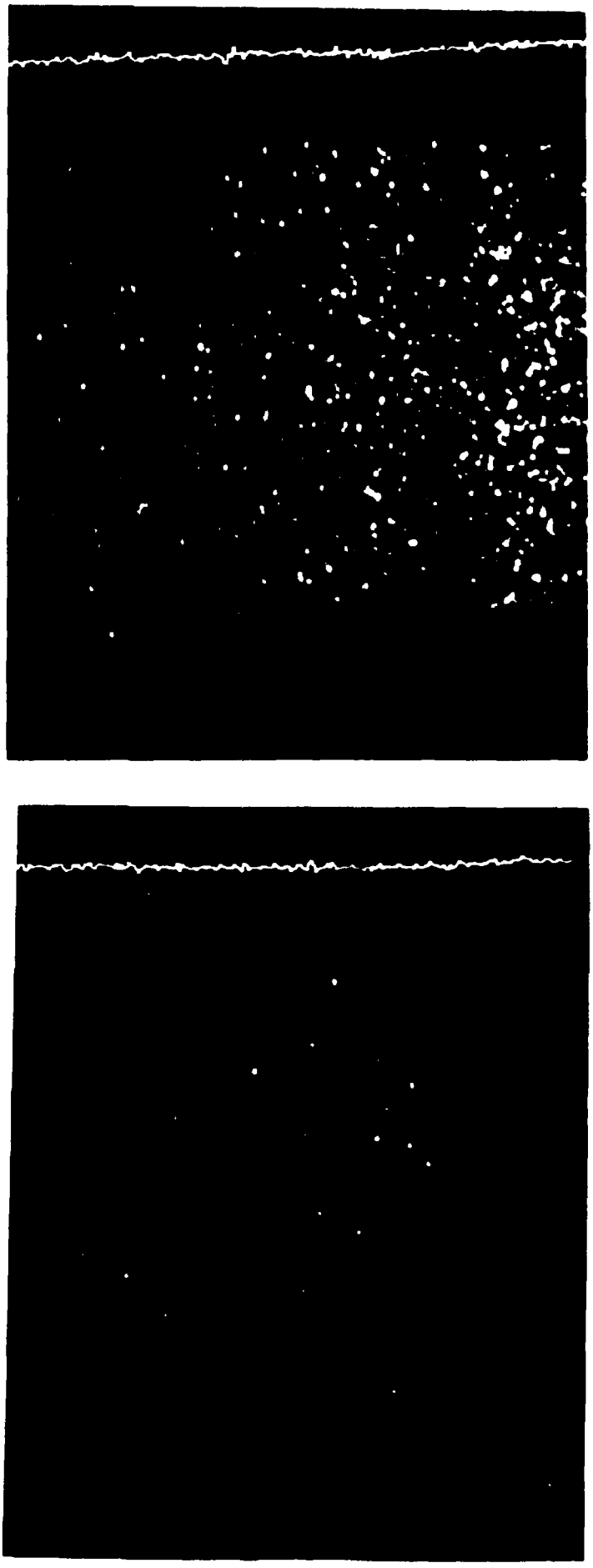

Figure 16. Streak data of Ar plasma column axis during the ... pulse. The upper photo is at τ_D = 1 ms and lower photo at ...

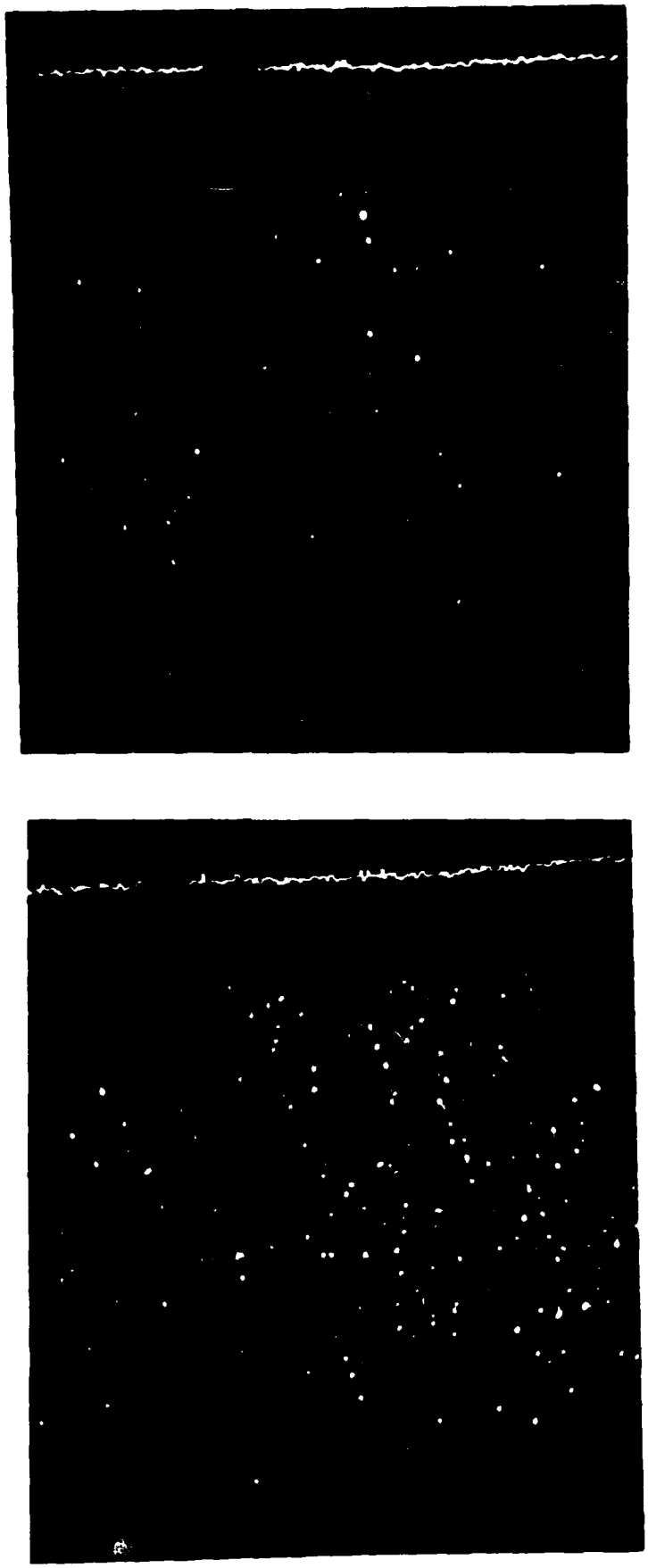

Figure 37. Streak data of Ar plasma column near the lucite window at τ_D = 10 μs. The upper photo is without the rf pulse and the lower photo is during the rf pulse.

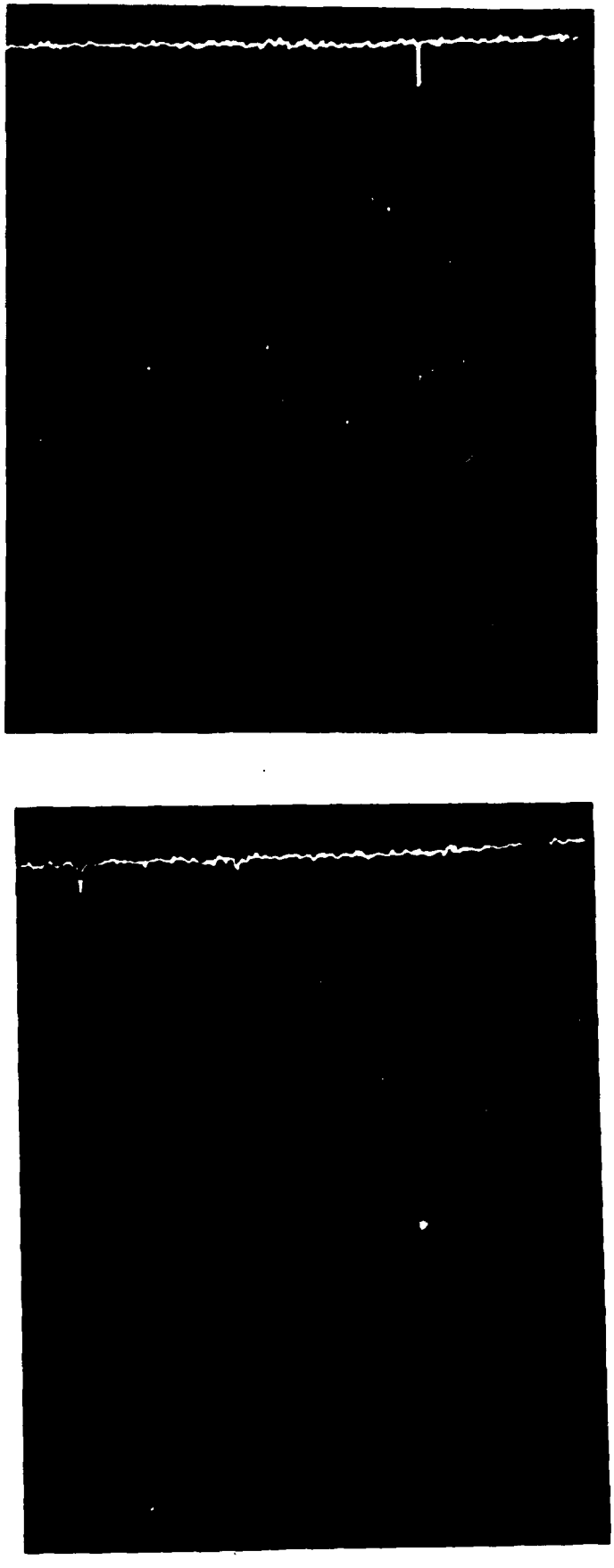

Figure 38. Streak data of Ar plasma column near the lucite window during the rf pulse. The upper photo is 1 ms into the afterglow, and the lower photo is 1 sec into the afterglow.

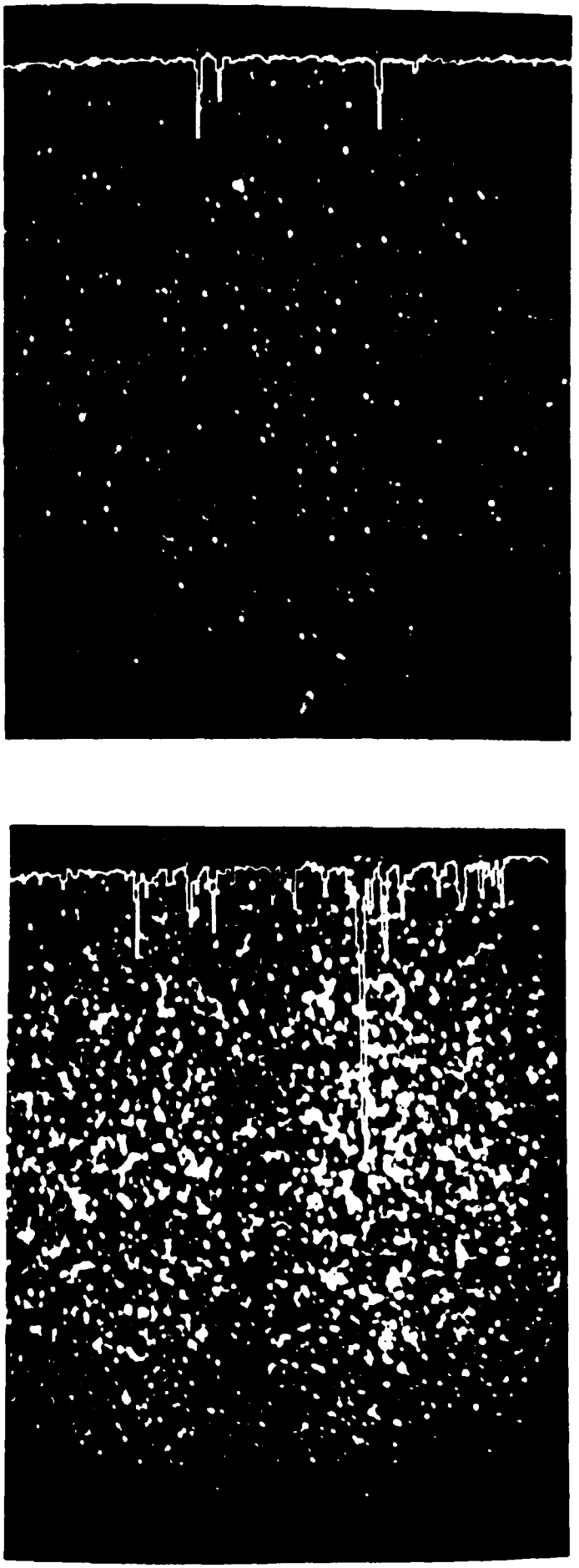

Figure 39. N_2 axis view at 10 μs afterglow time. The upper photo is without the rf pulse and the lower photo is during the rf pulse.

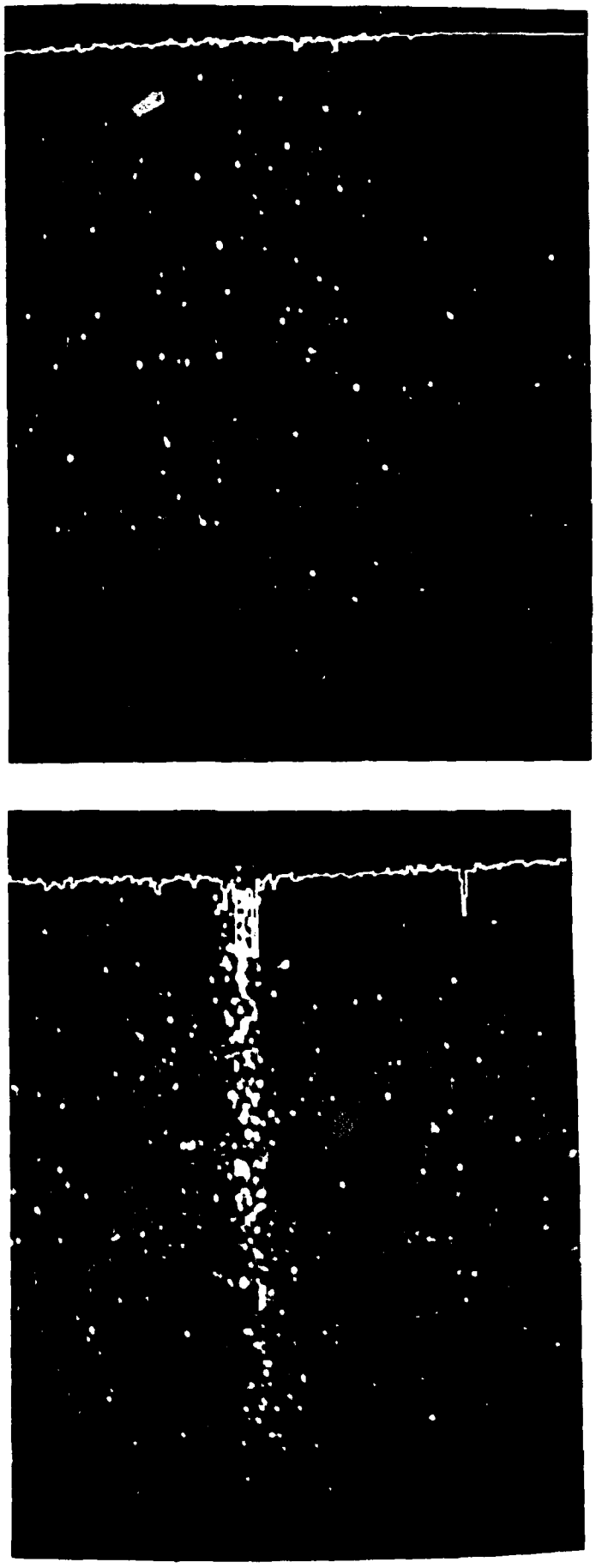

Figure 40. N_2 axis view at 1 ms afterglow time. The upper photo is without the rf pulse and the lower photo is during the rf pulse.

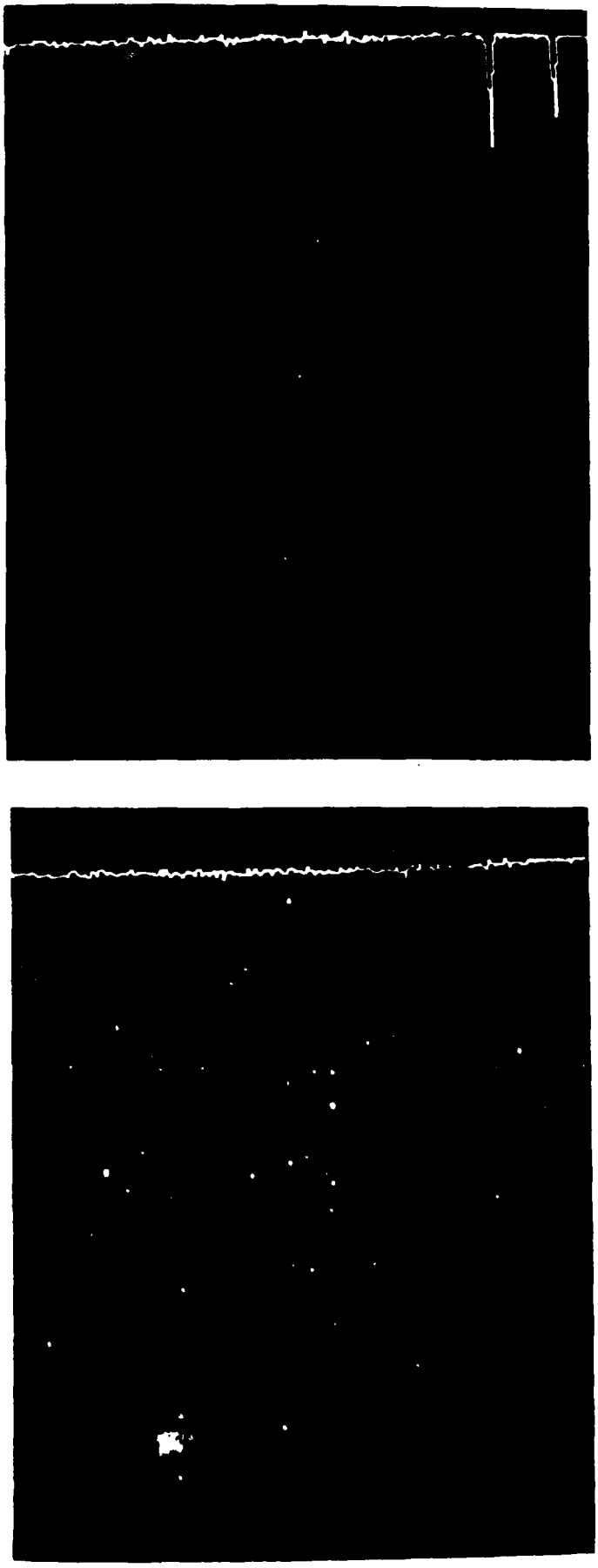

Figure 41. N_2 axis view at 1 sec afterglow time. The upper photo is without the rf pulse and the lower photo is during the rf pulse.

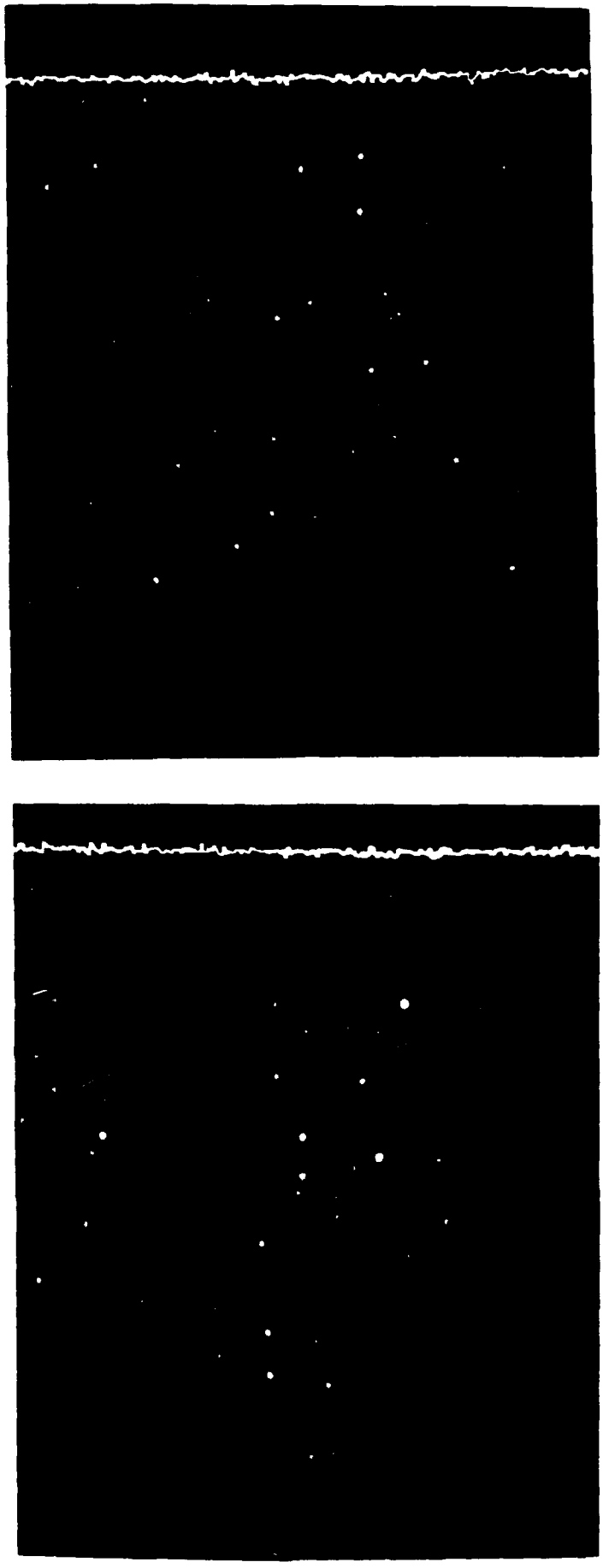

Figure 42. N_2 window view at 10 μs afterglow time. The upper photo is without the rf pulse and the lower photo is during the r- pulse.

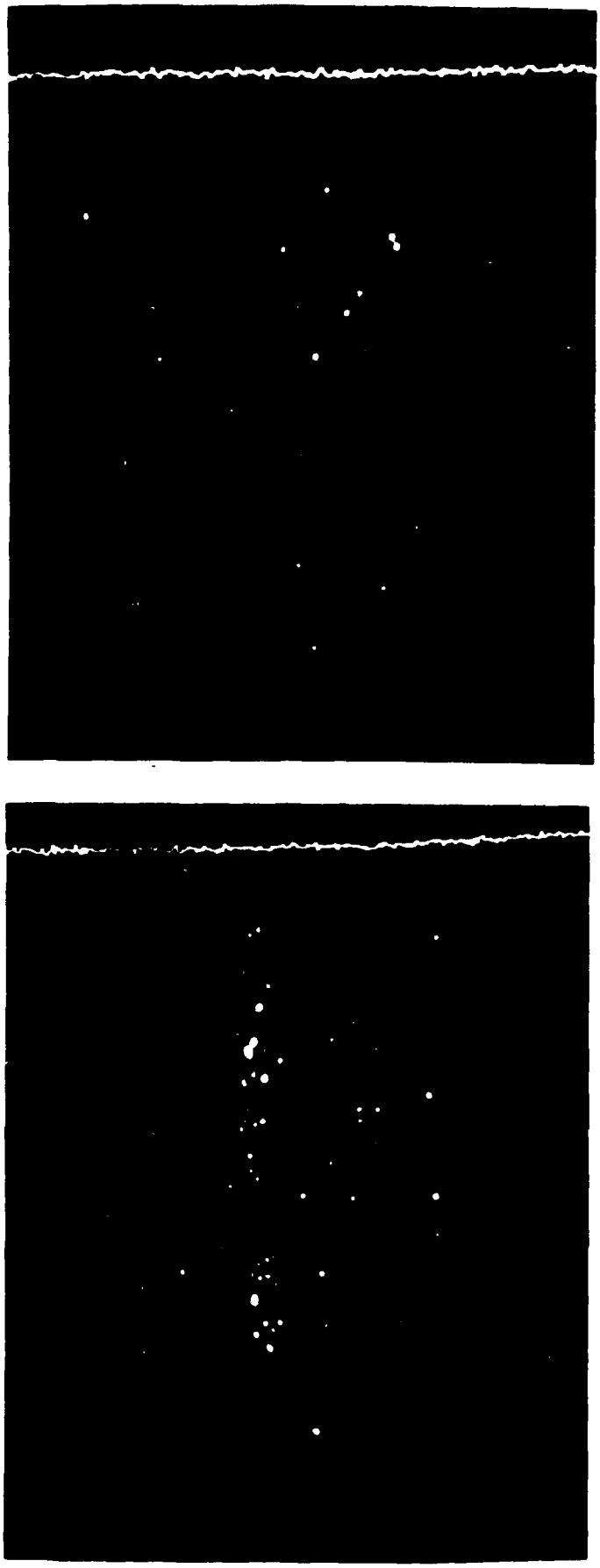

Figure 43. N_2 window view at 1 ms afterglow time. The upper photo is without the rf pulse and the lower photo is during the rf pulse.

Appendix 1. Double Langmuir Probes

This section describes how the measured current and the applied bias (V) are used to determine the double probe characteristics. A schematic of the double probe system is shown in Fig. 5. The data are generated on a point by point basis by varying the voltage from the battery supply across the probe tips. The oscilloscope photos (Fig. 6) show the voltage from the current monitor. A set of photos, typically 6 to 10, of various bias voltages are used to determine the curve shown in Fig. A1.1. The curve does not pass through the origin. This is not surprising because Borovsky[43] has shown that for probes used in monitoring high voltage discharges that the point of symmetry may lie at (I_0, V_0) rather than (0,0). If they were to pass through the origin, the normal equation to fit the points would be:

$$I(V) = I^*_{pi} \tanh (eV/T_e) \qquad (A1.1)$$

where I^*_{pi} is the ion saturation current and T_e is the plasma electron temperature. To account for the offset from the origin we replace I(V) by I(V) - I_0 and V by V - V_0. The resulting equation is:

$$I(V) = I_0 + I^*_{pi} \tanh [e(V-V_0)/T_e]. \qquad (A1.2)$$

A curve fitting the data is obtained by using a computer program which is provided the best estimate of the saturation values for $I(V_{max})$ and $I(V_{min})$, and a guess for the values of I_0 and V_0. The value of I^*_{pi} is simply ½ ($I(V_{max}) - I(V_{min})$). Equation A1.2 is then solved for T_e. Having found I^*_{pi} and T_e we can compute the plasma ion density as follows:

$$n\ (cm^{-3}) = 2\ I^{*}_{pi}/(e\ c_s\ A_{probe}), \qquad (A1.3)$$

where e is the electronic charge in coulombs, c_s is the ion acoustic velocity (cm/sec), A_{probe} is the double probe collecting area (cm^2). For the system considered the probe is constructed of 5 mil tungsten wire. A_{probe} is $2(\pi r^2+2\pi rl)$ = 0.0242 cm^2, where l= .3 cm (the probe length) and r=.00635 cm. Typical values on the plasma axis are $I^{*}_{pi} \sim .01$ A, $T_e \sim$ 5 to 10 eV. These values give $n \sim 1.8 \times 10^{13}\ cm^{-3}$.

The program then computes the plasma conductivity (σ) in cgs units, using the following formula[44]:

$$\sigma = \frac{\omega_{pe}^2}{4\ \pi\ \nu_c}\ . \qquad (A1.4)$$

Where ω_{pe} is the electron plasma frequency, and ν_c is the electron momentum transfer collision frequency. For weakly ionized gases, the major contribution to ν_c comes from the electron - neutral collision frequency (ν_{en}) For argon[45]:

$$\nu_{en} \approx 5.5 \times 10^{8}\ p_0\ T_e^{3/2} \qquad (A1.5)$$

where p_0 is the neutral gas pressure in Torr.

Equation A1.4 may also be used to compute the electron density (n) if σ is determined independently, since $\omega_{pe}^2 \propto n$. If the neutral gas is argon we find

$$n\ (cm^{-3}) = 4.4 \times 10^{11}\ \sigma\ (mho/m). \qquad (A1.6)$$

Likewise, while using nitrogen the relationship is

$$n\ (cm^{-3}) = 1.33 \times 10^{11}\ \sigma\ (mho/m). \qquad (A1.7)$$

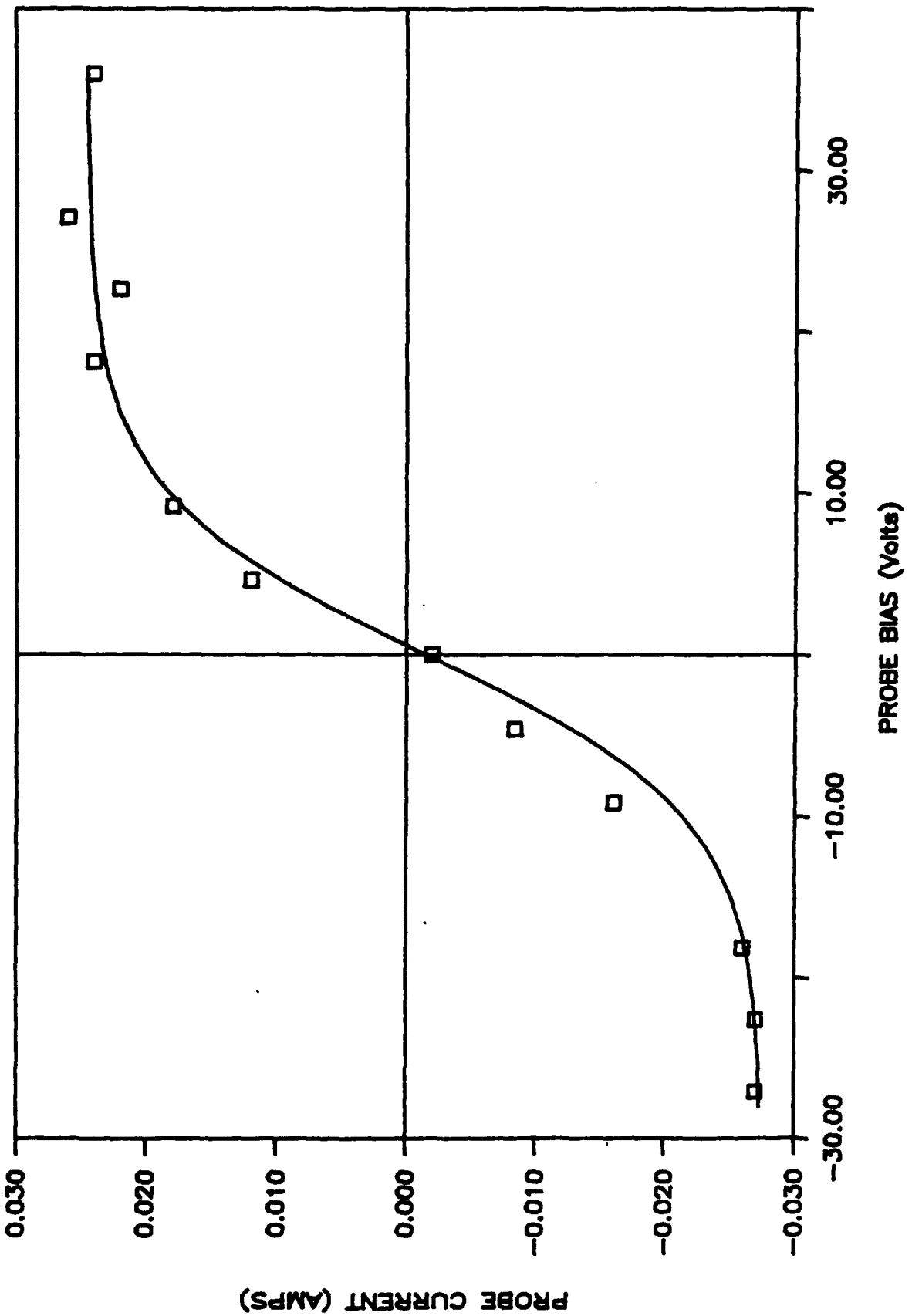

Figure A1.1 Double Langmuir probe curve fit to data

Appendix 2. Two Coil Conductivity Probe

The two coil conductivity probe was originally discussed by Mikoshiba and Smy[27]. The theory assumes that the conductivity of the medium is a scalar quantity. If one assumes that the plasma density or conductivity is homogeneous (over a radius $r \lesssim a$) the theory is greatly simplified. Our starting point is a system of coupled equations given by Faraday's and Ampere's laws:

$$\nabla \times \vec{E} = - i \omega \mu \vec{H} \qquad \text{(A2.1)}$$

$$\nabla \times \vec{H} = (\sigma + i \omega \epsilon) \vec{E}. \qquad \text{(A2.2)}$$

Where a harmonic time dependence is used ($e^{i\omega t}$), σ is the sample conductivity, and ϵ and μ are the dielectric permitivity and magnetic permeability. The field components are H_r, E_θ, and H_z. After some algebra one finds that the field components are:

$$H_r(r,z) = (A\, J_1(\alpha\, r) + B\, Y_1(\alpha\, r))e^{-mz} \qquad \text{(A2.3)}$$

$$H_z(r,z) = (F\, J_0(\alpha\, r) + G\, Y_0(\alpha\, r))e^{-mz} \qquad \text{(A2.4)}$$

$$E_\theta(r,z) = - \frac{m^2 - \alpha^2}{m\,(\sigma + i\omega\epsilon)} (H\, J_1(\alpha\, r) + L\, Y_1(\alpha\, r))e^{-mz}. \qquad \text{(A2.5)}$$

Where A, B, F, G, H, and L are constants to be set by the boundary conditions. J and Y are ordinary Bessel and Neumann functions of order 0 and 1. The final parameters are $\alpha^2 = m^2 + k^2 - i\lambda^2$ with m the eigenvalue from $d^2Z/dz^2 = m^2 Z$, $k^2 = \omega^2\mu\epsilon$, and $\lambda^2 = \omega\mu\sigma$. We also define a parameter $\gamma^2 = m^2 - k^2$, where α is replaced by γ for $r > a$ (where $\sigma = 0$).

Now for $r < a$, one wants the solution to be bounded,

this implies that B = G = L = 0. Using the E_θ equation from Ampere's law shows that for r < a, A=H=(m/α)F. Likewise for r > a, again A=H=(m/γ)F≡ β and B=G=(m/γ)L≡ η. We also know that the field components must be continuous at r = a for all z. This requires that m be the same for r<a and r>a. The field components are then given by:

r < a	r > a
$H_r = A\, J_1(\alpha r)e^{-mz}$	$H_r = (\beta J_1(\gamma r) + \eta Y_1(\gamma r))e^{-mz}$
$H_z = \frac{\alpha}{m} A J_0(\alpha r)e^{-mz}$	$H_z = \frac{\gamma}{m} (\beta J_0(\gamma r) + \eta Y_0(\gamma r))e^{-mz}$
$E_\theta = -\frac{m^2 - \alpha^2}{m(\sigma+i\omega\epsilon)} H_r$	$E_\theta = -\frac{m^2 - \gamma^2}{mi\omega\epsilon} H_r.$

Requiring continuity of the fields at r = a, we can write β and η in terms of A and the Bessel and Neumann functions evaluated at r = a. The constant A is determined from the fact that for σ = 0 we know that $H_z(r=b, z=0) = I/p$ where I is the current through the driver coil and p is a geometry factor. Therefore:

$$A = \frac{mI}{p} (J_1(\gamma a)\, Y_0(\gamma a) - Y_1(\gamma a)\, J_0(\gamma a)) \times \Big\{ \gamma J_1(\alpha a)\, [J_0(\gamma b)Y_0(\gamma a) - Y_0(\gamma b)J_0(\gamma a)] + \alpha J_0(\alpha a)\, [J_1(\gamma a)Y_0(\gamma b) - J_0(\gamma b)Y_1(\gamma a)] \Big\}^{-1}. \qquad \text{(A2.6)}$$

Then substituting into the equations for H_r and H_z at r = a one finds that

$$\beta = A \left\{ \frac{J_1(\alpha a)Y_0(\gamma a) - (\alpha/\gamma)\, J_0(\alpha a)Y_1(\gamma b)}{J_1(\gamma a)Y_0(\gamma a) - Y_1(\gamma a)J_0(\gamma a)} \right\} \quad \text{(A2.7)}$$

$$\eta = A \left\{ \frac{-J_1(\alpha a)J_0(\gamma a) + (\alpha/\gamma)\, J_0(\alpha a)J_1(\gamma a)}{J_1(\gamma a)Y_0(\gamma a) - Y_1(\gamma a)J_0(\gamma a)} \right\} . \quad \text{(A2.8)}$$

The above formalism is used to find E_θ for r > a. Then E_θ is used to determine the voltages induced on the receiver coils for cases with and without a conducting material within the coils. The voltage induced on one receiver coil while the conducting medium is inside the probe is $V = 2\pi b\, E_\theta(r=b,\ \sigma>0)$. The induced voltage without the conducting medium is $V_0 = 2\pi b\, E_\theta(r=b,\ \sigma=0)$. The ratio of the two voltages is given by:

$$\frac{V}{V_0} = \frac{J_0(\gamma b)}{J_1(\gamma b)}\, \phi(\sigma f) \quad \text{(A2.9)}$$

where

$$\phi(\sigma f) = \frac{\gamma\, J_1(\alpha a)\, C_1 + \alpha\, J_0(\alpha a)\, C_2}{\gamma\, J_1(\alpha a)\, C_3 + \alpha\, J_0(\alpha a)\, C_4}$$

$$C_1 = J_1(\gamma b)\, Y_0(\gamma a) - J_0(\gamma a)\, Y_1(\gamma b)$$
$$C_2 = J_1(\gamma a)\, Y_1(\gamma b) - J_1(\gamma b)\, Y_1(\gamma a)$$
$$C_3 = J_0(\gamma b)\, Y_0(\gamma a) - J_0(\gamma a)\, Y_0(\gamma b)$$
$$C_4 = J_1(\gamma a)\, Y_0(\gamma b) - J_0(\gamma b)\, Y_1(\gamma a) .$$

The equation for V/V_0 has been evaluated by computer for a range of σf values. These values of V/V_0 can then be used to determine the conductivity when the frequency is known or the frequency when the conductivity is known. For

verification purposes the frequency can be varied while σ, a, and b are held constant. The variation with frequency should generate a graph as shown in Fig. A2.1.

The useful frequency range is found by looking at both receiver coils independently for a given conductivity sample. The magnitudes of the voltages measured by each coil should be equal. When wide disagreement of the voltages occurs, the useful frequency range has been exceeded.

For the probe used the useful range of the product σf is 10^8 to 10^{11} Hz-mho/m. For example, using Poco graphite which has a conductivity of order 10^4 mho/m restricts the useful frequency range to 10^4 Hz $< f <$ 10^6 Hz. Likewise for a plasma with a conductivity of order 10 to 100 mho/m limits the useful frequency range to be 10^6 Hz $< f <$ 10^8 Hz.

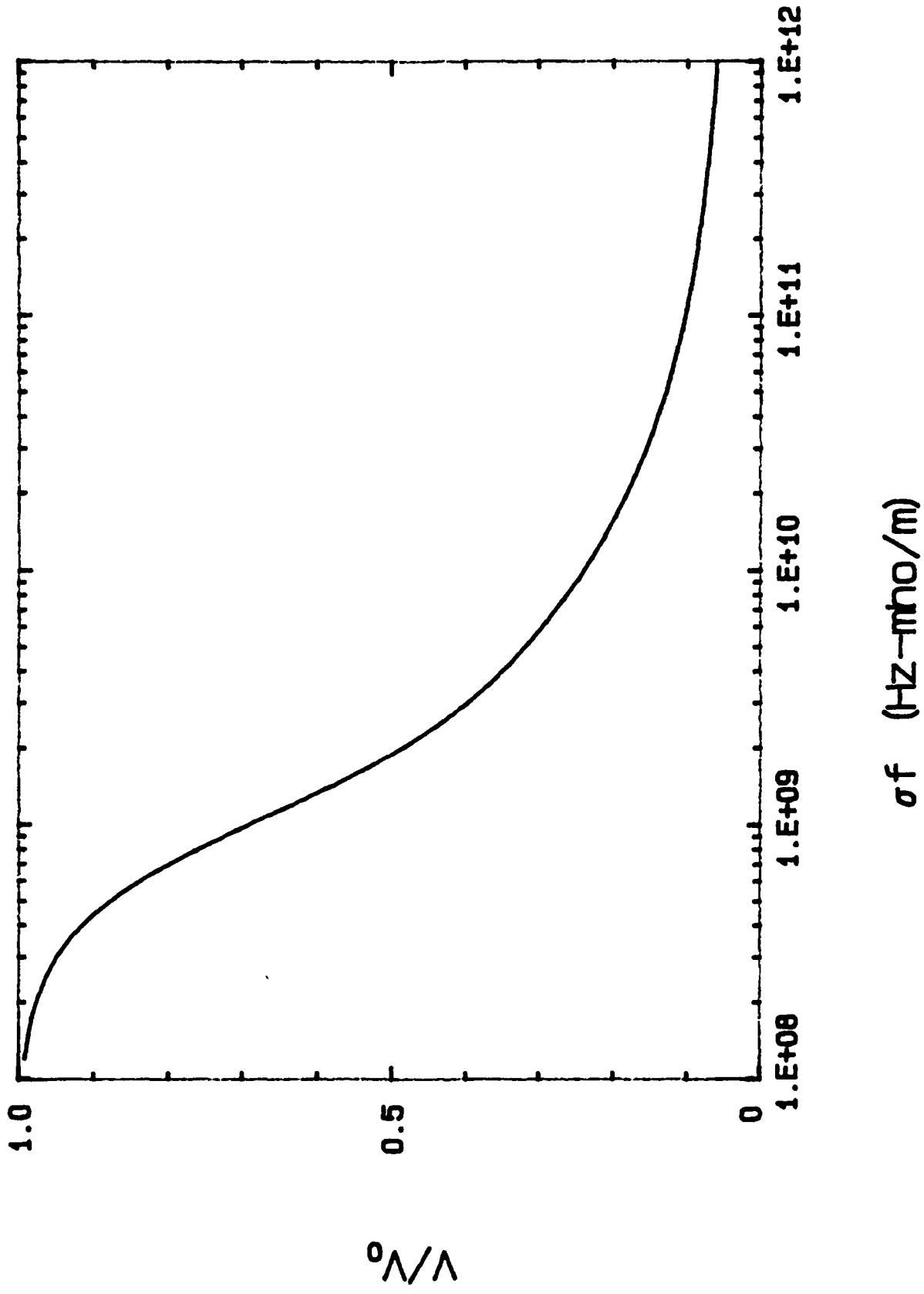

Figure A2.1 Calculated variation of V/V_0 with σf

Appendix 3. Criteria for Transmission through a Dielectric Window

The relationship between frequency, wavelength, and window thickness is derived[35] in this appendix. The derivation is independent of the microwave power level, but the angle of incidence is assumed to be very small, measured from the surface normal. The geometry is shown in Fig. A3.1. The angle of incidence is exaggerated for clarity. We define the following quantities for waves propagating toward $+\infty$: r_A and t_A are the reflection and transmission coefficients at interface A, and r_B and t_B are the coefficients at interface B. In addition we need coefficients for propagation toward $-\infty$ and we'll use r'_A, t'_A, r'_B, and t'_B where the convention is consistent with earlier use. Now using an incoming wave from $-\infty$ of amplitude E_0, the rays $r_A E_0$ and $t_A E_0$ are generated at interface A. The transmitted wave travels to the second surface with a phase change of e^{ikd} due to the distance traveled and then we generate a reflected wave $r_B t_A E_0$ and a transmitted wave $t_B t_A E_0$. The reflected wave from interface B will generate an infinite number of waves of decreasing amplitude. Summing all the waves propagating from interface A toward $-\infty$. We find:

$$\begin{aligned} E_r &= E_0 \left(r_A + t_A r_B t'_A e^{i2kd} + t_A r_B^2 r'_A t'_A e^{i4kd} + \ldots\right) \\ &= E_0 \left(r_A + t_A t'_A r_B e^{i2kd} \left(\Sigma_m \left(r_B r'_A e^{i2kd}\right)^m\right)\right) \\ &= E_0 \left(r_A + t_A t'_A r_B e^{i2kd} \left(1 - r_B r'_A e^{i2kd}\right)^{-1}\right). \end{aligned} \quad (A3.1)$$

Where $k = 2\pi \tilde{n}/\lambda$, $\tilde{n}$ is the index of refraction of the medium at wavelength λ, and d is the window thickness. We also assume that a plane wave is incident which means that H_0 =

E_0, $H_r = -E_r$, and $H_t = n E_t$ where we have equated the amplitudes of the incident, reflected and transmitted electric and magnetic fields. The matching condition on the tangential components of the electric and magnetic fields at interface A are:

$$E_0 + r_A E_0 = t_A E_0 \quad \text{or} \quad 1 + r_A = t_A \tag{A3.2}$$

and

$$H_0 + H_r = H_t \quad \text{or} \quad 1 - r_A = n t_A = n + n r_A \tag{A3.3}$$

therefore

$$r_A = (1 - n)/(1 + n). \tag{A3.4}$$

Now the matching condition at interface B is:

$$1 + r_B = t_B \tag{A3.5}$$

and

$$1 - r_B = t_B/n \tag{A3.6}$$

or

$$r_B = (n - 1)/(n + 1) = -r_A. \tag{A3.7}$$

We also know the Stoke's relations $r_A' = -r_A$ and $1 = t_A t_A' + r_A^2$. These tell us that:

$$\begin{aligned} E_r/E_0 &= [r_A - r_A r_B r_A' e^{i2kd} + r_B t_A t_A' e^{i2kd}]/(1 - r_B r_A' e^{i2kd}) \\ &= [r_A + r_B e^{i2kd}(t_A t_A' - r_A r_A')]/(1 - r_B r_A' e^{i2kd}) \\ &= [r_A + r_B e^{i2kd}]/(1 + r_B r_A e^{i2kd}). \end{aligned} \tag{A3.8}$$

If $E_r = 0$, $r_A + r_B e^{i2kd} = 0$. So that $r_A = 0$ or $e^{i2kd} = 1$. The latter, more general, condition requires that $2kd = 2\pi\ell$ where ℓ is an integer. The condition then is $d = \frac{1}{2}(\lambda/\tilde{n})\ell$, i.e. the window must be an integral number of half-wavelengths in the medium of the window.

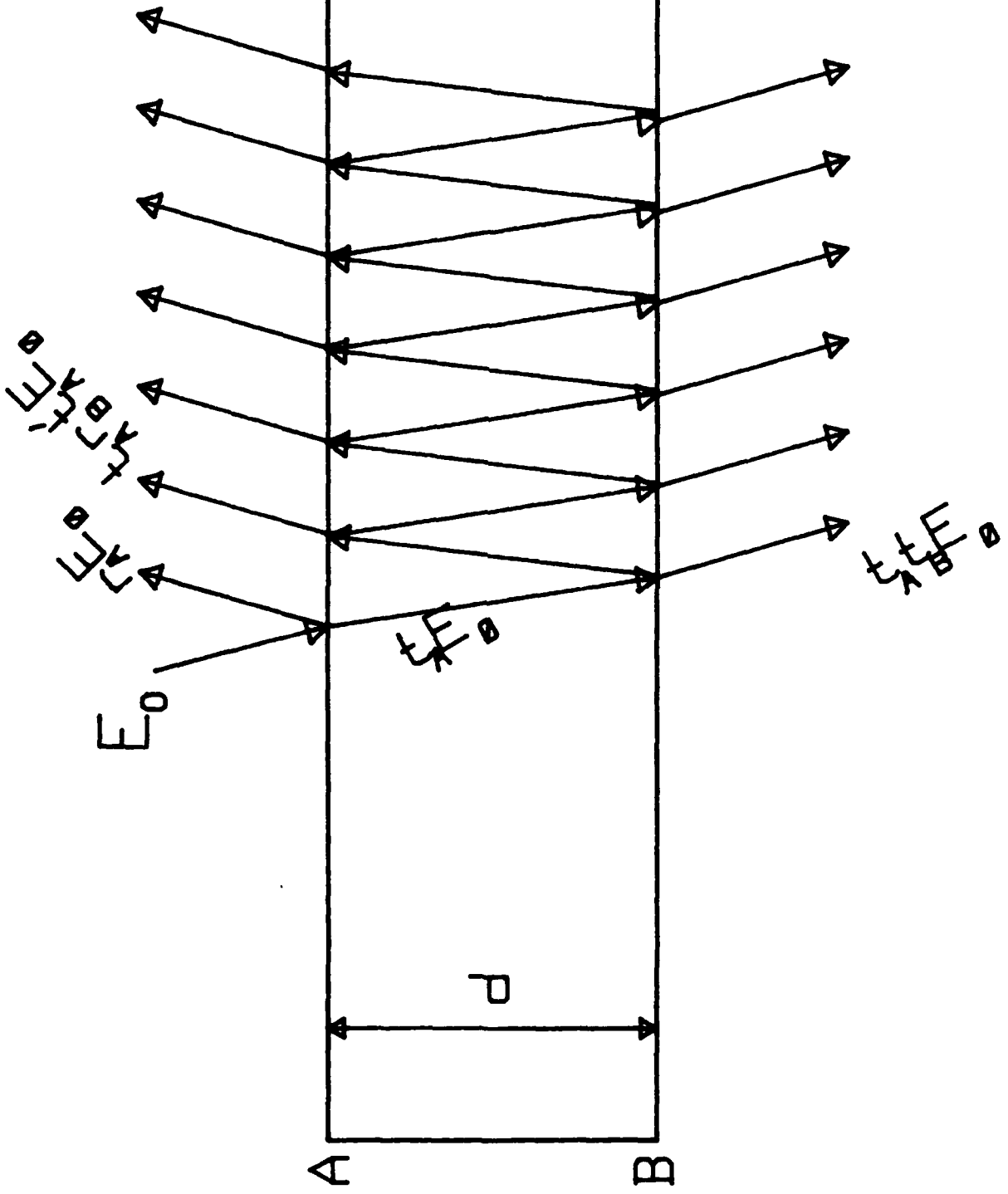

Figure A3.1 Diagram of microwave transmission through a dielectric window

Appendix 4. Microwave Detectors and Calibration

The apparatus used for measuring the various signals from the magnetron are typically uncalibrated. One has to use tables or graphs to relate the measured output to the applied input. A system of hardware and software exists to acquire and reduce calibration data[32,33].

The hardware involves a computer controller, a CAMAC crate containing an analog to digital converter(ADC), and a Hewlett-Packard sweep oscillator. The computer is used to direct the sweep oscillator as a standard output source, and the measurements with the various detectors are measured by the ADC and stored by the computer. The inputs to the computer are stored into a data file for later processing by other software on a mini-computer into a useable fashion. There is some additional hardware used, which includes thermistor and thermocouple rf power meters, x-y chart recorders, and a frequency counter.

The devices we need to calibrate are: 1) crystal diode detectors, 2) coaxial and waveguide directional couplers, 3) standard waveguide sections, and 4) coaxial cable. All of the above diagnostic components are power level insensitive except for the crystal detectors. Therefore our typical calibration will involve varying a continuous wave rf source in frequency and measuring the ratio of input to output power. The crystal diode detectors require variation of the power level and is done by an additional program loop which completes the variation of the frequency at each power level.

We begin our discussion with the calibration of the pickoff ratio of the coaxial and waveguide directional couplers. Next the calibration of the loss by coaxial attenuators and coaxial cables are discussed. Finally the calibration of the response of the crystal detectors to the applied microwave signal is discussed.

The directional couplers are calibrated by measuring the power on both the direct or through port and the pickoff port as a function of frequency. The power is measured by power meters and the output sent to the ADC for acquisition by the computer. The data file generated then has three entries per line (after the header data block) which are: 1) frequency, 2) through power level, 3) pickoff power level. A program is used to take the measured data and compute the dB value of the pickoff port below the through power as a function of frequency. The dB value is computed as:

$$dB = 10 \log(P_{in}/P_{out}) \qquad (A4.1)$$

The program also generates a graph of the dB value vs. frequency, and writes a data file of the frequency and dB value. Both are used in data reduction.

The coaxial attenuators and cables are calibrated in the following fashion. Two coaxial directional couplers are used to measure the power towards the test object and the power reflected from the test object. Power meters are used to measure the power on the pickoff ports of the directional couplers. A third power meter is used on the end of the device under test (cable/attenuator). A data file is

generated listing the frequency, incident pickoff power, reflected pickoff power, and through power. This raw data file is then accessed by another program to again compute the dB vs. frequency for a test object. This calculation involves deciding if the reflected power is to be used in computing a net power applied to the test object. One has the option of using either the net power or incident power for the calibration. Again a graph of dB vs. frequency and a data table are generated for later use.

As stated above, crystal calibration involved some extra work. The two complications are power variation, and small signal levels. The power sweep is incorporated as another loop in the program. The program sets the power level, loops through the frequency range, increments the power level, loops through the frequency range, and repeats until all power and frequency values are measured. The small signal level is due to the limited power handling ability of the crystals themselves, and the power output ability of our sweep oscillator. This problem is made worse by the input voltage ranges available on the ADC. When one has a signal <20 mV on a 5 V full scale range for a 12 bit ADC one loses almost all the accuracy of one's measurement. A solution to this is a variable gain amplifier. One simply sets the amplifier to a selected value, read the voltage, and then in software divide by the gain value. The amplifier uses a 741 operational amplifier with a potentiometer to give a variable gain inverting amplifier. The amplifier inverts the signal

because the ADC is setup for a positive input and the crystal detectors are setup to provide a negative voltage at the output.

The data files generated for the crystals have the following format for each power level used in the calibration. A line is written showing the power level. On the next line the frequency of the oscillator, the power from the oscillator on the incident directional coupler,the power reflected from the crystal on the reflected directional coupler, and last in the row is the crystal voltage into a 50 Ω terminator. The data file is then used by a program to generate two sets of tables and graphs. One of the tables shows the applied power, either net or incident, as a function of the oscillator power output and frequency. The second table shows the measured crystal voltage as a function of the oscillator power output and frequency.

The two data files can then be accessed by another program which computes the crystal voltage as a function of power for a chosen rf frequency. This program has been setup to allow one to give it a measured voltage and based on the two calibration files the program will provide the rf power level that generated the voltage. This is done by using a cubic spline interpolation on the measured values. Having the program compute the answer gives one at least three, and possibly four, significant digits.

Appendix 5. Interferometer

The theory behind using an interferometer[1,2] to relate the change in phase to a change in the plasma density is well understood for systems using microwave frequencies with critical densities far above the plasma density. The difficulty comes in when one tries to interpret the phase change as the plasma approaches the critical density. All the approximations typically used are useless, and other techniques such as numerical integration must be used to relate measured phase changes to related plasma density changes.

This technique has been used on both argon and nitrogen and a discussion of the method is given below. The relationship between the change in phase and the plasma density is:

$$\Delta\phi(t) = \frac{2\pi}{\lambda}\int_{-r_w}^{r_w}(1 - n(z,t))\,dz \qquad (A5.1)$$

where $n(z,t) < 1$ is the index of refraction of the plasma column. The variable of integration is the diameter of the plasma column. For the system under consideration $n(z,t) = \epsilon^{1/2}(z,t)$ where ϵ is the dielectric constant. The z dependence is given by $[1-(z/r_w)^4]$, while the time dependence for Argon is $[1 + \beta t]^{-1}$ and for N_2 is $e^{-\nu t}$. The equation then becomes:

$$\Delta\phi(t) = \frac{2(2\pi)}{\lambda}\int_0^{r_w}\left[1 - \left\{1 - \frac{n_0 g(t)}{n_c}\left[1 - \left(\frac{z}{r_w}\right)^4\right]\right\}^{1/2}\right] dz \qquad (A5.2)$$

where g(t) is a generic function to cover the decay for both argon and N_2. The front factor of 2 is due to using the symmetry of the plasma column to speed the numerical integration.

One immediate observation is that if the density on axis is beyond cutoff there will be a time delay before any microwave power is detected on the far side of the plasma. Again the only problem is having sufficient knowledge about the density profile along the path of integration.

REFERENCES

1. Plasma Diagnostics with Microwaves, by M.A. Heald and C.B. Wharton, Wiley, 1965

2. Intro. to Experimental Plasma Physics, by A.Y. Wong, UCLA Physics Dept., 1977

3. "The Plasma Resonator", A. Dattner, Ericsson Technics, 309(13), 1957

4. "Angular Distribution of Radiation Scattered Coherently by a Plasma Cylinder", A.R. Jones and E.R. Wooding, J. Appl. Phys., 37(13), Dec. 1966

5. "Breakdown in air-filled microwave waveguides during pulsed operation", D. Anderson, M. Lisak, and T. Lewin, J. Appl. Phys, 56(5), 1 Sept. 1984

6. "Intense Microwave pulse propagation through Gas Breakdown plasmas in a Waveguide", D.P. Byrne, Ph.D. Thesis, Lawrence Livermore Nat. Lab., UCRL-53764 (1986)

7. "High-power microwave energy coupling to Nitrogen during breakdown", W.M. Bollen, C.L. Yee, A.W. Ali, M.J. Nagurney, and M.E. Read, J. Appl. Phys., 54(1), Jan. 1983

8. "Microwave-energy coupling in a nitrogen-breakdown plasma", C.L. Yee, A.W. Ali, and W.M. Bollen, J. Appl. Phys., 54(3), March 1983

9. "Microwave absorption and plasma heating due to microwave breakdown in the atmosphere", W. Woo and J.S. DeGroot, Phys. Fluids, 27(2), Feb. 1984

10. "Air-Breakdown Limits for microwave pulse propagation: Pt 1", D.P. Byrne, R.A. Alvarex, R.M. Johnson, UCID-19877 Part 1, Sept. 1983

11. "Propagation and Breakdown in Air of Short Burst, High-Power Microwaves", C. Sullivan, H. Rappaport, P.E. Latham, W.W. Destler, and C.D. Striffler, Bull. of the APS, 32(9), October 1987

12. "High-frequency Breakdown of Gases" by J.D. Craggs, Chap. 8 of Electrical Breakdown of Gases by J.M. Meek and J.D. Craggs (John Wiley & Sons, New York)

13. Microwave Breakdown in Gases, A.D. McDonald (1966, John Wiley & Sons, New York)

14. "Theory of microwave pulse propagation during gas breakdown: Linear approximation", R.T. Robiscoe, J. Appl. Phys. 58(9), 1 Nov. 1985

15. "High E/n ionization rates and ionization induction times and High Intensity Microwave propagation in Molecular gases.", L.C. Pitchford, Y.M. Li, G.N. Hayes, J.B. Gerado, and J.T. Verdeyen, Proc. of the 3rd Nat. Conf on High Power Microwave Technology for Defense Applications, Dec. 1986

16. "High Power Microwave Propagation in the Atmosphere-Tail Erosion", C.L. Yee, R.R. Johnston, and D.A. Keeley, Proc. of the 3rd Nat. Conf on High Power Microwave Technology for Defense Applications, Dec. 1986

17. "Air Breakdown Limits for High Power Microwave Systems", G. August, Proc. of the 3rd Nat. Conf on High Power Microwave Technology for Defense Applications, Dec. 1986

18. "Kinetic Theory of Microwave Breakdown and Absorption in Air", R. Roussel-Dupre, T. Murphy, and A. Johnson, Proc. of the 3rd Nat. Conf on High Power Microwave Technology for Defense Applications, Dec. 1986

19. "Scaling Laws of Tail Erosion", B. Goldstein and C. Longmire, DNA-TR-86-298, Jan. 1987

20. "Results of High Power Microwave Propagation Research", Bart Goldstein and Conrad Longmire, Proc. of the 3rd Nat. Conf on High Power Microwave Technology for Defense Applications, Dec. 1986

21. W.T. Armstrong-private communication

22. Basic Data of Plasma Physics, 1966, by S.C. Brown, The M.I.T. Press, 1967

23. Classical Electrodynamics, by J.D. Jackson, John Wiley & Sons, 1975

24. "Breakdown Voltage Characteristics" by D.T.A. Blair, Chap. 6 of Electrical Breakdown of Gases by J.M. Meek and J.D. Craggs (John Wiley & Sons, New York)

25. Intro. to Electrical Discharges in Gases, by S.C. Brown, John Wiley & Sons, 1966

26. "Electric Probes", by F.F. Chen in Plasma Diagnostic Techniques, ed. by R.H. Huddlestone and S.L. Leonard, Academic Press, 1965

27. "Two Coil rf Determination of Plasma Conductivity", S. Mikoshiba and P.R. Smy, Rev. of Sci. Instrum., 40(9), Sept. 1969

28. "Plasma Conductivity Experiments on Pulsed High-Voltage Discharges by Two Coil Rf-Probe", K.J. Hendricks, M.C. Clark, D.J. Ulrich, and L.K. Len, AFWL-TR-84-06, July 1984

29. Instruction Manual on the CT-1 and CT-2 -Tektronix, 1963

30. POCO Graphite-Union 76 spec sheet, 1980

31. "X-Band Magnetron Source", K.J. Hendricks, AFWL-AWP-ITR-87-01, June 1987

32. "Microwave Calibration System", K.J. Hendricks, AFWL-MTYP-TN-84-004, July 1984

33. "Microwave Calibration System II", K.J. Hendricks, G. DeMuth, and L. Torraca, AFWL-TR-97-119, April 1988

34. Antenna Design using Personal Computers, by David M. Pozar, Artec House, 1985

35. Univ. of Chicago Graduate Problems in Physics, by J.A. Cronin, D.F. Greenberg, and V.L. Telegdi, Univ. of Chicago Press, 1979

36. Double Balanced Mixers-ANAREN Microwave Components Catalog 1984

37. Coaxial Phase Shifters-Narda Catalog 24, 1986

38. Hamamatsu Camera Manuals

39. Intro. to Plasma Physics, by F.F. Chen, Plenum Press, 1977

40. Spectra of Diatomic Molecules, 2nd ed., by G Herzburg, D. Van Nostrand Co., 1965

41. "The Absorption of Microwaves by Oxygen", J.H. Van Vleck, Phys. Rev., 413(7), April 1, 1947

42. "Improved electron emission by use of a cloth fiber cathode", R.J. Adler, G.F. Kiuttu, B.E. Simpkins, D.J. Sullivan, and D.E. Voss, Rev. Sci. Instrum., 56(5), May 1985

43. "The theory of Langmuir Probes in strong electrostatic potential structures", J.E. Borovsky, Phys. Fluids, 29(3), March 1986

44. Principles of Plasma Physics, by N.A. Krall and A.W. Trivelpiece, McGraw-Hill Book Co., 1973

45. NRL Plasma Formulary, by D.L. Book, 1987